



Project Number: R. 099350.002



# **Lasalle Causeway Bascule Bridge Main Trunnion Rehabilitation Study - Structural Evaluation Report**

# TABLE OF CONTENTS

<b>EXECUTIVE SUMMARY .....</b>	<b>1</b>
<b>1 INTRODUCTION .....</b>	<b>1</b>
<b>2 STRUCTURE DESCRIPTION.....</b>	<b>1</b>
<b>3 METHODOLOGY .....</b>	<b>3</b>
3.1 Loads .....	4
3.1.1 Dead loads .....	4
3.1.2 Live loads .....	4
3.1.3 Winds loads ( $W_0$ ).....	4
3.1.4 Horizontal force ( $H_0$ ) .....	4
3.1.5 Operating impact load ( $I_0$ ) .....	4
3.1.6 Loads caused by the operation of machinery ( $M_0$ ).....	5
3.2 Load Combinations and Load Factors .....	6
3.3 Member Resistances .....	6
3.3.1 Gusset plates and fasteners of the main trunnion assemblies.....	6
3.3.2 Material properties of the connecting members .....	7
3.3.3 Capacity of the connecting members.....	7
3.3.4 Capacity reduction .....	9
3.4 Structural Analysis .....	10
3.4.1 Global bridge models.....	10
3.4.2 Localized 2D models .....	11
3.5 Strain gauge testing.....	14
<b>4 STRUCTURAL EVALUATION RESULTS.....</b>	<b>15</b>
4.1 Strain Gauge Testing.....	15
4.1.1 Dynamic load amplification.....	15
4.1.2 Validation of structural analysis models .....	16
4.1.3 Testing variability.....	18
4.2 Connecting Members of the Main Trunnion Assemblies.....	18
4.3 Gusset Plates and Fasteners .....	20
4.3.1 Influence of fastener stiffness .....	20



4.3.2	Influence of the operating impact ( $I_0$ ).....	25
4.3.3	Influence of loads caused by the operation of machinery ( $M_0$ ) .....	25
4.3.4	Influence of wind load ( $W_0$ ) .....	26
4.3.5	Influence of deterioration.....	28
4.3.6	Summary of results .....	32
<b>5</b>	<b>CONCLUSIONS AND RECOMMENDATIONS.....</b>	<b>37</b>
<b>6</b>	<b>CLOSURE.....</b>	<b>38</b>
	<b>REFERENCES.....</b>	<b>39</b>
	<b>APPENDIX A – UPDATED MAPPING OF THE TRUNNION PLATE DETERIORATION .....</b>	<b>40</b>
	<b>APPENDIX B – UTT INSPECTION REPORT FROM BROUCO NDT.....</b>	<b>45</b>
	<b>APPENDIX C – STRAIN GAUGE TESTING.....</b>	<b>66</b>
	<b>APPENDIX D – DEVIATION REQUEST FOR THE 2017 MOTOR AND DRIVE REHABILITATION PROJECT.....</b>	<b>67</b>

---

**LIST OF FIGURES**

Figure 1	- South elevation.....	2
Figure 2	- Dimensions and Truss Member Designation.....	2
Figure 3	- Main Trunnion Assembly (a) Left: Moveable part (b) Right: Fixed part.....	3
Figure 4	- Discontinuity in cover plates of members 14-15 and 14-16 near main trunnion plate .....	8
Figure 5	- Diagonal 13N-16N a) Left: Section loss of $\pm 25\%$ on the webs of both channels (b) Right: Existing strengthening on the outside .....	9
Figure 6	- Local deterioration at member 15-17.....	10
Figure 7	- Localized section loss near the middle of member 15S-18S.....	10
Figure 8	- Global bridge model.....	10
Figure 9	- 2D model of the Main Trunnion Plate.....	11
Figure 10	- Meshing of the Main Trunnion Gusset Plate.....	11
Figure 11	- Links representing fasteners between different plates.....	12
Figure 12	- (a) Left: Modeling example of the fasteners (b) Right: Identification of the fastener's zones .....	13
Figure 13	- Boundary conditions at the trunnion pin (Gusset plate shown only).....	13
Figure 14	- Strain gauge configurations (a) Left: Uni-axial (b) Right: Tri-axial.....	15
Figure 15	- Strains on inner face of member 15-17 during Scenario 6 with maximal impact factor recorded .....	16
Figure 16	- Strains on diagonal 13-16 during Scenario 6 compared to global bridge model results.....	17
Figure 17	- <i>von Mises</i> stresses on north exterior gusset plate during Scenario 6 compared to localized 2D model results .....	17
Figure 18	- Strain measurements on bottom chord (13N-16N) during lifts 3, 4 and 5 .....	18
Figure 19	- Intersection between members 14-15 and 14-16.....	20
Figure 20	- <i>von Mises</i> stresses at undeteriorated state for maximum compression in strut 14-15 (ULS B2) (a) Left: Upper bound case (b) Right: Lower bound case .....	21
Figure 21	- <i>von Mises</i> stresses at undeteriorated state for maximum tension in diagonal 13-16 (ULS B2) (a) Left: Upper bound case (b) Right: Lower bound case .....	22
Figure 22	- <i>von Mises</i> stresses at undeteriorated state for maximum compression in strut 14-15 (ULS B2) with modified lower bound fastener stiffness.....	23
Figure 23	- <i>von Mises</i> stresses at undeteriorated state for maximum tension in diagonal 13-16 (ULS B2) with modified lower bound fastener stiffness.....	23
Figure 24	- Fasteners with insufficient shear resistance at undeteriorated state for upper bound fastener stiffness (a) Left: ULS B1 to ULS B3 (b) Right: ULS 1.....	24



Figure 25 - Fasteners with insufficient shear resistance at undeteriorated state for lower bound fastener stiffness (a) Left: ULS B1 to ULS B3 (b) Right: ULS 1..... 24

Figure 26 - *von Mises* stresses at undeteriorated state for maximal compression in strut 14-15 (ULS B3) (a) Left:  $I_0$  taken as per S6-14 (b) Right:  $I_0$  taken as zero..... 25

Figure 27 - *von Mises* stresses at undeteriorated state for maximal compression in strut 14-15 (ULS B2) (a) Left: with  $M_0$  level 3 (b) Right: with  $M_0$  level 1..... 26

Figure 28 - *von Mises* stresses at undeteriorated state caused by unfactored  $W_0$ ..... 27

Figure 29 - *von Mises* stresses at undeteriorated state caused by (a) Left: unfactored dead loads (b) Right: unfactored  $M_0$  level 3 ... 27

Figure 30 - *von Mises* stresses at undeteriorated state for maximal compression in strut 14-15 (ULS B2) (a) Left: with  $W_0$  according to S6-14 (1.5 kPa) (b) Right: with reduced  $W_0$  (0.75 kPa)..... 28

Figure 31 - *von Mises* stresses for maximal tension in diagonal 13-16 (ULS B2) in south interior gusset plate without triangle reinforcement plate (a) Left: Upper bound fastener stiffness (b) Right: Lower bound fastener stiffness..... 29

Figure 32 - *von Mises* stresses in south interior gusset plate due to (a) Left: dead loads in model A (b) Right: maximal tension in diagonal 13-16 (ULS B2) in Model B ..... 30

Figure 33 - *von Mises* stresses in south interior gusset plate for maximum compression in strut 14-15 (ULS B2) (a) Left: at undeteriorated state (b) Right: with deterioration ..... 31

Figure 34 - *von Mises* stresses in south interior gusset plate for maximum tension in diagonal 13-16 (ULS B2) (a) Left: at undeteriorated state (b) Right: with deterioration ..... 31

Figure 35 - Gusset plate expected yielding and fasteners with insufficient resistance at undeteriorated state according to S6-14 (a) Left: ULS 1 (b) Right: ULS B1 to B3..... 33

Figure 36 - Gusset plate expected yielding for ULS 1 considering deterioration (a) South exterior plate (b) South interior plate (c) North exterior plate (d) North interior plate..... 34

Figure 37 - Gusset plate expected yielding for ULS B1 to B3 according to S6-14 considering deterioration (a) South exterior plate (b) South interior plate (c) North exterior plate (d) North interior plate ..... 35

Figure 38 - Gusset plate expected yielding and fasteners with insufficient resistance at undeteriorated state for ULS B1 to B3 (a) Left: with loads taken according to S6-14 (b) Right: with restrictions during bridge operation ..... 36

---

#### LIST OF TABLES

Table 1 - Different Levels of  $M_0$ .....5

Table 2 - Load combinations and load factors used for the structural evaluation.....6

Table 3 - Gusset plate and fastener material properties .....6

Table 4 - Gusset plates and fastener resistances for ULS.....7

Table 5 - Capacity reduction factors .....9

Table 6 - Stiffnesses considered for the fasteners in the different zones and cases ..... 12

Table 7 - D/C ratios of the connecting members (including deterioration)..... 19

Table 8 - *von Mises* stresses for maximum tension in diagonal 13-16 (ULS B2) in south interior gusset plate with upper bound fastener stiffness case..... 30

Table 9 - *von Mises* stresses for maximum tension in diagonal 13-16 (ULS B2) in south interior gusset plate with lower bound fastener stiffness case..... 30

Table 10 - Results for gusset plates and fasteners at undeteriorated state in accordance with the CHBDC ..... 32

Table 11 - Results for gusset plates and fasteners at undeteriorated state with restrictions during bridge operation..... 36

## Executive Summary

In September 2019, Public Services and Procurement Canada (PSPC) retained Parsons to provide professional engineering services related to the rehabilitation of the main trunnion bearings of the LaSalle Causeway Bascule Bridge. The scope of work for the current mandate includes: a detailed close-up inspection (including ultrasonic thickness testing) of the main trunnion assemblies and six adjacent steel members and connections; measuring the dynamic amplification of the bridge during opening and closing of the bridge using strain gauges; a structural evaluation of the main trunnion assemblies and adjacent steel members and connections in accordance with the Canadian Highway Bridge Design Code CAN/CSA S6-14 (CHBDC); development of repair and/or replacement concepts, steel coating requirements, construction staging strategies, including Class 'C' cost and working day estimates; and a traffic impact analysis.

This report presents the findings of the detailed close-up inspection, the in-situ testing using strain gauges and the structural evaluation of the main trunnion assemblies in accordance with the CHBDC.

The strain gauge testing performed at the bridge allowed validation of the static dead load distribution obtained with the structural analysis models with the bridge in the closed and various open positions. For the dynamic amplification effect, a lower operating impact factor ( $I_0$ ) was measured compared to the CHBDC factor. However, given the lower than expected influence of the operating impact factor on the results of the evaluation and high variability of the recorded values, the use of the operating impact factor specified in the CHBDC for bascule bridges is recommended.

The results of the structural evaluation showed that when the bridge is operated, i.e. in the open position, four truss members (13-16, 14-15, 14-16 and 15-17) are significantly overstressed with demand over capacity (D/C) ratios greater than 1.6, and all four trunnion gusset plates are also overstressed. When the bridge is in the closed position, i.e. open for road traffic, the six members evaluated have adequate resistance but both interior (north and south) gusset plates are locally overstressed. Therefore, if the requirements of the CHBDC are strictly adhered to, members 13-16, 14-15, 14-16 and 15-17, and all four gusset plates should be repaired or strengthened.

It should be noted however, that the analyses performed showed that, contrary to what was expected, the forces in the main trunnion assemblies when the bridge is in the open position are mainly influenced by the wind and not by the operating impact. Therefore, consideration should be given to deviating from the loads prescribed in the CHBDC and setting a limit on the maximum permissible wind speed for bridge operation, in order to reduce significantly the extent of the required strengthening. As the existing mechanical system also has insufficient capacity to meet current CHBDC requirements, a rational and coherent approach considering both mechanical and structural capacities should be considered in order to establish the restrictions during the operation of the bridge.

## 1 Introduction

The LaSalle Causeway, owned and operated by Public Services and Procurement Canada (PSPC), carries Highway 2 across the Cataraqui River within the City of Kingston, providing a critical transportation link between the downtown area on the west side of the river with the Barriefield/CFB Kingston area on the east side of the river. Approximately 23,000 vehicles cross the Causeway daily. The Causeway consists of five (5) interconnecting structures: The West Bridge (including its west approach), the West Wharf, the Bascule Bridge, the East Wharf, and the East Bridge (including its east approach). The Bascule Bridge also provides marine access to the inner harbour of Kingston, lifting an average of 900 times per year, and access to the southern entrance of the Rideau Canal.

In September 2019, Parsons was retained by PSPC to provide professional engineering services related to the Main Trunnion Bearings Rehabilitation of the LaSalle Causeway Bascule Bridge. The mandate includes the following tasks: a detailed close-up inspection (including ultrasonic thickness testing) of the main trunnion assemblies and adjacent steel members and connections; measuring the dynamic amplification of the bridge during opening and closing of the bridge using strain gauges; a structural analysis of the main trunnion assemblies; development of repair and/or replacement concepts; steel coating requirements; construction staging strategies, including Class 'C' cost and working day estimates; and a traffic impact analysis. This draft technical memorandum presents the results of the structural evaluation and discuss the results of the measurements that were carried out to evaluate the dynamic effects during the bridge operation.

It should be noted that two structural evaluations of the bridge were previously carried out: the 2015 Trunnion Joint Inspection and Analysis Report by MMM Group [1] and the 2017 Structural Evaluation Report by Parsons [2]. Both reports indicate that the main trunnions and adjacent truss members of the Bascule Bridge do not meet the requirements of Section 13 of the Canadian Highway Bridge Design Code CSA S6-14 (CHBDC) [3], primarily due to ongoing deterioration of the structural steel and the operating impact ( $I_0$ ) special load factor applied to the maximum dead load effect in all members caused by the movement of the bridge.

Finally, mechanical movable bridge specialist engineers from Stafford Bandlow Engineering (SBE), a division of Wiss, Janney, Elstner Associates (WJE), have collaborated with Parsons during this study to ensure that the dynamic and the machinery effects are well reflected in our analyses.

## 2 Structure Description

The Bascule Bridge is a single-leaf Strauss heel trunnion bascule bridge, designed by The Strauss Bascule Bridge Co. of Chicago (Figure 1 and Figure 2). Construction of the bridge was completed in April 1917. The structure is supported on two concrete abutments (also known as piers) founded on timber piles (based on available original drawings), the front faces of which are protected with steel sheet piling.

The main leaf truss span of the bridge spans between the East Wharf and West Wharf and consists of a Modified Warren through truss with a span length of 48.77 m (160'). The centre-to-centre truss width is 8.23 m (27') and the centre of bottom chord to centre of top chord height varies from the east to the west end from 6.10 m (20') to 7.92 m (26'). The bridge has a posted vertical clearance of 4.2 m and a vertical clearance above the water of approximately 0.6 m.

The roadway width on the bridge is 7.32 m (24') and carries one eastbound and one westbound vehicular traffic lane on an open steel deck grating. The deck grating is supported by a floor system comprised of transverse sills, nine longitudinal stringers, and transverse floor beams located at each panel point. A 1.2 m (4') wide timber plank sidewalk is cantilevered from the exterior of the south truss.

The fixed tower truss supports the counterweight truss and machinery room. The lower members of the north and south trusses are located directly adjacent to the roadway. The counterweight truss above supports the concrete counterweight.



The top chords, bottom chords, verticals, diagonals, cantilevered sidewalk floor beams, sway bracing and struts, top lateral bracing, fixed tower, counterweight link, operating strut, and counterweight truss members consist of built-up sections of plates, channels, angles, and/or lattice. Repairs carried out under previous contracts have strengthened or repaired some deteriorated members and replaced lattices with cut out steel plates on others.

The concrete counterweight weighs approximately 550 tons (1,220,000 lbs.) and is suspended from the counterweight truss. The counterweight has an internal steel truss structure and is reinforced at the exterior faces by steel bars and wire mesh. There are steel plates mounted on the north and south faces which are secured in place by threaded steel rods. Two pockets are provided in both the east and top faces of the counterweight, which can accommodate additional dead load required to balance the bridge.

The machinery room containing the span drive machinery (brakes, motors, open gearing, etc.) is located over the roadway and is supported within the fixed tower truss. Access to the machinery room, top of the counterweight, bearings and pins is provided by various catwalks, stairs, and access ladders. The operator's control house containing the electrical systems for bridge operations is located to the northwest of the structure on the east end of the West Wharf. The building containing the PSPC office and workshop is located on the West Wharf.



Figure 1 - South elevation

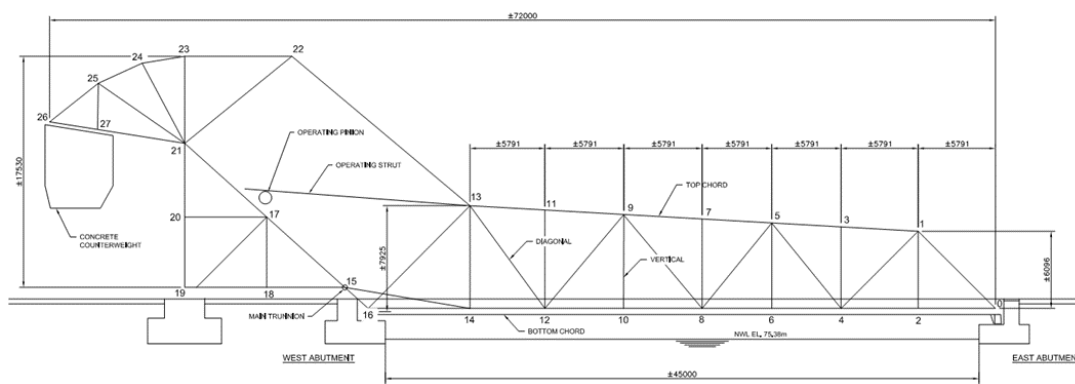


Figure 2 - Dimensions and Truss Member Designation

The main trunnion assemblies consist of 6 truss members: the diagonal 13-16, the strut 14-15, the bottom chord 14-16 (all through-truss members), the fixed diagonal 15-17 and tie 15-18 (both tower truss members) and the post (Figure 3). The main trunnion pin is located at node 15.

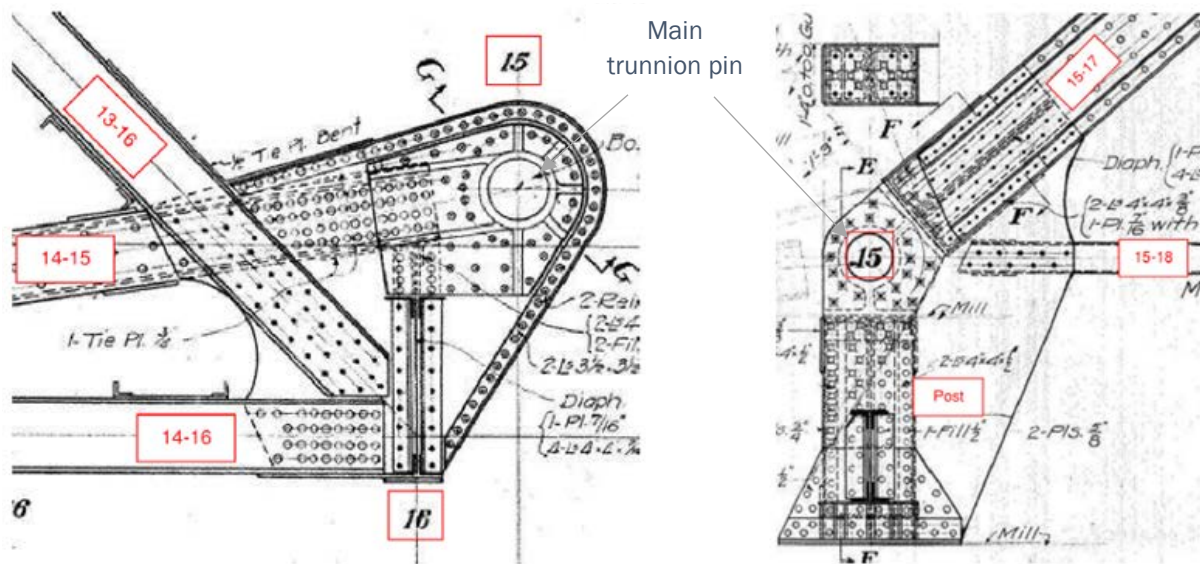


Figure 3 - Main Trunnion Assembly  
(a) Left: Moveable part (b) Right: Fixed part

### 3 Methodology

The structural evaluation of the trunnion plates and the connecting members was performed for the bridge in the closed position (open to vehicular traffic) and the bridge in four open positions at the following angles: 0°, 21°, 42° and 63°. The maximum opening angle according to the original drawings is 84°, but the current maximum operating angle is only 65° according to PSPC (refer to Parsons 2017 report). Moreover, the bridge analysis at 63° is deemed sufficiently close to 65° to be representative.

Demand/Capacity factors (D/C) were calculated using the design Ultimate Limit States (ULS). In the closed position, the evaluation was performed under ULS1 per Section 3 of the CHBDC. In the open position, the evaluation was performed per Section 13, considering ULS B1 to B4.

All loads and materials used for the study were taken in accordance with Sections 3 and 13 of the CHBDC and are summarized in the following sections. The following loads were not considered in this study:

- Ice accretion load;
- Loads due to earth pressure and hydrostatic pressure;
- Earthquake load;
- Loads due to stream pressure and ice forces or to debris torrents;
- Collision load arising from highway vehicles or vessels;
- Braking force;
- All strains, deformations, and displacements and their effects, including the effects of their restraint and the effects of friction or stiffness in bearings. Strains and deformations include strains and deformations due to temperature change and temperature differential, but not elastic strains;
- Load due to differential settlement and/or movement of the foundation;
- Sidewalk loading per Clause 14.9.5.1 (significant sidewalk loading not considered likely to occur with maximum traffic loading);

- Snow loads per clause 14.9.5.2 (not deemed significant due to open deck grating system);
- Wind load on traffic per Clause 14.9.5.3; and
- Wind load on the closed structure per Clause 14.9.5.3.

## 3.1 Loads

---

### 3.1.1 DEAD LOADS

For truss members, built-up sections consisting of angles, channels, and plates are used in this bridge. These members are modeled in the 3D models of the bridge using the cross-section identified in the original drawings as well as drawings for any rehabilitated members. A weight modifier is used for all truss members to account for the weight of lattices, batten plates, and bolts. The original concrete counterweight is modeled with solid elements whereas the steel grating and the steel railings are not modeled, but additional dead loads are applied in the model to represent them. As the 3D model is based on the one used in the 2017 Structural Evaluation Report [2], the reader can refer to it for additional information.

### 3.1.2 LIVE LOADS

Live Loads and their associated Dynamic Load Allowances (DLA) were taken in accordance with Section 3 of the CHBDC. The CL-625-ONT truck load and the CL-625-ONT Lane load were used in the analysis. The envelope of live-load effects was used for the member evaluations. However, concurrent forces were considered for the main trunnion plate evaluation. In this specific case, concurrent forces not only refer to the associated forces within a member (i.e. associated shear for the maximum bending moment), but to concurrent forces in all the members connecting to the main trunnion plate.

### 3.1.3 WINDS LOADS ( $W_0$ )

Wind loads on the structure and on traffic when the bridge is in its closed position were not considered in this study. Wind loads ( $W_0$ ) were considered for the bridge in the open position as defined in Clause 13.6.4 of the CHBDC. For bascule bridges, the horizontal transverse wind pressure as well as the horizontal longitudinal wind pressure is taken as 1.50 kPa (Clause 13.6.4.9). These two cases were not considered simultaneously. Moreover, different diagonal wind load cases were considered using the algebraic transverse and longitudinal components of the wind load as recommended by AASHTO LRFD Movable Highway Bridge Design Specifications [4] Clause 2.4.1.3.

### 3.1.4 HORIZONTAL FORCE ( $H_0$ )

A horizontal force ( $H_0$ ) taken as 5% of the total moving load (i.e. the leaf span) was applied per Section 13 of the CHBDC. This load has to be applied in all directions through the centre of gravity of the moving load, but it is only considered for the three members of the fixed part of the bridge (and only included in load combination ULS B4).

### 3.1.5 OPERATING IMPACT LOAD ( $I_0$ )

An operating impact load ( $I_0$ ) of 20% was applied to the maximum dead load effect in all members that are in motion and to the load effect on a stationary member caused by the moving dead load. Due to the nature of impact forces, this load was applied in either an upward or downward direction to find the maximum effect.

It is acknowledged that the code-prescribed factors may be overconservative and more applicable to setting the standard for new bascule bridge design rather than evaluating an existing structure that has already operated for 100 years. Strain gauge testing was performed to measure the dynamic amplification during the bridge operation and is discussed in Section 3.5.



### 3.1.6 LOADS CAUSED BY THE OPERATION OF MACHINERY ( $M_0$ )

The forces applied by the operating struts as the bridge opens or closes are to be considered in the load case  $M_0$ . The CHBDC defines this load case as the maximum loads on structural parts caused by the operation of machinery, increased 100% for impact. It does not state what is the maximum machinery force to be considered. AASHTO LRFD [4] Clause 2.4.1.2.3 specifies the machinery forces shall be taken as those specified for the service limit state for machinery design which is 150% of the full load motor torque. This corresponds to 256 kN per operating strut according to SBE.

Using the value defined per AASHTO appears to be very conservative as the  $M_0$  load case is combined with other load case forces in the operating struts. For example, the unfactored horizontal longitudinal wind pressure can cause force of up to 560 kN in each operating strut. As the wind is combined with  $M_0$  in the load combination ULS B2 ( $1.3W_0 + 1.25M_0$ ), it results in a total force of 1368 kN (excluding the contribution of the other load cases). Based on the data received from SBE, there is a safety mechanism on the machinery limiting the maximum force to 457 kN. When this force is exceeded, the brakes will continue to resist this maximum force, but they will allow a movement of the operating struts if the force is maintained. In fact,  $M_0$  alone with 100% impact exceeds this limit ( $256 \text{ kN} \times 2 = 512 \text{ kN}$ ), before multiplying it by the load factors 1.25 or 1.55 according to Table 13.2 of the CHBDC.

An attempt was made to rationalize a better approach to integrate  $M_0$  into this existing bridge evaluation, because the axial force in the operating struts is associated with important axial forces at some of the connecting members of the main trunnion plates. During normal operations with negligible wind, the force in the operating struts is caused by three factors: the unbalanced dead loads between the main leaf and the counterweight, the friction in the pins, and the acceleration and deceleration of the moving mass. Strain measurements taken on the shafts by SBE during testing runs performed in October 2019 show the following results:

- During operations without an emergency stop, the peak loads applied to the operating struts are 98 kN. These loads are when the span just starts to move and are a result of overcoming starting friction and acceleration. With the new drives and VFD motors the span is very well controlled and the loads applied to the machinery during starting and stopping were noticed to be repeatable.
- When the span is operating at a constant velocity the operating strut loads were less than 62 kN and around 31 kN on average.
- When performing emergency stops a peak load of 238 kN was applied to the operating strut. This was an extreme condition achieved by applying the motors at the control desk to move the bridge while simultaneously applying the emergency brake.

Three (3) levels of  $M_0$  have been considered and are summarized in Table 1. Level 1 corresponds to the maximum value measured without any emergency stops during the testing. Level 2 corresponds to the measurement made while performing the emergency stops, slightly rounded up to match the theoretical value of 256 kN. Levels 1 and 2 do not include any additional force for impact. Level 3 is calculated per the definition of AASHTO LRFD [4]. For all the levels, the load factors per Chapter 13 of the CHBDC are applied.

Table 1 - Different Levels of  $M_0$

	<b>Machinery Force (kN)</b>	<b>Contingency for Impact (kN)</b>	<b><math>M_0</math> Total Force (kN)</b>
LEVEL 1	98	0	98
LEVEL 2	256	0	256
LEVEL 3	256	256	512

These three  $M_0$  levels were defined to help PSPC understand how they influence the results. We believe these additional load cases will be useful as part as the broader discussion on the extent of the required strengthening, especially since the bridge has been operating without any major structural issues related to the trunnions for more than 100 years. It is not possible to guarantee that the results recorded in October 2019 will not vary with time, as they depend on the tuning of

the brakes. However, it might be possible to include frequent tuning of the brakes (adjusting time delays and verifying set torques) to accept a lower level of forces caused by the machinery.

### 3.2 Load Combinations and Load Factors

The structural evaluation is conducted in accordance with Sections 3 and 13 of the CHBDC. For the bridge in the closed position, ULS 1 of Section 3 was used to find the maximum concomitant forces in the members and the trunnion plates. As this bridge evaluation will be used to determine the strengthening required for the bridge rehabilitation, the use of ULS1 is justified as S6-14 Clause 15.5.2 specifies the load factors and the load combinations shall be in accordance with Section 3. For the bridge in open position, ULS B1, ULS B2, ULS B3 and ULS B4 of Cl. 13.6.10.2 of the CHBDC were considered. This special load combinations apply to bascule bridges and consider various loading situations during the operation of the bridge, such as the dead load plus dynamic amplification effect plus peak force coming from the machinery (ULS B1) or the dead load plus a dynamic amplification effect plus a strong wind (ULS B3). It should be noted that ULS B4 only applies to the fixed members, which are the diagonal 15-17, the tie 15-18 and the post. Table 2 summarizes the load combinations used for the structural evaluation.

Table 2 – Load combinations and load factors used for the structural evaluation

LOADS	Load combination for normal traffic	Special load combinations for bascule bridges			
	ULS 1	ULS B1	ULS B2	ULS B3	ULS B4
D1	$\alpha_{D1}$	$\alpha_{D1}$	$\alpha_{D1}$	$\alpha_{D1}$	$\alpha_{D1}$
D2	$\alpha_{D2}$	$\alpha_{D2}$	$\alpha_{D2}$	$\alpha_{D2}$	$\alpha_{D2}$
D3	$\alpha_{D3}$	$\alpha_{D3}$	$\alpha_{D3}$	$\alpha_{D3}$	$\alpha_{D3}$
L	1.7	-	-	-	-
H <sub>0</sub>	-	-	-	-	1.55
W <sub>0</sub>	-	-	1.3	1.6	-
I <sub>0</sub>	-	1.2	1.2	1.2	1.2
M <sub>0</sub>	-	1.55	1.25	-	1.55

### 3.3 Member Resistances

The member resistances were calculated according to Section 10 of the CHBDC. The main assumptions are presented in the following sub-sections.

#### 3.3.1 GUSSET PLATES AND FASTENERS OF THE MAIN TRUNNION ASSEMBLIES

The material properties considered in the evaluation are presented in Table 3.

Table 3 - Gusset plate and fastener material properties

Element	E <sub>s</sub>	F <sub>y</sub>	F <sub>u</sub>	Justification
GUSSET PLATES (INCLUDING COLLAR AND INTERIOR-SIDE PLATES)	200 000 MPa	210 MPa	-	S6-14 Cl. 14.7.4.2
RIVETS	200 000 MPa	-	320 MPa	S6-14 Cl. 14.7.4.6
BOLTS	200 000 MPa	-	830 MPa	ASTM Grade A325M

To evaluate the possibility of failure of the gusset plates, the *von Mises* yield criterion is used. Based on the maximum distortion strain energy theory, this criterion is commonly used to evaluate the yielding of steel submitted to multi-axial

stresses. In this theory, yielding occurs when an equivalent stress, also called *von Mises* stress, exceeds the yield strength. *Von Mises* stresses are calculated from both axial and shear stresses obtained using the finite element (FE) model with shell elements and consider the interaction between tension/compression and shear forces in the gusset plates.

A factored yield strength is used in this assessment to serve as a limit for the *von Mises* stresses. A resistance factor of 0.90 for plate strength was taken. This value is consistent with requirements of the CHBDC Section 10 for steel in compression, which was found to be the major failure mode in the gusset plates.

Table 4 presents the resistance criteria that was used to evaluate the gusset plates and the fasteners of the main trunnion assemblies.

Table 4 - Gusset plates and fastener resistances for ULS

Element	Type of force	Resistance limit	Justification
GUSSET PLATES (INCLUDING COLLAR AND INTERIOR-SIDE PLATES)	<i>von Mises</i> stresses	$\Phi_s F_y = 0.9 \times 210 \text{ MPa}$ = 189 MPa	No specific indication for gussets in the CHBDC, other well-documented references used [5], [6], [7]
RIVETS (19 MM - 3/4" DIAMETER)	Shear force per rivet per shear plane	$0.75 \Phi_r A_r F_u$ = $0.75 \times 0.67 \times 283 \text{ mm}^2 \times 320 \text{ MPa}$ = 45.5 kN	S6-14 Cl. 14.14.1.4.2
BOLTS (22 MM - 7/8" DIAMETER)	Shear force per bolt per shear plane	$0.60 \Phi_b (0.7A_b) F_u$ = $0.60 \times 0.80 \times 0.7 \times 380 \text{ mm}^2 \times 830 \text{ MPa}$ = 106 kN	S6-14 Cl. 10.18.2.3.3 (threads considered as intercepted)

### 3.3.2 MATERIAL PROPERTIES OF THE CONNECTING MEMBERS

In the absence of other information, Table 14.1 of CHBDC states that for bridges constructed between 1905 and 1932, the specified yield strength of steel ( $F_y$ ) shall be taken as 210 MPa and the ultimate strength ( $F_u$ ) taken as 420 MPa. Since the Bascule Bridge is constructed between 1915 to 1917, the above values were taken as the strength of steel for the purposes of this evaluation.

In 1997, the tie-plates of members 14N-15N, 14S-15S and 14S-16S were replaced by new plates. As the yield strength ( $F_y$ ) is not specified on the drawings, it is assumed to be 300 MPa as per Table 14.1 of CHBDC. Moreover, the drawings indicate the tie-plates on member 14S-16S had already been replaced in 1997, but no drawing showing this retrofit is available. It was assumed this retrofit was done after 1978 so an  $F_y$  of 300 MPa was also considered.

### 3.3.3 CAPACITY OF THE CONNECTING MEMBERS

The resistances were calculated per Section 10 of the CHBDC, with additional criteria utilized for the members in compression as noted below.

#### 3.3.3.1 Compression

Compression resistance is calculated for built-up members according to Clauses 10.9.3, 10.9.4 and 10.14 of the CHBDC. In addition, the use of an equivalent slenderness ratio per CAN/CSA-S16-19 [8] Clause 19.2.4 was used:

$$\text{in } C_r \text{ (S6 - 14 art. 10.9.3.1) use: } \left(\frac{KL}{r}\right)_{eq} = \sqrt{\left(\frac{KL}{r}\right)_{global}^2 + \left(\frac{KL}{r}\right)_{individual-max}^2}$$

The above equation is not applied when the individual component's slenderness controls. In that case, compression resistance is limited to the individual component's resistance:

$$\text{if } \left(\frac{KL}{r}\right)_{individual max} > \left(\frac{KL}{r}\right)_{global}$$



in  $C_r$  (S6 – 14 art. 10.9.3.1) use:  $\left(\frac{KL}{r}\right)_{individual\ max}$

Moreover, the compressive resistance of the built-up members has been verified using the equations suggested by Galambos [9] for lacing members and batten members. The most critical verification was used to determine the D/C ratio.

### 3.3.3.2 Detailing of the Built-up Members

Members 13-16, 15-17 and 15-18 are built-up members composed of lacing similar to many other members on this bridge. It is important to mention that CHBDC Clause 10.4.2.1 states that built-up members shall be connected by solid plates unless otherwise approved. The CAN/CSA-S16-19 is less stringent as it allows the use of laced members, batten members and perforated cover plates. It also mentions the use of batten members is not recommended for members in compression carrying primary bending in addition to axial load, but it does not exclude laced members. Most laced members on this bridge resist some bending in the plane of the lacings, but it is important to note that it is especially the case for the two 13-16 members. These two diagonals are part of the end portal of the bridge and they act as unbraced members. When the bridge is in the open position, they resist the transverse loads applied to the bridge by deforming in double curvature, resulting in very large bending moments at both ends of member 13-16. This evaluation has been carried out considering compressive laced members are adequate even if they resist bending in the plane of the lacing and the resistance of the lacings has been checked according to Clause 19.2.9 of CAN/CSA-S16-19.

Similarly, CHBDC Clause 10.4.2.2 states that the separate components of tension members shall be connected by tie plates or other approved means. Members 13-16 and 15-18 are in tension under certain load cases. They are connected at both extremities by tie plates, but instead of intermediate tie plates, they have lacing. This is considered acceptable.

Perforated cover plates were installed on members 14-15 and 14-16 in 1997. Even though the CHBDC does not state it explicitly, it is well established in practice [8], [9], [10] that the net area of the cover plates can be considered in the total area of the member to calculate its compressive resistance. Unfortunately, it has not been possible to take full advantage of them in this evaluation. Firstly, it was found the cover plates do not meet one of the criteria of Clause 10.14.2.3, which is that the minimum longitudinal distance between the openings must be larger than the distance between the connecting members. Considering the number of bolts connecting each component to the cover plates, it appears reasonable to still consider the benefit of the net area of the cover plates in the member’s resistance. Secondly, the 3D model results clearly showed that the critical locations of these members are near their ends where larger bending moments occur. As shown on Figure 4, the new cover plates do not reach the member ends so all the forces must be transmitted through the original section making these locations the critical D/C ratios.



Figure 4 - Discontinuity in cover plates of members 14-15 and 14-16 near main trunnion plate

Considering the cover plates of members 14-15 and 14-16 do not comply to all the requirements of Clause 10.14.2.3, a verification was done by considering these members as batten members. The steel section of the cover plate in between two openings is considered as the member linking the two separate components. In both cases, this check found the capacity of the members to be adequate.

### 3.3.4 CAPACITY REDUCTION

As a first step, the previous structural evaluation had assigned reductions of 20% and 5% section loss to the members located in the splash zone (i.e. at or below deck level) and above the splash zone, respectively. If a member was found to be understrength for the live load demands (ULS1), a more accurate determination of the actual section loss was then established. This approach was deemed too conservative for the current study as only a few members are evaluated, and the critical load combinations have been found to be when the bridge is open (ULS B1 to ULS B4). Thus, a structural capacity reduction factor was assigned to each element per the detailed inspection that was carried out as part of this assignment and is summarized in Table 5. An overall capacity reduction factor was considered for each member and it applies to the full length of the member as it represents the general deterioration of the member. In addition, three localized areas of deterioration were also considered in this evaluation as explained in next paragraphs.

Table 5 – Capacity reduction factors

Member type (North and South)	Overall capacity reduction (full length of member)	Localized capacity reduction
13-16	5%	0% because localized deterioration at connection with strut 14-15 fully compensated by reinforcement
14-15	15%	0%
14-16	15%	0%
15-17	5%	10% at the member end connected with the trunnion
15-18	5%	10% at the middle of the member

As shown in Figure 5, a significant area of section loss is present on the interior face of both webs of the diagonal 13-16, just above strut 14-15. This section loss was visually estimated to represent 25% of the web thickness. However, this section loss is assumed to be compensated by the additional plates installed on the outside in 2011.



Figure 5 - Diagonal 13N-16N  
a) Left: Section loss of  $\pm 25\%$  on the webs of both channels (b) Right: Existing strengthening on the outside

Deterioration representing approximately 10% loss of the section was found on member 15-17 near the trunnion. As shown in Figure 6, it is located near the base, on area which has been holding water. By inspection, it was determined that this is not critical because it is located in a section where additional plates are added to stiffen the member. Finally, as shown on

Figure 7, two perforations representing approximately 10% loss of the section were found on the 15S-18S and were considered at their specific location in the evaluation.



Figure 6 - Local deterioration at member 15-17



Figure 7 - Localized section loss near the middle of member 15S-18S

For the main trunnion plates, the results of the detailed inspection combined with the results of the ultrasonic thickness testing were used to update the deterioration mapping drawings (refer to Appendix A – Updated Mapping of the Trunnion Plate Deterioration and Appendix B – UTT Inspection Report from Brouco NDT). The different areas of deterioration (i.e. reduced thickness, perforations, etc.) were explicitly modeled in the finite element model (FEM) of the main trunnion plates.

### 3.4 Structural Analysis

#### 3.4.1 GLOBAL BRIDGE MODELS

The three-dimensional finite element model of the Bascule Bridge created in CSI-Bridge during the 2017 Parsons Structural Evaluation was re-used for this evaluation. It should be noted that some modifications have been made to the model by the authors of the current study. The model was run in CSiBridge® version 21.1.0 and it was used to determine the forces in all the frame elements. A thorough description of the global model is available in the 2017 report and will not be reproduced herein. The global model was used to determine the concomitant forces in the members. Five (5) global models were used: one model when the bridge in the closed position (open to vehicular traffic) and four models when the bridge is in the open positions at various angles: 0°, 21°, 42° and 63°. The difference between the closed position and the 0-degree open position is that, for the latter, there is no support at the end of the leaf span, which is retained by the motors and therefore considered as cantilevered. In addition, special load combinations from the CHBDC apply for the open positions and not for the closed one. Figure 8 shows a 3D view of the global bridge model in the closed position.

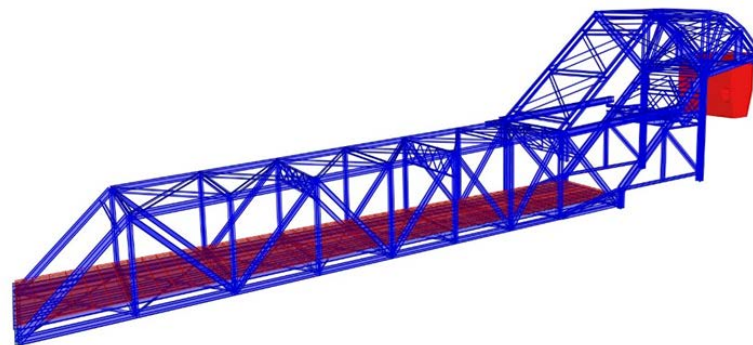


Figure 8 - Global bridge model

### 3.4.2 LOCALIZED 2D MODELS

A 2D model of the main trunnion assemblies has been made using shell elements. This finite element modeling consists of one gusset plate, one outside collar plate, one interior-side plate, the webs of the three connected members (diagonal 13-16, strut 14-15 and bottom chord 14-16) as shown in Figure 9. Meshing consists mainly of four-node quadrilateral shell elements of a size of approximately 10 mm by 10 mm. This dimension is very close to the thickness of the thinnest plate and was found to be a good compromise between accuracy and analysis time. Some three-node triangular shell elements were used to connect quadrilateral elements in areas of transition. Figure 10 shows the meshing used for the main trunnion gusset plate. Moreover, as shown on Figure 11, the plates are connected to each other with link elements that represent the existing fasteners (rivets and bolts).

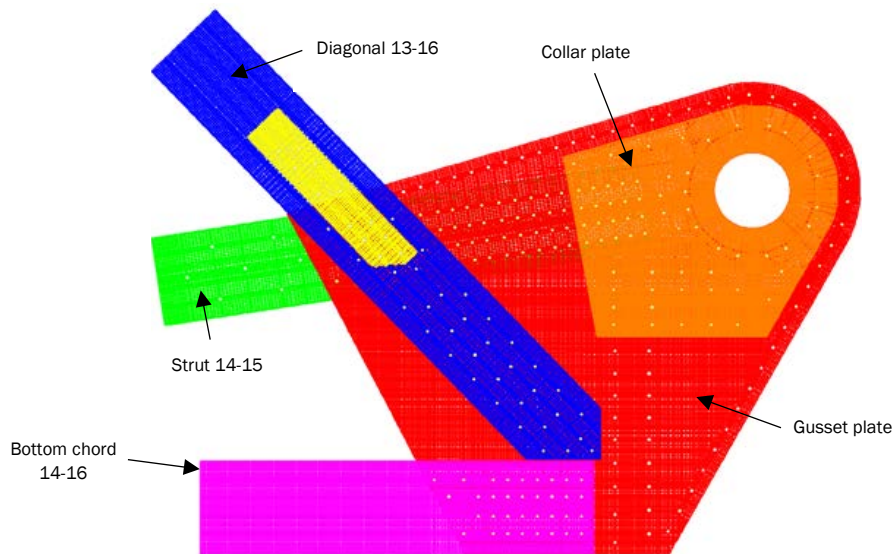


Figure 9 - 2D model of the Main Trunnion Plate

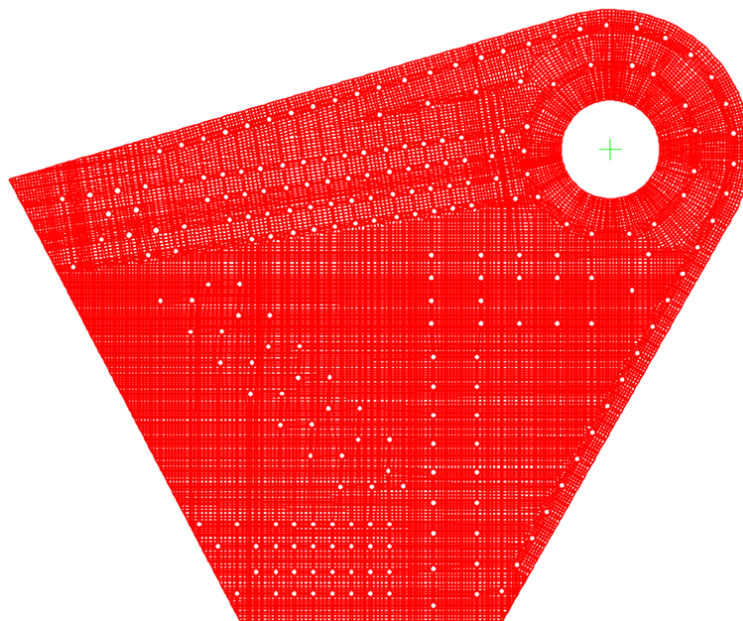


Figure 10 - Meshing of the Main Trunnion Gusset Plate



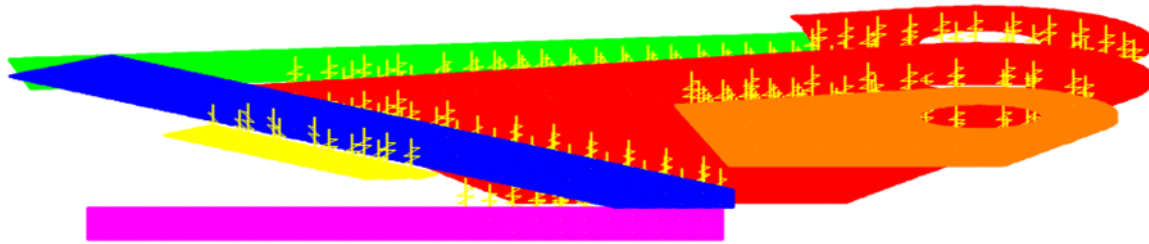


Figure 11 – Links representing fasteners between different plates

The link elements have a linear behavior and only have a degree of freedom for transverse shear in both orthogonal directions. The link stiffness that was used depends on the case considered in the analyses to evaluate the influence of the fastener flexibility.

Table 6 presents the fastener stiffnesses used in the analyses for the two cases considered. The same stiffness was used for both orthogonal directions. In the upper bound case, fasteners are considered semi-flexible and the stiffness is calculated with the equation given by Huth [11]. An upper bound case with infinite stiffness has not been considered because it would have been too conservative and not realistic. In the lower bound case, fasteners are considered infinitely flexible, in order to model a force distribution in the plates that would represent a final state after redistribution of the forces in the fasteners, considering the strain-hardening capacity in the rivets. To calculate the stiffness, different zones were defined depending on the groups of fasteners that assemble the same plates. These zones are shown in Figure 12 (b).

Table 6 - Stiffnesses considered for the fasteners in the different zones and cases

Fasteners	Stiffness for Upper Bound (UB) case (calculated with Huth equation [11])	Stiffness for Lower Bound (LB) case (UB stiffness divided by 1000)
ZONE 1 (RIVETS)	513 kN/mm	0.5 kN/mm
ZONE 2 (RIVETS)	513 kN/mm	0.5 kN/mm
ZONE 3 (RIVETS)	1230 kN/mm	1.2 kN/mm
ZONE 4 (BOLTS)	1458 kN/mm	1.5 kN/mm
ZONE 5 (RIVETS)	726 kN/mm	0.7 kN/mm
ZONE 6 (RIVETS)	2012 kN/mm	2.0 kN/mm
ZONE 7 (RIVETS)	1671 kN/mm	1.7 kN/mm
ZONE 8 (RIVETS)	513 kN/mm	0.5 kN/mm
ZONE 9 (BOLTS)	421 kN/mm	0.4 kN/mm

The holes for the rivets are generally 21 mm in diameter (19+2mm) while bolt holes are 24 mm in diameter (22+2mm). Links are located in the center of each hole. A body constraint was assigned to the end-node of the link and to all the nodes located at the perimeter of the hole to transfer the force from the plate to the link to reduce possible stress concentrations in one node (Figure 12 (a)). This modeling technique doesn't capture any hole ovalization behavior due to bearing but we consider it acceptable because linear analyses are performed.



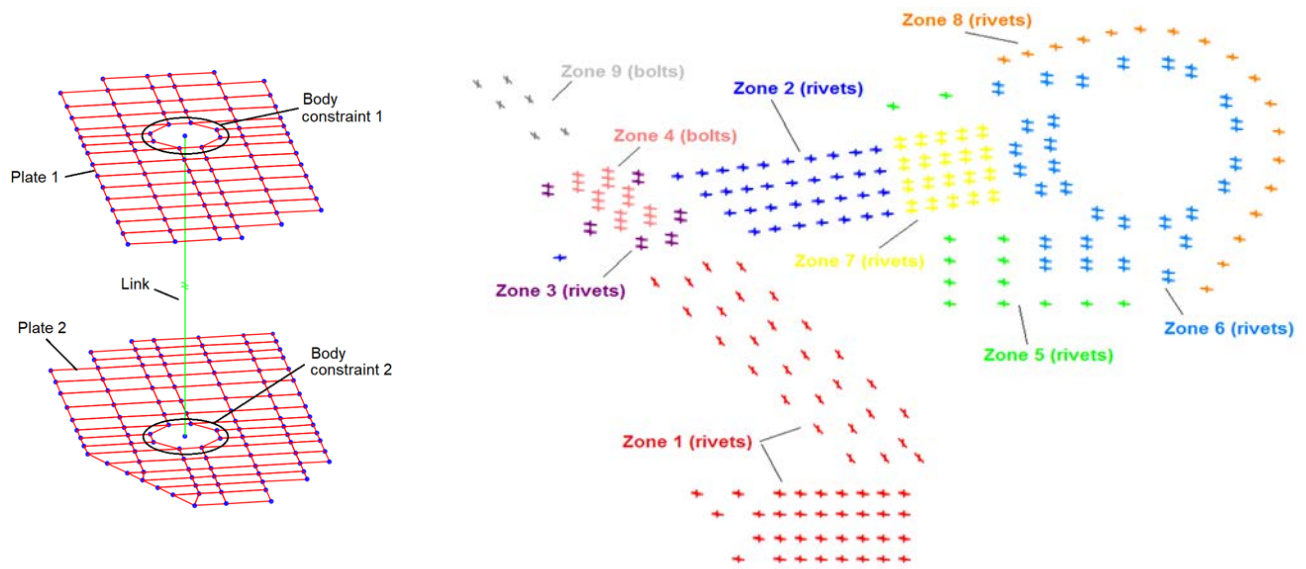


Figure 12 - (a) Left: Modeling example of the fasteners (b) Right: Identification of the fastener's zones

At the center of the trunnion pin hole, a support has been added to restrain the in-plane translation and the rotation about an axis normal-to-the-plane. Restraining the rotation is necessary for numerical stability of the analysis because theoretically, if friction is neglected, the summation of moments should be null and pin support should only transfer in-plane forces. However, in practice, because of the slight differences between both global and localized models, and because friction has been considered in the global model, an overturning moment exists. To transfer the forces between the plates and the pin support, frame members have been added to connect the node located at the circumference of the ring to the pin restraint at the center of the ring. Figure 13 gives an overview of the modeling at the trunnion pin.

The possibility to use compression-only axially rigid frame elements has been studied in order to model more accurately the stress distribution in the plates around the pin (i.e. with contact elements, no tension induced behind the pin). However, it was found that this modeling technique slightly changes the stresses but not enough to change the findings. Because this would require a non-linear analysis, it has been decided to keep linear axially rigid frame elements to model the contact between the plates and the pin.

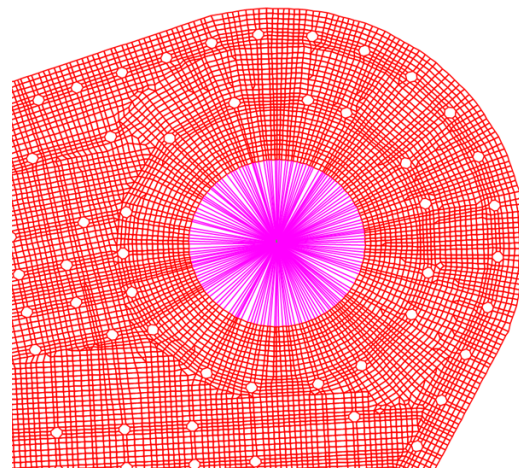


Figure 13 - Boundary conditions at the trunnion pin (Gusset plate shown only)

Concurrent forces (axial, shear and moment) in the three connecting members (strut 14-15, diagonal 13-16 and bottom chord 14-16) were obtained from the global bridge models and applied in the 2D model on the shell elements representing the web of these members. The end floorbeam connected to the main trunnion and the bottom lateral bracing connected to the gusset plate are not modeled in the 2D model. Therefore, concurrent forces in both the floorbeam and lateral bracing, that are also obtained with the global bridge models, are applied in the 2D model directly on the gusset plate nodes.

### 3.5 Strain gauge testing

---

The strain gauge testing of the north and south main trunnions and connecting truss members was conducted during several opening and closing cycles of the bridge. The strain measurements allowed the determination of stresses on the trunnion plates and forces on the truss members with two objectives: to rationalize the dynamic load amplification during the operation of the bridge; and to validate structural analysis models.

Previous evaluations (MMM in 2015 [1] and Parsons in 2017 [2]) recommended further research on the operating impact factor of the bridge. The main reason for this recommendation was that in both studies, the capacity of most truss members and trunnion plates was found to be insufficient compared to load cases where the theoretical value of the operating impact factor ( $I_0$ ) calculated as per the CHBDC was applied. However, regular opening and closing cycles (approximately 193,000 times since 1917) have not caused visible impact damage to the bridge. This is a possible indication that the impact coefficient may be lower than the theoretical value.

As described earlier, five global models of the bridge were built in order to obtain the forces in the connecting members of the main trunnions for different bridge opening positions. Dead loads obtained in these models were based on the original plans and available documents describing the repairs and modifications carried out on the bridge. However, all the information available was not always accurate or complete, and the strain gauge testing was key to validate the models based on those assumptions.

The strain gauge testing was carried out by BMT Canada Ltd. (BMT) in conjunction with Brouco NDT under the supervision of Parsons. Installation of the strain gauges started on October 15, 2019 and the testing operations were conducted on October 17 between 12:00 a.m. and 6:00 a.m.

Strain gauges were installed in a combination of single uni-axial units and tri-axial configurations. All truss members were tested with two uni-axial strain gauges, one gauge on each side (Figure 14 (a)). Tri-axial measurement points were installed on the inner and outer plates of the trunnions (Figure 14 (b)).

A total of five (5) lift scenarios were defined to include different operating speeds as well as regular braking and emergency stops. In order to assess the variability of the test, one of these lift scenarios was carried out three (3) times. These lift scenarios were:

- Lift 1: Opening and closing at regular speed (3) with only one regular (i.e. non-emergency) stop at current maximum permissible opening position (65°);
- Lift 2: Opening and closing at speed 2 with only one regular stop at 65°;
- Lifts 3, 4 and 5: Opening and closing at speed 2 with regular stops at 5°, 21°, 42°, 60° and 65°;
- Lift 6: Opening and closing at speed 2 with emergency stops at 5°, 21°, 42°, 60° and 65°; and
- Lift 7: Opening and closing at speed 3 with regular stops at 5°, 21°, 42°, 60° and 65°.

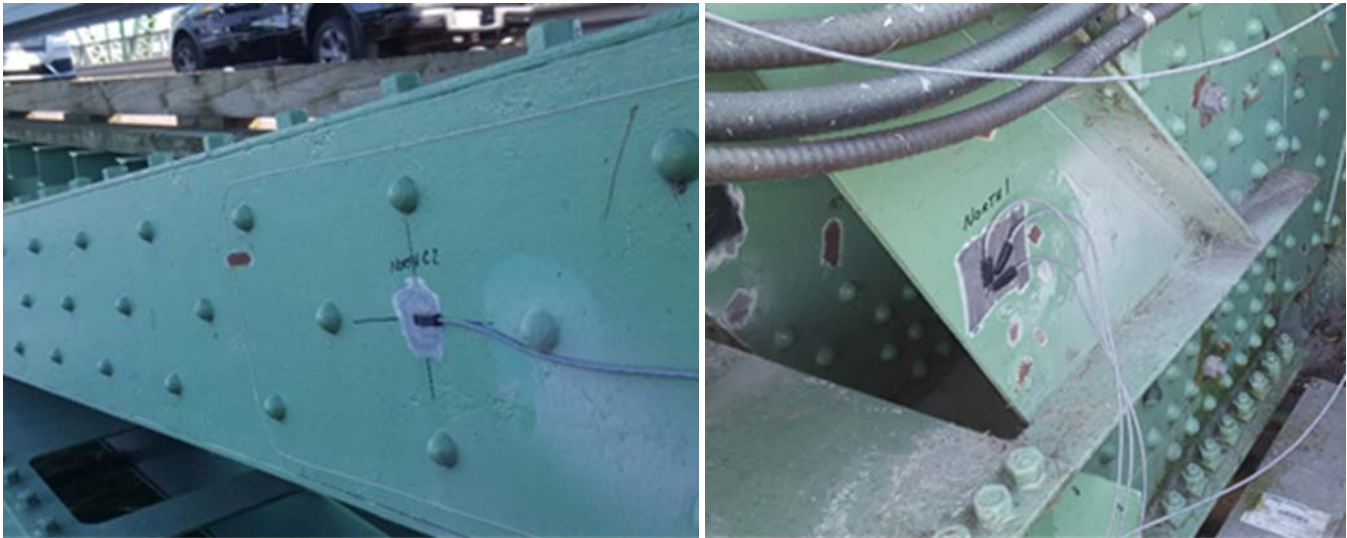


Figure 14 – Strain gauge configurations  
(a) Left: Uni-axial (b) Right: Tri-axial

Due to the important number of strain gauges required (a total of sixty-four (64)), the test operations were conducted twice since the data acquisition system (DAS) available was only able to record thirty-two (32) channels at a time. For the duration of the entire test, data acquisition frequency was about 1.6 Hz. This value was the largest allowed by the DAS, given the duration of the test. Testing results and discussion are included in Section 4.1.

## 4 Structural Evaluation Results

### 4.1 Strain Gauge Testing

This section presents the findings of the in-situ testing conducted at the bridge. Refer to Appendix C for the raw data.

#### 4.1.1 DYNAMIC LOAD AMPLIFICATION

The measurement of the operating impact factor has been considered in order to rationalize its value. The CHBDC states that the operating impact load ( $I_o$ ) shall be considered to be 20 % of the dead load. The load factor corresponding to  $I_o$  being 1.2, operating impact comes to a maximum of 24% of dead load. Moreover, operating impact load, is part of four of five load combinations (refer to Table 2) to be considered for design or evaluation of bascule bridges.

Measured strains for all members and plates, for several speeds and for several types of braking have been analyzed and the highest value recorded for  $I_o$  is 11 % of dead load (see Figure 15). The maximal value was recorded during the scenario (Scenario 6) when the emergency brake was applied. Compared to the theoretical value of 20% from the CHBDC, this value confirms that the CHBDC factor is conservative.

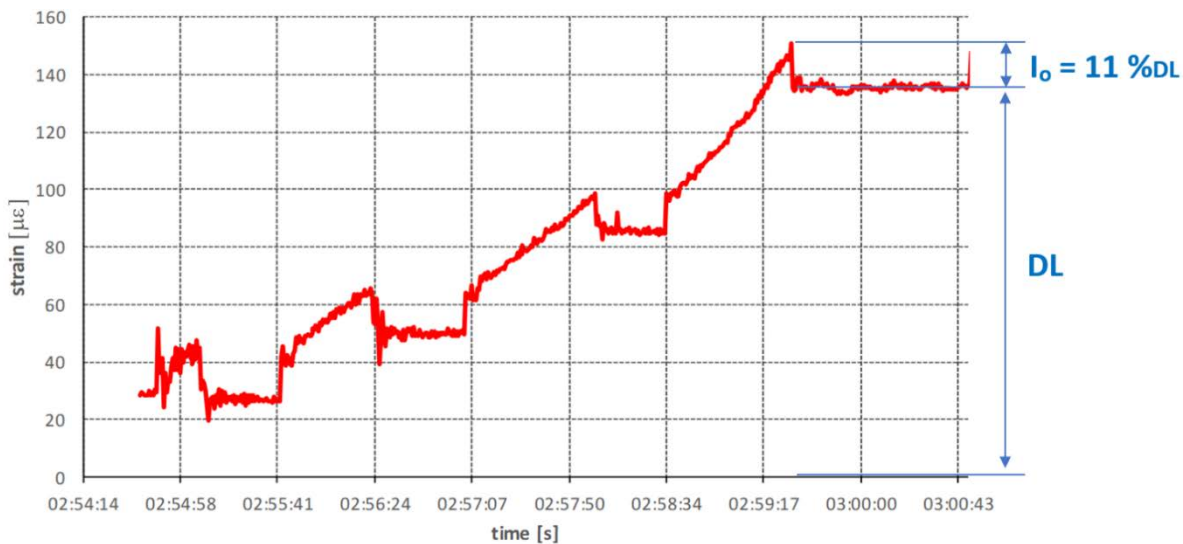


Figure 15 - Strains on inner face of member 15-17 during Scenario 6 with maximal impact factor recorded

However, it should be noted that this measured value could change to some extent with the data acquisition frequency. High variability in the recorded strains was found in some gauges, in particular during regular stops and emergency stops. Considering the uncertainty of any in situ test and taking the measurement error into consideration, the maximal value may be higher. Therefore, we recommend adopting the operating impact factor value recommended by the CHBDC for the structural evaluation.

However, as discussed in subsequent sections, the influence of the impact factor was found to be lower than expected on the forces in the members and on the stresses in the gusset plates. Indeed, both wind load ( $W_0$ ) and operation of machinery load ( $M_0$ ) are more significant than the operating impact load. Therefore, we believe there is no need to further analyses the data nor perform any other tests or measurements as any adjustment of the value of the operating impact factor would not change the findings of the structural evaluation.

#### 4.1.2 VALIDATION OF STRUCTURAL ANALYSIS MODELS

Strains measured during the in-situ testing were compared to the expected strains that were calculated from the global bridge models developed for each of the five bridge positions, i.e. closed, open to  $0^\circ$ ,  $21^\circ$ ,  $42^\circ$ , and  $63^\circ$  positions. During the testing, the regular and emergency stops were applied so that span stopped approximately at these positions. Although it was not possible to achieve the exact same angles each time, it was still very close.

Strain data was analyzed and different comparisons between the measured and expected values were done. These comparisons have shown that the global models on which this evaluation is based are considerably close to the results of the test. The following figures show the comparisons for the results that are the closest. The highest differences between test results and models were found to be just under 20%. As an example, for the connecting members, Figure 16 shows the comparison in strains for the diagonal 13-16 during lift 6.

It should be noted that the comparison can only be done for a difference in strains in relation to the closed position, and not for the total strain measured. Indeed, the gauges were installed when the bridge was closed, and the measured strain gives only the strain difference between the open position and the closed one. At  $42^\circ$  for example, measured strain is approximately  $375 \mu\text{m/m}$ , which would be equivalent to an axial tensile stress of roughly 80 MPa in the member under dead load. However, this member is in compression at the closed position and then goes into tension when the bridge is lifted. Therefore, the 80 MPa recorded corresponds to the addition of the tensile stress at  $42^\circ$  and the compressive stress



at closed position, which means that at 42° the diagonal sees a much lower axial tensile stress than 80 MPa under dead load.

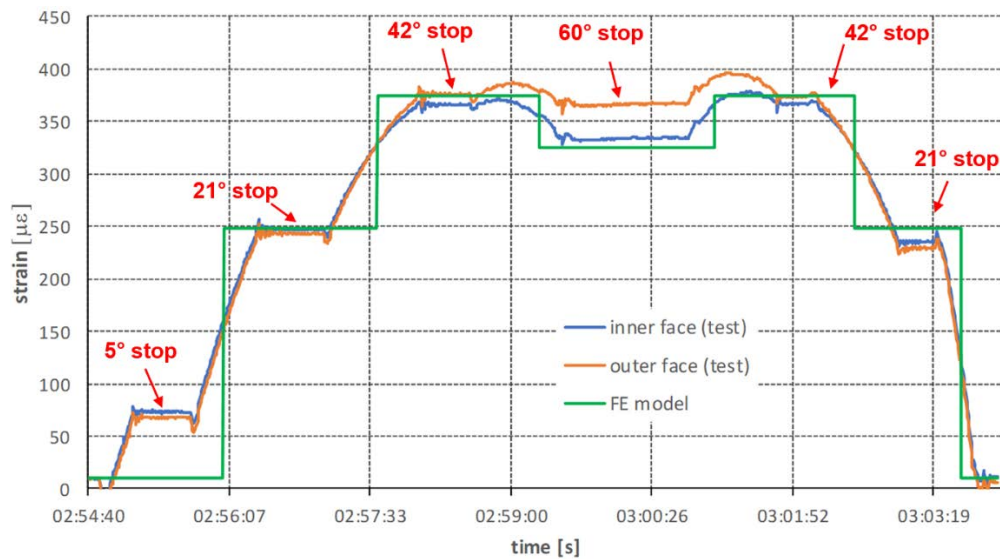


Figure 16 - Strains on diagonal 13-16 during Scenario 6 compared to global bridge model results

Figure 17 presents a comparison for the tri-axial gauge shown in Figure 14 (b). This gauge was placed on the north exterior gusset plate. Measured strains were converted in *von Mises* stresses and then compared to the results of the localized 2D model (FE model) in which the dead loads coming from each connecting member were applied for each bridge position. These dead loads were obtained with the global bridge models for each different position before being integrated into the 2D model.

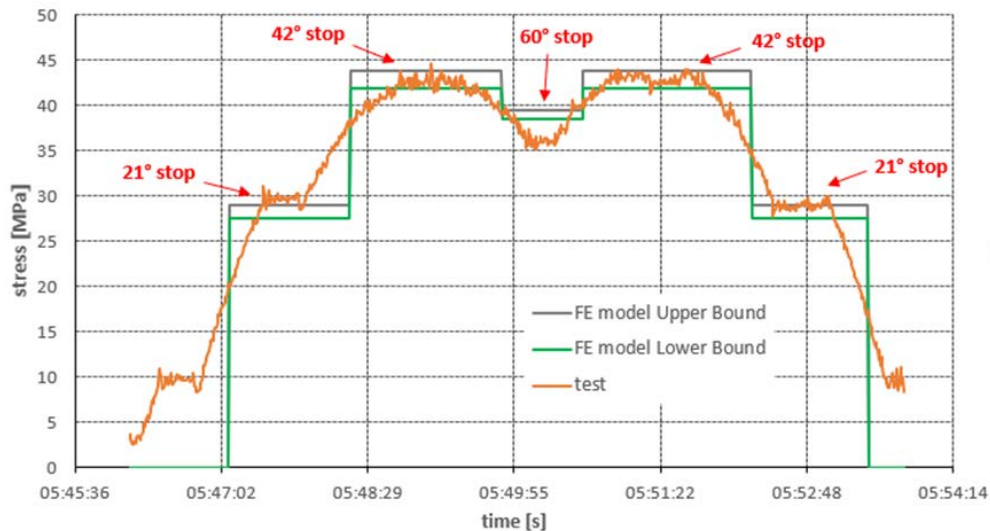


Figure 17 - *von Mises* stresses on north exterior gusset plate during Scenario 6 compared to localized 2D model results

This comparison shows that the stresses obtained at the same position in the gusset plate are very close. The 2D model considering an upper bound stiffness for the fasteners seems to give even better results. This allows us to say that the finite element models are representative of the bridge behavior as observed during the testing.



### 4.1.3 TESTING VARIABILITY

As already mentioned, lifts 3, 4 and 5 are repetitions of the same lift scenario to determine a possible variability of the test. First, it should be noted that all the stops planned for the test could not be carried out automatically, but manually by the operator. There is then a certain variability between the lifts because the stopping angles were not exactly the same for each repetition. However, it was observed that these inaccuracies of human origin were the only source of error in the test. In addition, since the stop angles were known, it was possible to exclude the measurements too far from the planned angle.

For example, Figure 18 shows the strain measurements on bottom chord (13N-16N) during lifts 3, 4 and 5. Stops planned at 21° and 42° are highlighted. On the one hand, it can be noted that when the stop angles are sufficiently close, the strain measurements are practically identical. On the other hand, for the stop at 18° during lift 3, which was the furthest during the whole test from the planned angle (21°), we can notice that the difference with the equivalent readings is about 10%. However, this difference between the stop angle and the planned angle is known, it is therefore possible to discard this reading.

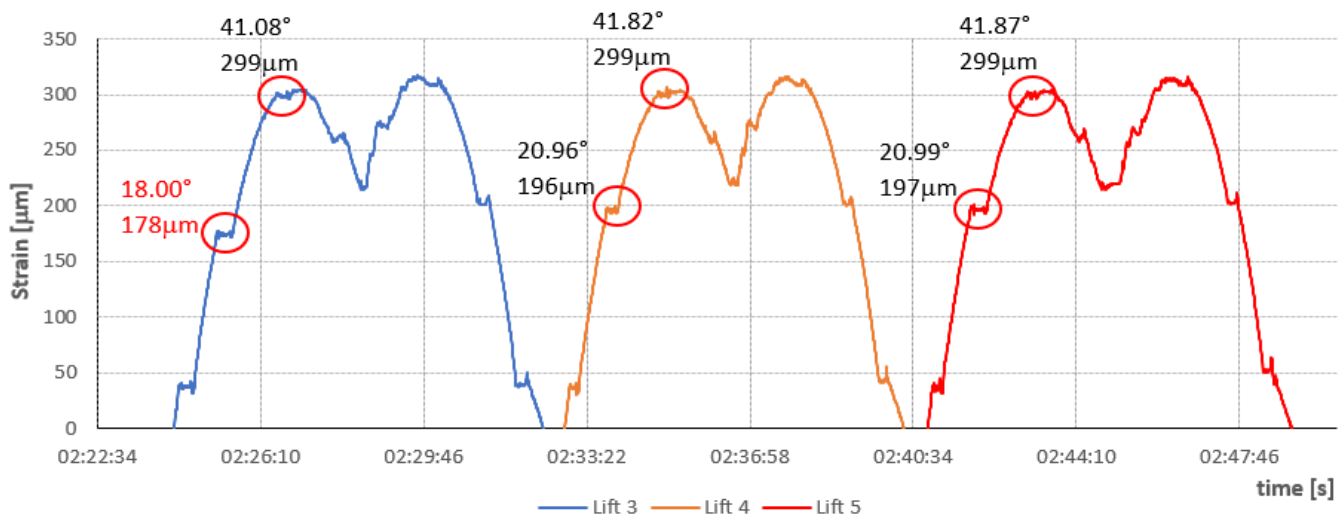


Figure 18 - Strain measurements on bottom chord (13N-16N) during lifts 3, 4 and 5

## 4.2 Connecting Members of the Main Trunnion Assemblies

Table 7 presents the calculated Demand over Capacity (D/C) ratios for the load combinations defined in Section 3.2. In the closed position, when vehicle traffic is allowed on the bridge, all the members evaluated are found to have adequate capacity (i.e. D/C < 1,0). However, when the bridge is in the open position, almost all the members evaluated are found to be inadequate by a significant margin.

A close look at the detailed results shows that the wind load ( $W_0$ ) is clearly the most predominant load case for the trunnion main plates and their connecting members. Since it is acknowledged that PSPC does not currently operate the bridge in high winds, design exception to the code could be considered to limit the extent of the strengthening. For reference purposes only, the last column of Table 7 presents the D/C ratios that have been determined by reducing the wind load ( $W_0$ ) by a factor of 2 as well as using a reduced machinery force ( $M_0$ ) as discussed in Section 3.1.6 (corresponding to Level 2). This does not suggest that we recommend using these specific values or any other deviations to the code, it is only provided to give some insights to the owner on how such an exception would affect the result.

If such an approach is used, a limiting operating wind speed would need to be determined. The determination of such a limiting operating wind speed would need to consider many factors and could require a dedicated wind speed monitoring equipment installed at the bridge. For example, to reduce the wind pressure by a factor of 2 as suggested in the previous

paragraph, a mean hourly wind speed of 60 km/h at a standard anemometer height of 10 m would need to be respected. A wind specialist could help determine how frequent and how long these shutdowns would be required if such a limiting wind speed is adopted based on the historical data. It could also provide some insight on the most predominant wind directions and how this relates to the structural evaluation, which could help us reduce as much as possible the down times (i.e. a longitudinal wind is less critical than a transverse wind).

As part of the recent motor and drive rehabilitation project, a similar approach was implemented (see Appendix D). It was determined that the existing prime mover (i.e. motor system) was overloaded by a factor of 1.50 from the wind loads. Moreover, it was determined that this existing machinery components were appropriately sized for the existing prime mover. However, there was little reserve capacity in the existing gears and therefore increasing the capacity of the prime mover as part of the motor and drive replacement project was not possible unless the scope of the replacement work was increased to include virtually all the existing gearing. Therefore, a reduced wind pressure corresponding to the maximum permissible wind pressure was recommended in 2017, but we are unsure if this is currently implemented as part as the bridge operations.

Finally, AASHTO LRFD [4] states that when the movable span is normally left in the closed position (similar to LaSalle Causeway Bascule Bridge), the open position can be evaluated for a load combination using only 60 percent of the reference wind pressure.

Table 7 - D/C ratios of the connecting members (including deterioration)

Member	Failure mode	Load combinations per CHBDC		Deviation from CHBDC (limited to 60 km/h winds)
		ULS 1	ULS B1 to B4	ULS B1 to B4
DIAGONALS (MEMBER 13-16)	TENSION INTERACTION	0.58	1.64	1.26
	COMPRESSION INTERACTION	0.71	1.10	0.54
BOTTOM CHORDS (MEMBER 14-16)	TENSION INTERACTION	0.74	0.84	0.44
	COMPRESSION INTERACTION	0.51	2.11	1.68
STRUTS (MEMBER 14-15)	TENSION INTERACTION	N/A	1.06	0.59
	COMPRESSION INTERACTION	0.77	1.87	1.26
FIXED DIAGONALS (MEMBER 15-17)	TENSION INTERACTION	N/A	N/A	N/A
	COMPRESSION INTERACTION	0.71	1.62	1.33
TIES (MEMBER 15-18)	TENSION INTERACTION	0.17	1.00	0.59
	COMPRESSION INTERACTION	N/A	0.90	0.37
POSTS (AT NODE 15)	TENSION INTERACTION	N/A	0.76	0.34
	COMPRESSION INTERACTION	0.19	0.81	0.44

The governing case for all the D/C ratios presented in Table 7 is for the interaction between the axial force and the bending moments. When the load combinations are applied according to the CHBDC, the governing load combination is either ULS B2 or ULS B3. The D/C ratio of member 14-16 exceeds 2,0 at the location where this member intersects member 14-15. As shown in Figure 19, the two channels of 14-16 are considered laterally unsupported over a length of approximately 2.2 m as the top cover plate is interrupted to allow the passage of member 14-15. The buckling resistance of an individual

channel reduces significantly the resistance of the entire section. If the outward buckling of a single channel would be restricted, the D/C ratio of this specific member would be 1.65 instead of 2.11.



Figure 19 - Intersection between members 14-15 and 14-16

Moreover, the lacing was verified for members 13-16, 15-17 and 15-18. For member 13-16, it was found that the lacing rivets are overstressed and would need to be replaced by bolts. The lacing of 15-17 was found to be inadequate for both the rivets and the lacing compressive capacity, whereas the lacing of 15-18 was found to be acceptable.

The number of members requiring strengthening does not reduce if we consider the suggested deviation from the CHBDC requirements, but the D/C ratios have reduced significantly. Table 7 does not reflect this well, but the extent of the strengthening would be much less with the latter case.

### 4.3 Gusset Plates and Fasteners

From the main localized 2D model presented in section 3.4.2, various versions were made and analyzed in order to study the influence of specific parameters on the results. This section describes the different analyses that were done and presents the associated results for the gusset plates and the fasteners of the main trunnion assemblies.

The loads applied on the 2D models were obtained from the global bridge models. Only concurrent forces in the connecting members were used for the different bridge positions (closed and open at 0°, 21°, 42° and 63° angles). Forces are also differentiated depending on the side of the bridge (north/south) to consider the imbalance between the trusses. Analyses considered the undeteriorated state and the actual deterioration of the four gusset plates.

#### 4.3.1 INFLUENCE OF FASTENER STIFFNESS

In the 2015 MMM evaluation [1], two cases were considered in the analyses to consider the flexibility of the fasteners. In design, it is generally assumed that all fasteners connecting a member to the gusset carry an equal share of the load, i.e. a uniform force distribution is considered. However, in these main trunnion assemblies, it may be possible to have a non-uniform force distribution, because of the long-riveted connections, the high numbers of rivets and the complex pattern of forces that goes through the gusset. Therefore, two cases, i.e. non-uniform and uniform force distribution, have been considered.

The first case is an upper bound case in which the fastener stiffnesses have been calculated using the equation proposed by Huth. This equation predicts a certain stiffness for each group of fasteners, depending on the type of the connection

(riveted, bolted), the plate thicknesses and the diameter of the fasteners. In this upper bound case, the force distribution in a group of fasteners is non-uniform, and it is expected that the fasteners located first in a row transmit the most shear force. The second case is a lower bound case in which a very small stiffness has been used for the flexibility of the fasteners. In this case, the expected force distribution in a group of fasteners is uniform, and therefore all fasteners transmit the same shear force.

#### 4.3.1.1 Stresses in the Gusset Plates

As noted in the previous evaluation, the stiffness of the fasteners considered in the model influences the distribution of the stresses in the gusset plate. The previous evaluation used a model in which the collar plate was modeled separately, and it seems that the gusset plate thickness around the pin was increased to consider the presence of the interior plate. In this evaluation, a more refined model has been done to model the collar, the gusset and the interior plates separately in order to better capture stress distribution in the gusset plate area located between the pin and the end of the strut 14-15.

Figure 20 and Figure 21 show a comparison of the *von Mises* stresses in the gusset plate obtained with both upper and lower bound fastener flexibility cases. In Figure 19, results are shown for concurrent force case in the connecting members where the strut 14-15 is in maximal compression at a 0-degree opening angle. Figure 21 shows the concurrent force case in which the diagonal 13-16 is in maximal tension at a 42-degree opening angle. Stress areas in blue are where the gusset plate reaches yielding (including a resistance factor of 0.90).

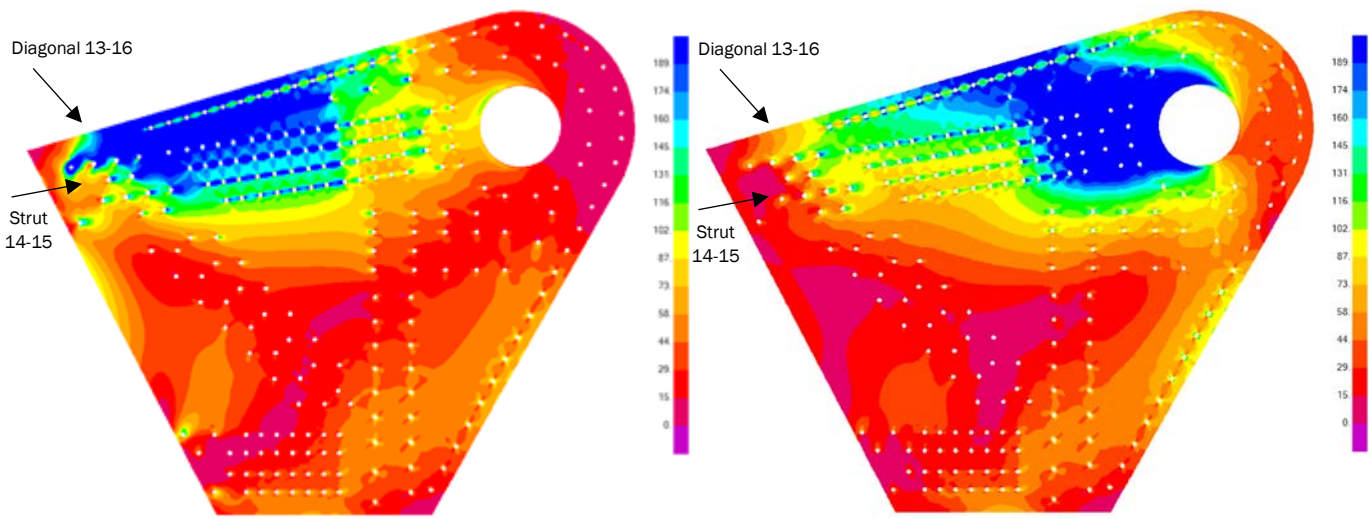


Figure 20 - *von Mises* stresses at undeteriorated state for maximum compression in strut 14-15 (ULS B2)  
 (a) Left: Upper bound case (b) Right: Lower bound case

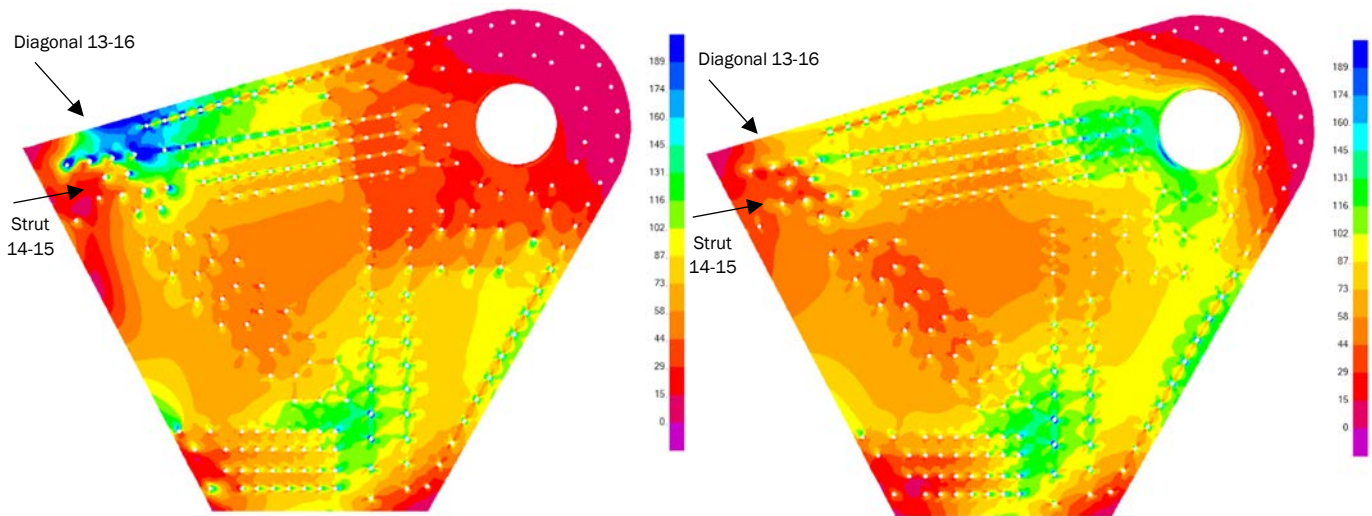


Figure 21 - von Mises stresses at undeteriorated state for maximum tension in diagonal 13-16 (ULS B2)  
(a) Left: Upper bound case (b) Right: Lower bound case

As expected, a different stress distribution occurs because of the fastener stiffness. For the two upper bound cases, forces coming from the connecting members (strut 14-15 and diagonal 13-16 in the cases shown in particular) are mainly transmitted by the first rivets and therefore, the gusset plate presents higher stresses in these areas. For the two lower bound cases, stresses are higher at the end of the connections of the connecting members. However, in the lower bound case it was found that no force goes through the fasteners that connect the collar, the interior and the gusset plates around the pin, because the fastener stiffness is very low. Therefore, stresses in the gusset plate are much higher around the pin. In our opinion, it is too conservative (regarding the stresses in the gusset plate) to consider that both collar and interior plates take no force. Therefore, this lower bound case should not be used to evaluate the stresses in the vicinity of the collar plate but can be still useful to evaluate the stresses in other parts of the gusset and the forces in the fasteners.

In order to better evaluate the stresses in the area between the strut end and the pin, an intermediate and more realistic case was analyzed. In this case, the fasteners connecting the collar, interior and gusset plates have been considered semi-flexible (stiffness calculated using the Huth equation like in the upper bound case) while all other fasteners have been considered infinitely flexible (with very small stiffness equal to the lower bound case). Figure 22 and Figure 23 show the stresses in the gusset plate obtained with this modified fastener stiffness distribution. This distribution will be designated as *modified lower bound fastener stiffness* later in this report. As expected, stresses are lower in the gusset plate at the end of the strut 14-15 than compared to the lower bound case, because both collar and interior plates take some forces transmitted by the rivets.



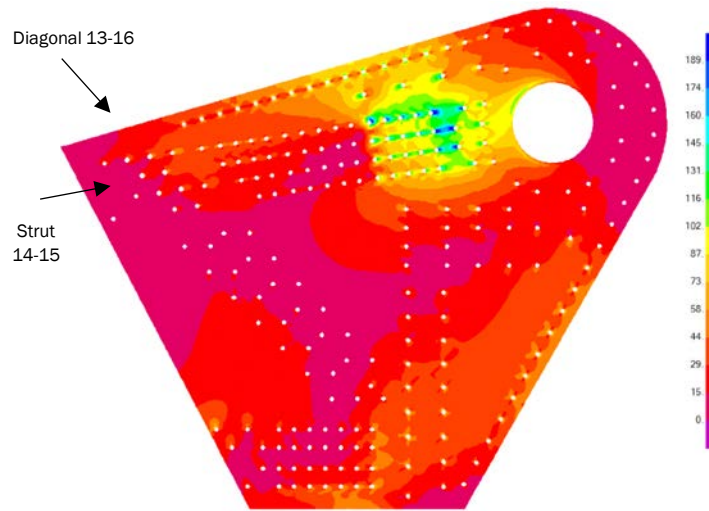


Figure 22 - *von Mises* stresses at undeteriorated state for maximum compression in strut 14-15 (ULS B2) with modified lower bound fastener stiffness

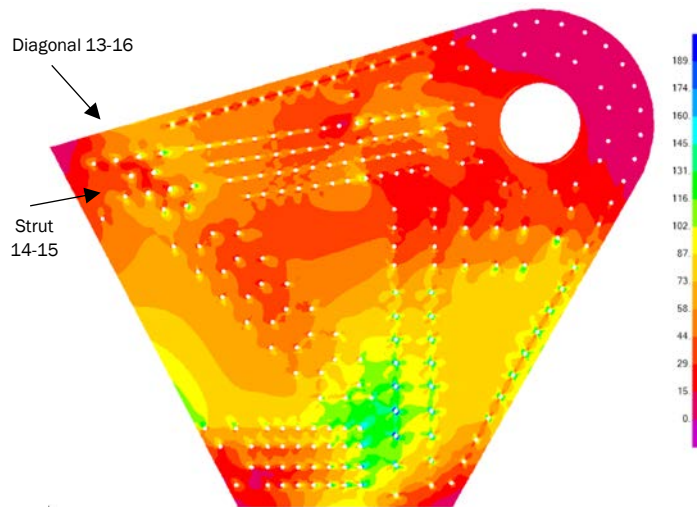


Figure 23 - *von Mises* stresses at undeteriorated state for maximum tension in diagonal 13-16 (ULS B2) with modified lower bound fastener stiffness

#### 4.3.1.2 Forces in the Fasteners

Regarding the forces obtained in the fasteners, it was found as expected that, in the upper bound stiffness case, the force coming from the connecting members is mostly transmitted by the first rows of fasteners encountered. Therefore, shear forces are much higher in these fasteners and their resistance is more likely to be exceeded. In the case of the lower bound stiffness, the results show that the forces are uniformly distributed in all the fasteners of a same assembly and therefore the maximal shear forces are lower than the ones obtained with the upper bound case.

To compare the influence of the force distribution on the results, Figure 24 and Figure 25 show the fasteners with insufficient shear resistance in red color. Left figures are when the bridge is an open position (ULS B1 to ULS B3) and right figures are for ULS 1 when the bridge is closed.



Figure 24 - Fasteners with insufficient shear resistance at undeteriorated state for upper bound fastener stiffness  
 (a) Left: ULS B1 to ULS B3 (b) Right: ULS 1

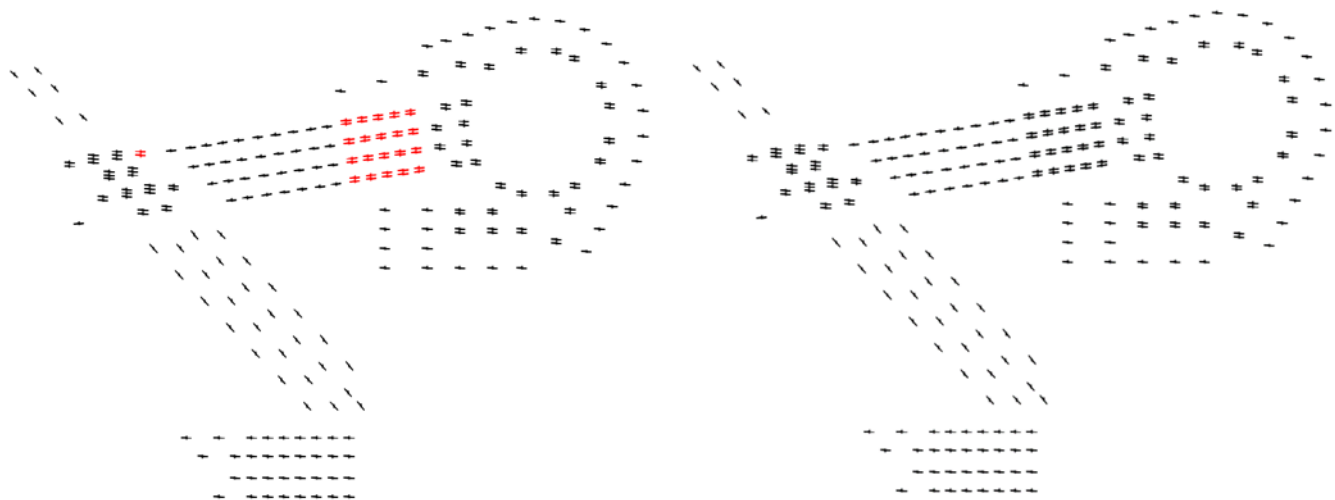


Figure 25 - Fasteners with insufficient shear resistance at undeteriorated state for lower bound fastener stiffness  
 (a) Left: ULS B1 to ULS B3 (b) Right: ULS 1

As shown in these two figures, more fasteners have an exceeded resistance with a non-uniform force distribution (upper bound case). For this case however, it should be noted that other fasteners next to the ones in red may also have an exceeded resistance. As linear analyses were performed, force redistribution in a same group of fasteners was not carried out and redistribution during strain-hardening wasn't captured. Therefore, if one would look to replace overloaded rivets by bolts in the design phase, we recommend using nonlinear analyses to consider force redistribution in the fasteners with this upper bound case.

From the uniform force distribution case, two connections appears to be a concern: the connection that assembles the strut 14-15, the diagonal 13-16 and the gusset plate (zones 3 and 4 shown in Figure 12 (b)) and the connection at the end of the strut 14-15 that assembles together the strut, the gusset and the collar plate (zone 7 shown in Figure 12 (b)). It is likely that the rivets in these two connections will need to be replaced by bolts. However, it should be noted that these results are for the most conservative case, i.e. with the loads taken according to the CHBDC (with  $M_0$  level 3). For the

second connection, for example, the shear resistance is slightly exceeded (D/C ratio is 1.1). Therefore, replacement of the rivets may be avoided if the loads considered during bridge operation are reduced.

#### 4.3.2 INFLUENCE OF THE OPERATING IMPACT ( $I_0$ )

The operating impact ( $I_0$ ) has to be taken into account in the three special load combinations ULS B1 to ULS B3 used to evaluate the gusset plates when the bridge is in an open position. Its effect on the stresses in the gusset plate has been studied using two limit cases.

The first case considers an operating impact as per the CHBDC, i.e. equals to 20% of the dead load effect. This effect is supposedly the maximum that will occur and therefore constitutes an upper bound limit. To compare its importance, a second case has been analyzed in which the operating impact has not been considered in the three special load combinations. This later case constitutes a lower bound limit.

Figure 26 shows the stresses in the gusset plate for these two cases.

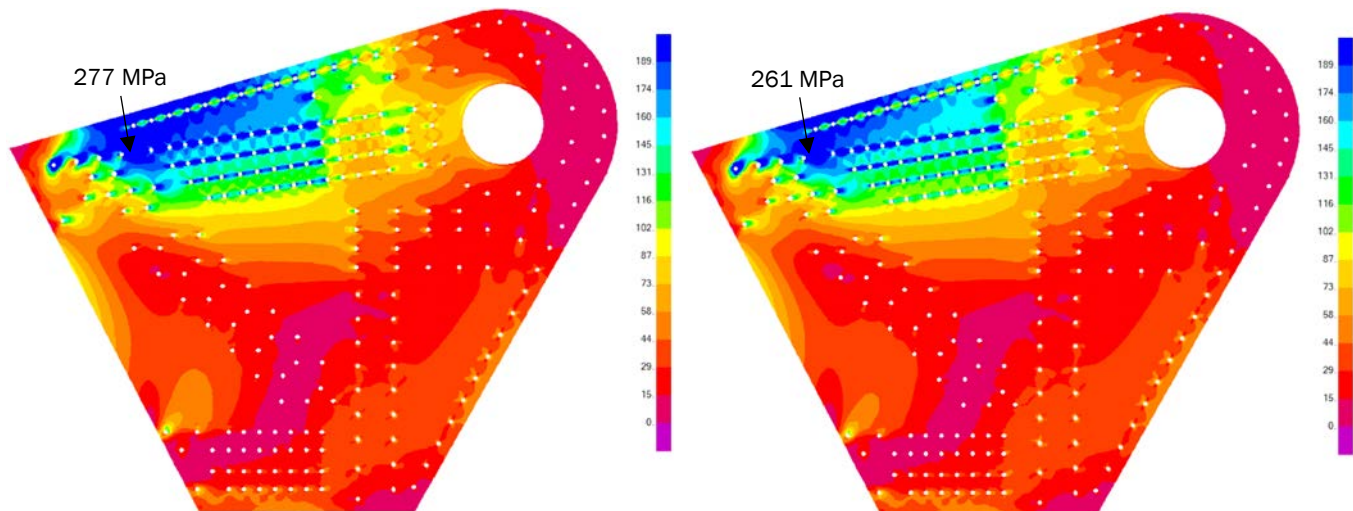


Figure 26 - *von Mises* stresses at undeteriorated state for maximal compression in strut 14-15 (ULS B3)  
 (a) Left:  $I_0$  taken as per S6-14 (b) Right:  $I_0$  taken as zero

Comparing both figures, it was found that the influence of the operating impact is quite low on the stresses in the gusset plate. In the most stressed region, the difference between both cases is 16 MPa in *von Mises* stress, which represents only 9% of the factored yield stress.

Moreover, the case in which  $I_0$  has not been considered (Figure 26 (b)) shows that stresses are high, and yielding is expected regardless of the value that is taken for  $I_0$ . Therefore, we believe that, for the gusset plate, it's not relevant to refine further the value of the impact factor, because our understanding and our findings will not change significantly.

Considering these results, it appears that other parameters come into play and influence the stresses in the gusset plates more than the operating impact. The following sections will present the results of the analyses that have been done in order to improve our understanding and will show that other factors have greater influence on the stresses.

#### 4.3.3 INFLUENCE OF LOADS CAUSED BY THE OPERATION OF MACHINERY ( $M_0$ )

The loads caused by the operation of machinery ( $M_0$ ) are considered in special load combinations ULS B1 and ULS B2. As discussed in Section 3.1.6, this load may present high variability depending on the context during the lifting operation. Two limit cases were analyzed to study the effect of  $M_0$  on the gusset plates. Figure 26 shows the result of this analysis.

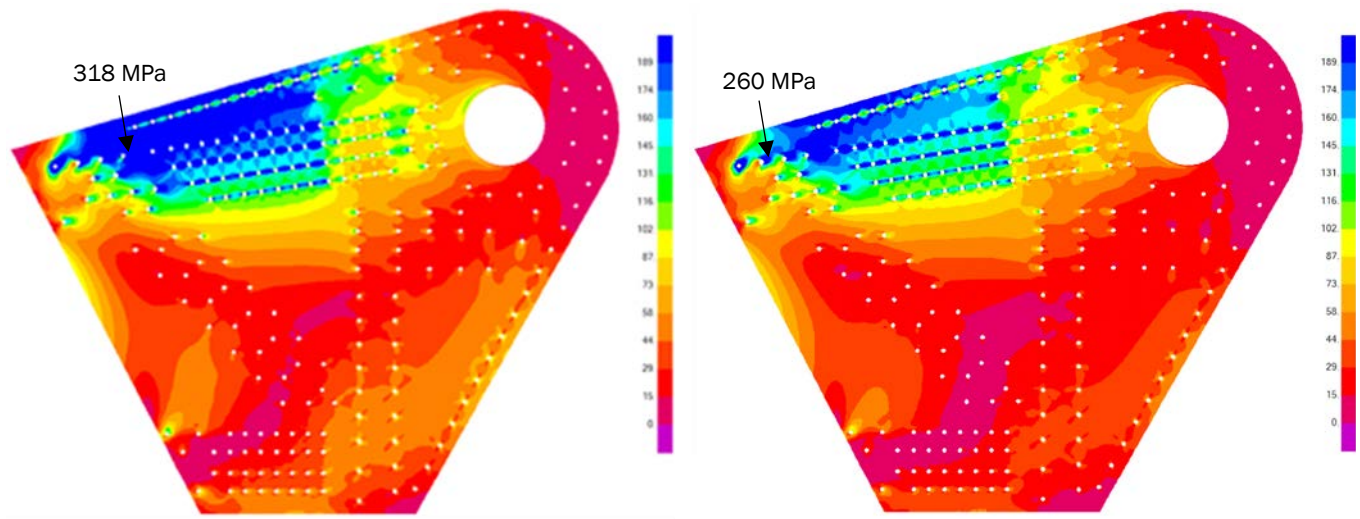


Figure 27 - *von Mises* stresses at undeteriorated state for maximal compression in strut 14-15 (ULS B2)  
 (a) Left: with  $M_0$  level 3 (b) Right: with  $M_0$  level 1

In Figure 27 (a), a value of 512 kN has been taken for  $M_0$ , corresponding to Level 3 indicated in Table 1. In Figure 26 (b), a value of 98 kN has been considered for  $M_0$ , corresponding to the Level 1. The overall difference in stresses between the two cases is small; in terms of *von Mises* stresses, the difference is 58 MPa in the most stressed region, which represents 31% of the factored yield stress.

Moreover, depending on the value for  $M_0$  considered in the analysis of the bridge, the governing load combination can change for the gusset plates. When  $M_0$  is equal or less than Level 1 it was found that ULS B3 is the governing load combination, while when  $M_0$  is equal to Level 3, combination ULS B2 controls with all other parameters remaining unchanged. When Level 2 is considered for  $M_0$ , ULS B2 stresses becomes equivalent to ULS B3 stresses. This means that refining the loads to reduce the stresses in the gusset plates, there is no clear benefit to reduce  $M_0$  beyond Level 2, because combination ULS B3 will then govern and  $M_0$  is not part of ULS B3.

These results show that the loads caused by the operation of machinery have a much greater influence than the operating impact ( $I_0$ ) on the stresses in the gusset plates. Moreover, it shows that the value that will be taken for  $M_0$  can influence the extent of the strengthening for the gusset plates.

#### 4.3.4 INFLUENCE OF WIND LOAD ( $W_0$ )

To evaluate the importance of the wind load on the stresses of the gusset plate, a case including only the unfactored  $W_0$  load was analyzed. For this case, wind load was taken as specified by CHBDC Cl.13.6.4.9, i.e. a wind pressure of 1.50 kPa. Figure 28 shows the stresses caused by the unfactored  $W_0$  load. For comparison, Figure 29 shows the stresses due to unfactored dead loads and to unfactored  $M_0$  Level 3 for the most critical bridge open position (0 degree opening). These results show that  $W_0$  causes the highest stresses in the gusset plates compared to other special load cases. Moreover, stresses shown are unfactored, which means that in special load combinations ULS B2 and ULS B3, the influence of  $W_0$  is even more important because factors on  $W_0$  are the highest.

Although *von Mises* stresses cannot be combined linearly, we expect that in the ULS B2 load combination, the factored  $W_0$  load case represents approximately between 40% and 50% of the total stresses, while in ULS B3, it represents between 60 and 70%. Therefore,  $W_0$  has a major influence on the stresses in the gusset plate.



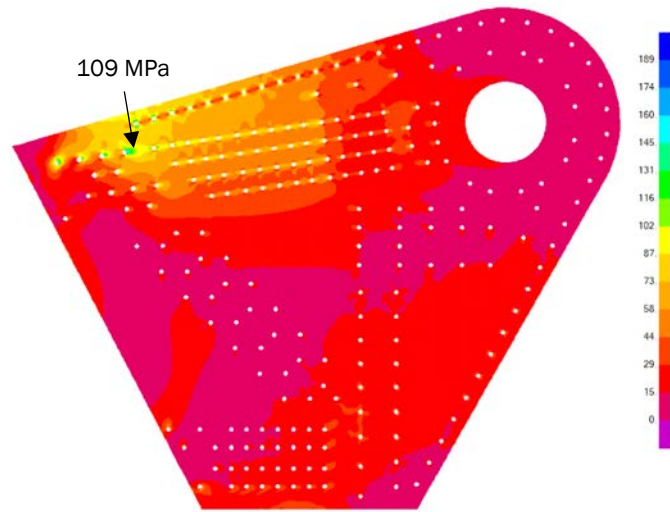


Figure 28 - *von Mises* stresses at undeteriorated state caused by unfactored  $W_0$

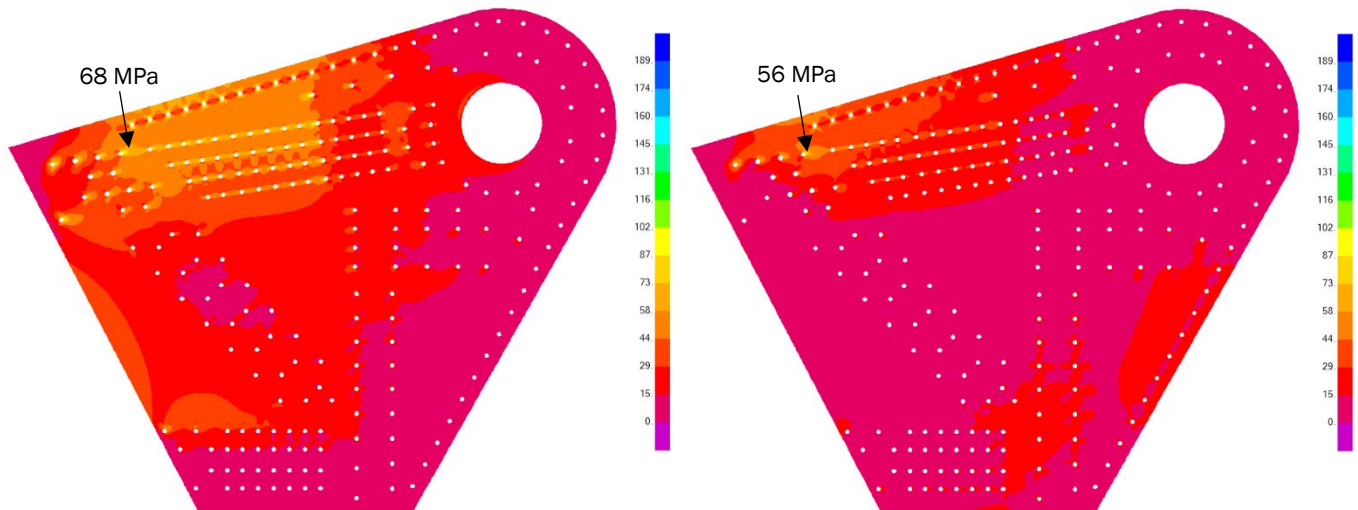


Figure 29 - *von Mises* stresses at undeteriorated state caused by  
 (a) Left: unfactored dead loads (b) Right: unfactored  $M_0$  level 3

The high wind pressure used according to the CHBDC explains why the stresses obtained in the gusset plates are so high when the bridge is open. In our opinion, refining and limiting the operation of the bridge under high wind loads would significantly reduce the stresses in the gusset plates and probably limit the extent of the strengthening required.

As an indication, Figure 30 presents the results for a reduced pressure wind of 0.75 kPa, corresponding roughly to a wind speed of 60 km/h.



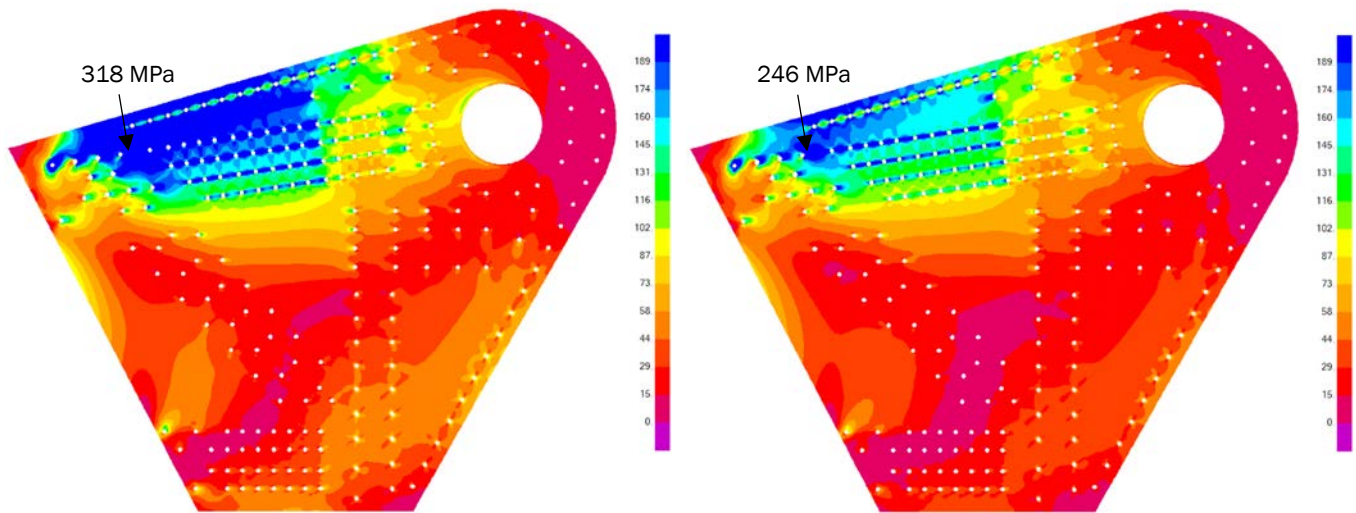


Figure 30 - *von Mises* stresses at undeteriorated state for maximal compression in strut 14-15 (ULS B2)  
 (a) Left: with  $W_0$  according to S6-14 (1.5 kPa) (b) Right: with reduced  $W_0$  (0.75 kPa)

Figure 30 (b) shows a stress reduction of 72 MPa in terms of *von Mises* stress in the critical area for the governing and most conservative case (with upper bound fastener stiffness, strut 14-15 in maximal compression at a 0-degree opening angle, impact load  $I_0$  taken as per S6-14 and  $M_0$  level 3). The yielding area becomes more localized and local redistribution would take place in the gusset plate. Furthermore, it should be noted that at the top edge of the gusset plate, an angle is riveted on the exterior side. As this angle is not taken into account in the 2D model, stresses on the edge are on the conservative side.

These results clearly show that by imposing a lower wind speed limit to operate the bridge, the strengthening requirements for the gusset plates would be greatly reduced.

#### 4.3.5 INFLUENCE OF DETERIORATION

In an undeteriorated state, the critical location in the gusset plate is adjacent to the crossing area between the strut 14-15 and the diagonal 13-16 as shown previously in Figure 20, Figure 26, and Figure 30. These high stresses appear when the strut is in maximal compression with the diagonal also in compression, which happens to be at the 0-degree position.

When considering deterioration in the trunnion plates, it is possible that other regions become more stressed because of the reduction in the plate thickness. First, we checked the influence of the triangle plates welded on both interior gusset plates in 2009. Then, we considered the actual deterioration of the plates based on the latest field measurements.

It should be noted that the deterioration was taken into account in the finite element model by modifying the thickness of the plate elements in the affected regions.

##### 4.3.5.1 Influence of the Triangular Reinforcement Plate

In 2009, a triangular reinforcement plate was welded onto the interior gusset plates because of severe section loss due to corrosion. To evaluate the influence of these reinforcement plates, the interior gusset plate of the south trunnion was considered, as it is the most deteriorated and takes slightly more loads than the north side.

First, the reinforcement plate was neglected, and the gusset plate was analyzed with a hole instead. Figure 31 shows the result of this analysis for the case of concurrent forces in the connecting members that causes the most stresses around the cut-out. It appears that the stresses rise significantly around this hole, i.e. between the diagonal 13-16 and the bottom

chord 14-16. This behavior is consistent with previous evaluation done by MMM in 2015, in which the triangle reinforcement plate has been neglected. However, it appears too conservative to neglect it.

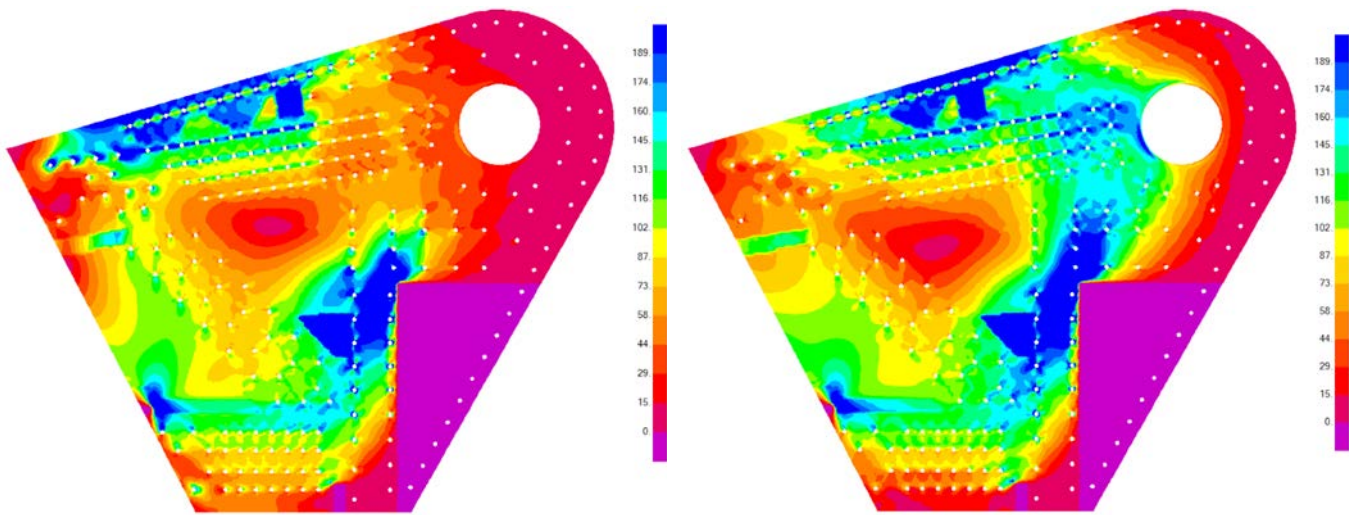


Figure 31 - *von Mises* stresses for maximal tension in diagonal 13-16 (ULS B2) in south interior gusset plate without triangle reinforcement plate  
 (a) Left: Upper bound fastener stiffness (b) Right: Lower bound fastener stiffness

It is not possible to take into account the reinforcement plate in the FEM analysis, because linear elastic analyses are done. To evaluate precisely the stresses in and around the reinforcement plates, the effect of construction phasing has to be considered and a non-linear analysis has to be done. However, a simpler method, using the superposition principle, can be used to consider construction phasing and roughly evaluate these stresses. The assumptions are the following:

- All locked-in stresses due to welding are neglected;
- There is a perfect strain compatibility between both gusset and reinforcement plates;
- The triangle reinforcement plate was welded when the bridge was in a closed position;
- When the bridge is in the closed position, the dead load is taken by the remaining section of the gusset plate and no dead load is taken by the triangular reinforcement plate;
- When the bridge is in the closed position, the live load is taken by both gusset and reinforcement plates; and
- When the bridge is open, the exterior loads (wind, impact, etc.) and the variation of dead load due to the opening angle is taken by both gusset and reinforcement plates.

Two different models have been used and analyzed: in Model A, the gusset plate has a hole instead of the reinforcement and in Model B, the gusset plate is continuous. Model A represents the state before the welding of the reinforcement plate, so it is used to have the factored dead loads in the critical region around the hole when the bridge is closed. Model B represents the state after the welding of the reinforcement plate (gusset plate thickness increased to 19 mm in the triangle to consider the reinforcement plate). Therefore, to have an approximation of the stresses in the critical region around the hole when the bridge is open, the stresses due to special load combinations ULS B1 to ULS B3 (obtained from Model B) were linearly added to the stresses due only to dead loads when the bridge is closed (obtained from Model A). The linear superposition was done only for the local stresses obtained with both models. Principal stresses and *von Mises* stresses were calculated after.

Figure 32 shows results obtained with models A and B, in terms of *von Mises* stresses and illustrates the two critical regions that have been checked. Only the upper bound fastener stiffness case, assuming non-uniform force distribution in the fasteners, is shown.

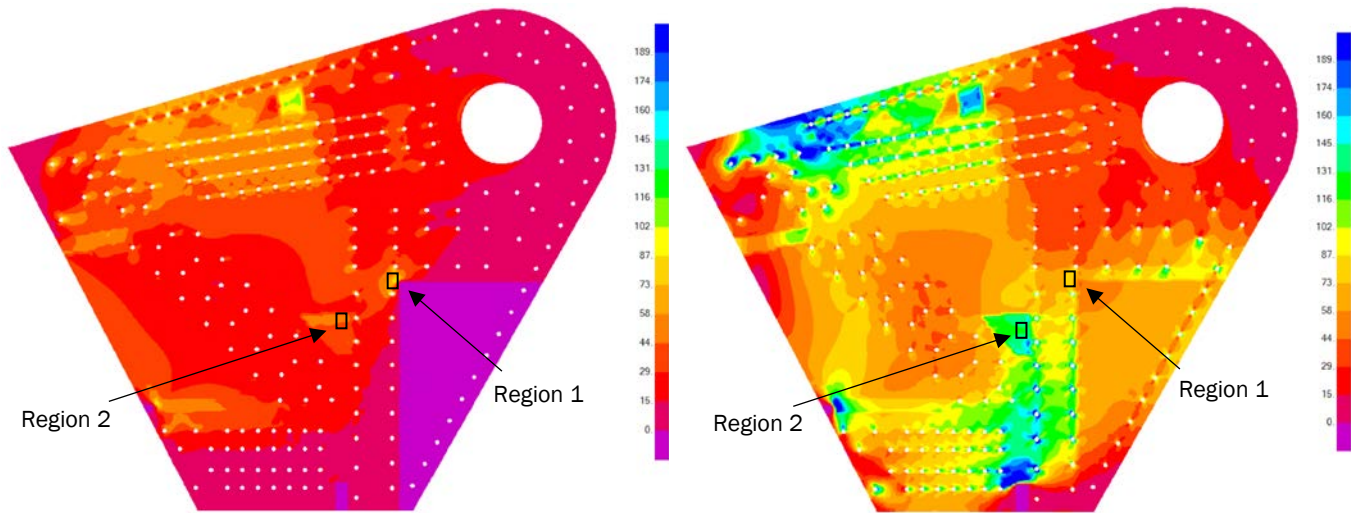


Figure 32 - *von Mises* stresses in south interior gusset plate due to  
 (a) Left: dead loads in model A (b) Right: maximal tension in diagonal 13-16 (ULS B2) in Model B

Table 8 and Table 9 summarize the calculated *von Mises* stresses using linear superposition in the two critical regions around the triangular reinforcement plate (details of the local stresses on which the linear superposition was done are not shown). Table 8 is for the case assuming upper bound fastener stiffness and Table 9 concerns the case with lower bound fastener stiffness.

Table 8 - *von Mises* stresses for maximum tension in diagonal 13-16 (ULS B2) in south interior gusset plate with upper bound fastener stiffness case

	Dead loads in Model A	ULS B2 in Model B	ULS B2 calculated with linear superposition	ULS B2 in Model A <sup>(1)</sup>
REGION 1	69 MPa	66 MPa	122 MPa < 189	436 MPa > 189
REGION 2	46 MPa	133 MPa	178 MPa < 189	280 MPa > 189

(1) Conservative case shown in Figure 30 (a), neglecting the triangular reinforcement plate

Table 9 - *von Mises* stresses for maximum tension in diagonal 13-16 (ULS B2) in south interior gusset plate with lower bound fastener stiffness case

	Dead loads in Model A	ULS B2 in Model B	ULS B2 calculated with linear superposition	ULS B2 in Model A <sup>(1)</sup>
REGION 1	84 MPa	63 MPa	124 MPa < 189	483 MPa > 189
REGION 2	52 MPa	125 MPa	176 MPa < 189	280 MPa > 189

(1) Conservative case shown in Figure 30 (a), neglecting the triangular reinforcement plate

As expected, the stresses are lower when the reinforcement plate is taken into account. These results confirm that it is too conservative to neglect the reinforcement plate to evaluate the stresses in the region located between the reinforcement plate, the diagonal 13-16 and the bottom chord 14-16. Moreover, in our opinion, it shows that this region is not a concern and probably has adequate capacity.

For both interior gusset plates (north and south), it is preferred to model the gusset plate continuously instead of a hole at the triangular plate location. As noted previously, as this evaluation was done with linear analyses, construction phasing has not been considered and results around the reinforcement plate may not be accurate. The stresses around the reinforcement plate are somewhat underestimated and the stresses in the reinforcement plate are overestimated. For this



evaluation, we believe this approximation is acceptable as long as it does not change our findings and conclusions. However, for the strengthening design, it is important to refine the analysis method and consider the construction phasing.

#### 4.3.5.2 Influence of section loss due to corrosion

The residual thicknesses of the gusset plates, which were measured during the field investigation, have been integrated into the analyses. Figure 33 and Figure 34 present the stresses obtained for the interior plate of the south trunnion as an example. The upper bound stiffness is used for the fasteners in both figures.

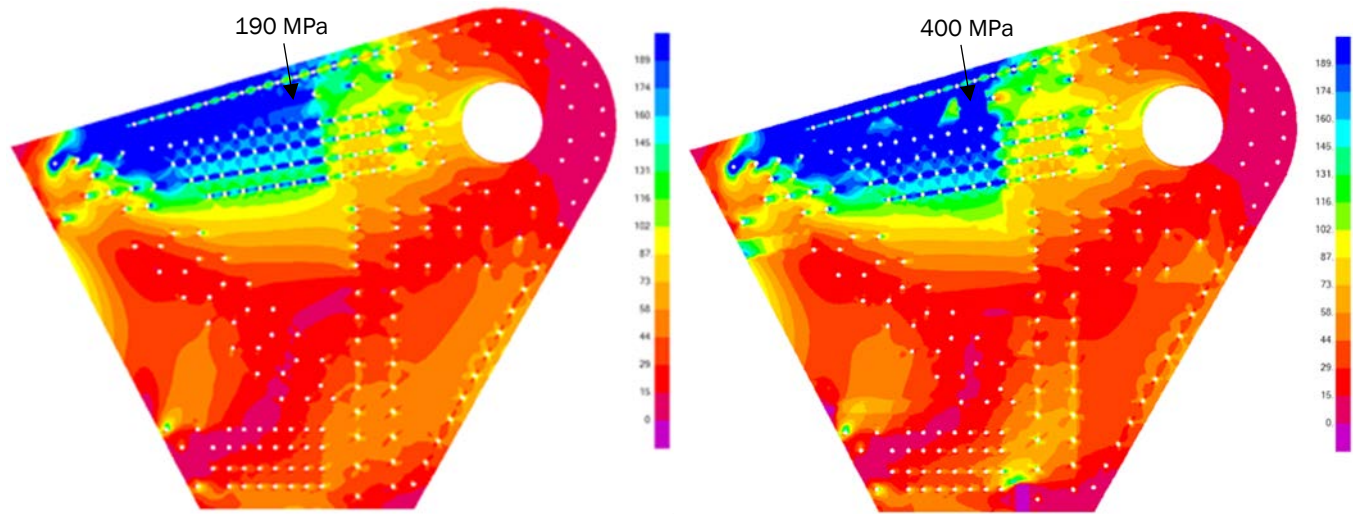


Figure 33 - *von Mises* stresses in south interior gusset plate for maximum compression in strut 14-15 (ULS B2)  
(a) Left: at undeteriorated state (b) Right: with deterioration

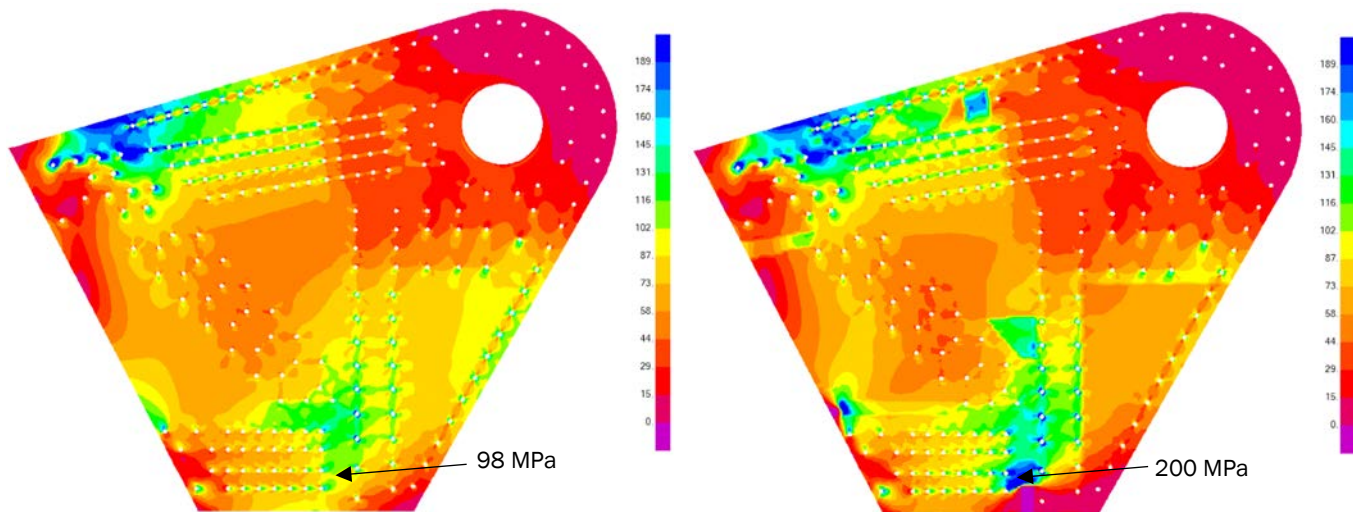


Figure 34 - *von Mises* stresses in south interior gusset plate for maximum tension in diagonal 13-16 (ULS B2)  
(a) Left: at undeteriorated state (b) Right: with deterioration

As expected, integrating the section losses caused a local increase in stresses. As shown in Figure 34, new regions near the bottom chord and the end of the diagonal, where significant section losses are found, become critical and may yield. This load case occurs when the diagonal 13-16 is in maximum tension at a 42-degree opening angle. As these section losses are generalized on all gusset plates, local yielding is expected to occur in this region for the four gusset plates.

#### 4.3.6 SUMMARY OF RESULTS

This section summarizes the findings of the different structural analyses that were carried out to evaluate the gusset plates and the fasteners.

##### 4.3.6.1 Results in accordance with the CHBDC

##### 4.3.6.1.1 At Undeteriorated State

Table 10 shows the results obtained with the 2D model of the main trunnion assemblies. Plates were considered without any deterioration and the loads were applied according to the CHBDC. For special load combinations ULS B1 to ULS B3, critical opening angles were found to be 0° and 42°. Results in green means the resistance is sufficient while results in red means the resistance is exceeded.

Table 10 - Results for gusset plates and fasteners at undeteriorated state in accordance with the CHBDC

Results	Fastener stiffness	Load combination for normal traffic	Special load combinations for bascule bridges		
		ULS1	ULS B1	ULS B2	ULS B3
MAX. <i>VON MISES</i> STRESS IN GUSSET PLATES  $\Phi_s F_y = 189 \text{ MPA}$	LOWER BOUND	185 MPa	250 MPa	372 MPa	338 MPa
	MODIFIED LOWER BOUND	73 MPa	96 MPa	145 MPa	132 MPa
	UPPER BOUND	196 MPa <sup>(1)</sup>	193 MPa <sup>(1)</sup>	318 MPa	277 MPa
	RECOMMENDED	196 MPa <sup>(1)</sup>	193 MPa <sup>(1)</sup>	318 MPa	277 MPa
	<i>VON MISES</i> STRESS / $\Phi_s F_y$	1.04	1.02	1.68	1.47
MAX. RIVET SHEAR FORCE PER SHEAR PLANE  $V_R = 45.5 \text{ KN}$	LOWER BOUND	25 kN	38 kN	52 kN	47 kN
	MODIFIED LOWER BOUND	135 kN	167 kN	268 kN	240 kN
	UPPER BOUND	157 kN	192 kN	310 kN	279 kN
	RECOMMENDED	157 kN	192 kN	310 kN	279 kN
	RIVET SHEAR FORCE / $V_R$	3.45	4.21	6.81	6.13
MAX. BOLT SHEAR FORCE PER SHEAR PLANE  $V_R = 106 \text{ KN}$	LOWER BOUND	27 kN	46 kN	56 kN	55 kN
	MODIFIED LOWER BOUND	27 kN	46 kN	56 kN	55 kN
	UPPER BOUND	84 kN	112 kN	178 kN	162 kN
	RECOMMENDED	84 kN	112 kN	178 kN	162 kN
	BOLT SHEAR FORCE / $V_R$	0.79	1.06	1.68	1.53

(1) Stress at a localized area, redistribution in surrounding material is expected to occur

Figure 34 illustrates the results in accordance with the CHBDC for the gusset plates and fasteners considering an undeteriorated state and an upper bound fastener stiffness. Areas in blue are where yielding (including a resistance factor of 0.9) is expected in the gusset plates according to the analyses and the *von Mises* criterion. These results include both upper and lower bound cases for fastener stiffnesses. Fasteners with insufficient resistance are also indicated. However, as linear analyzes were made, force redistribution in a same group of fasteners was not carried out. Thus, note that other adjacent fasteners could also have exceeded resistance when redistribution occurs. Consequently, this figure has to be interpreted as an indication that the group of fasteners is not adequate, rather than a recommendation for each individual fastener.



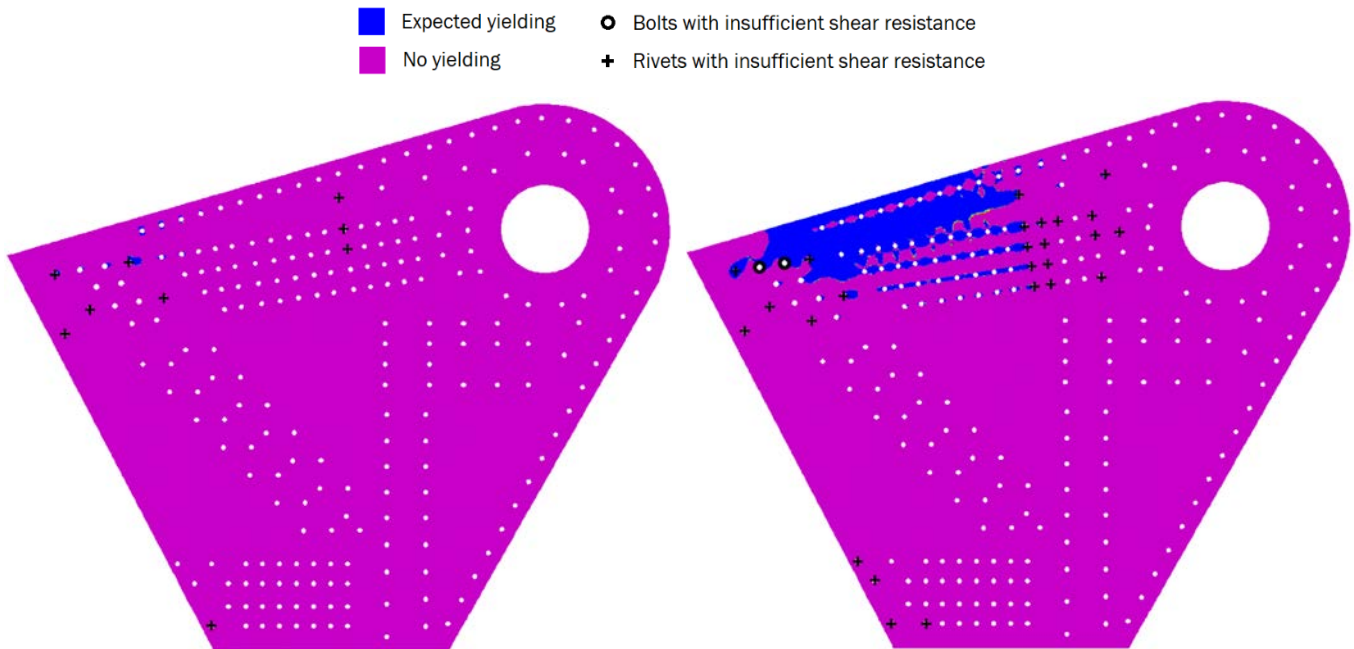


Figure 35 - Gusset plate expected yielding and fasteners with insufficient resistance at undeteriorated state according to S6-14  
 (a) Left: ULS 1 (b) Right: ULS B1 to B3

It should be noted that Figure 35 shows the results for the most conservative case at undeteriorated state, i.e. with an upper bound fastener stiffness and with  $M_0$  level 3. For ULS 1 shown in Figure 35 (a), as the yielding is expected to occur in a limited area, it would not be a concern, although some rivets would need to be replaced to meet CHBDC requirements. For special load combinations when the bridge is operated (shown in Figure 35 (b)), a large area located between strut 14-15 and the top edge is expected to yield. Although our 2D model is conservative at the edge because the existing top angle has not been modeled, we recommend that the plates should be strengthened at this location. Also, various rivets should be replaced by bolts, particularly those connecting the strut 14-15 to the gusset plates.

### 4.3.6.1.2 With Actual Deterioration

Figure 36 presents the expected yielding under load combination ULS 1 taking into account the actual deterioration for each plate while Figure 37 presents the expected yielding for special load combinations ULS B1 to ULS B3. Areas in blue are where yielding is expected in the gusset plates according to the analyses and the *von Mises* criterion. These results include both upper and lower bound cases for fastener stiffnesses.

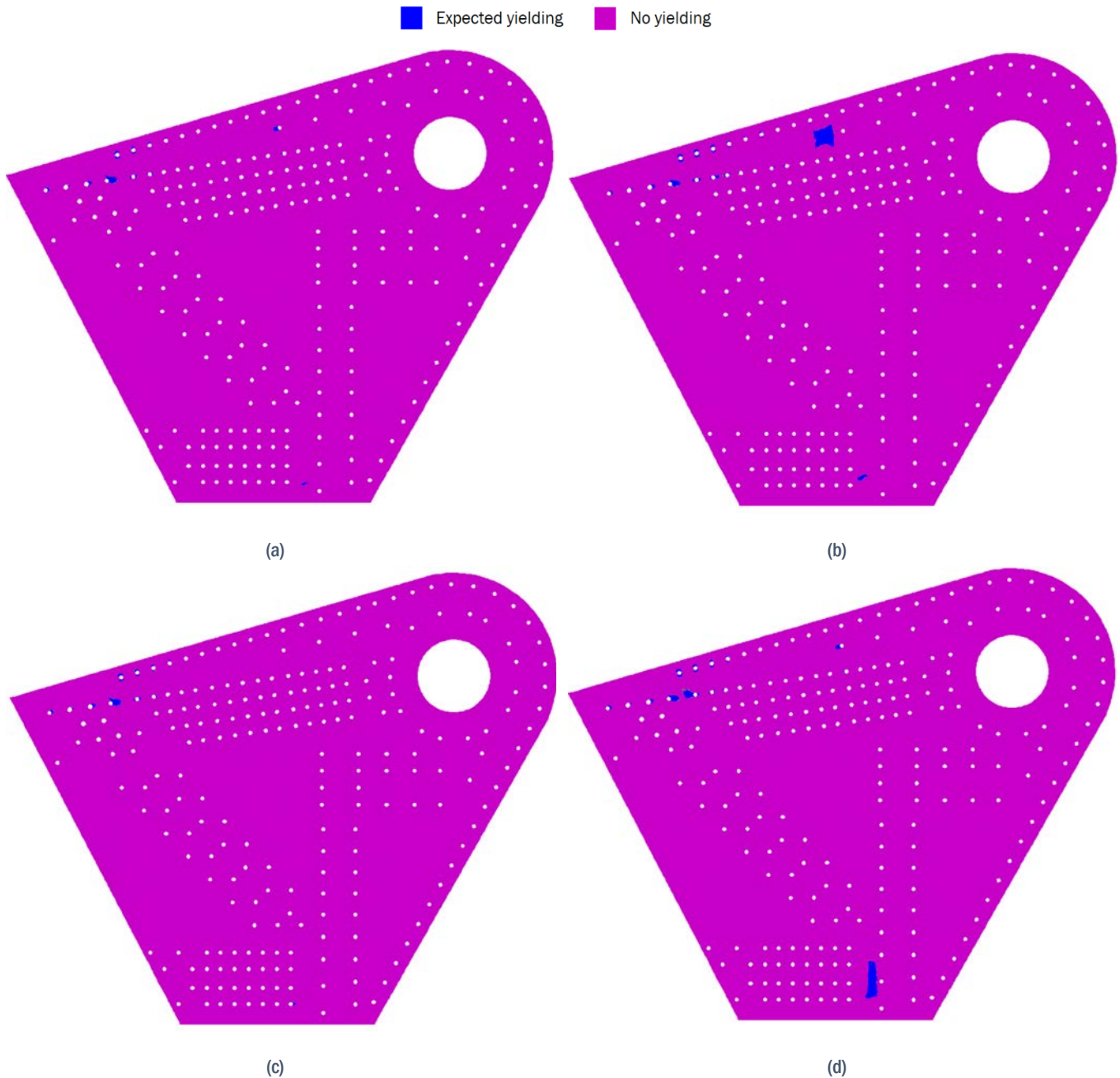


Figure 36 - Gusset plate expected yielding for ULS 1 considering deterioration  
(a) South exterior plate (b) South interior plate  
(c) North exterior plate (d) North interior plate

■ Expected yielding    ■ No yielding

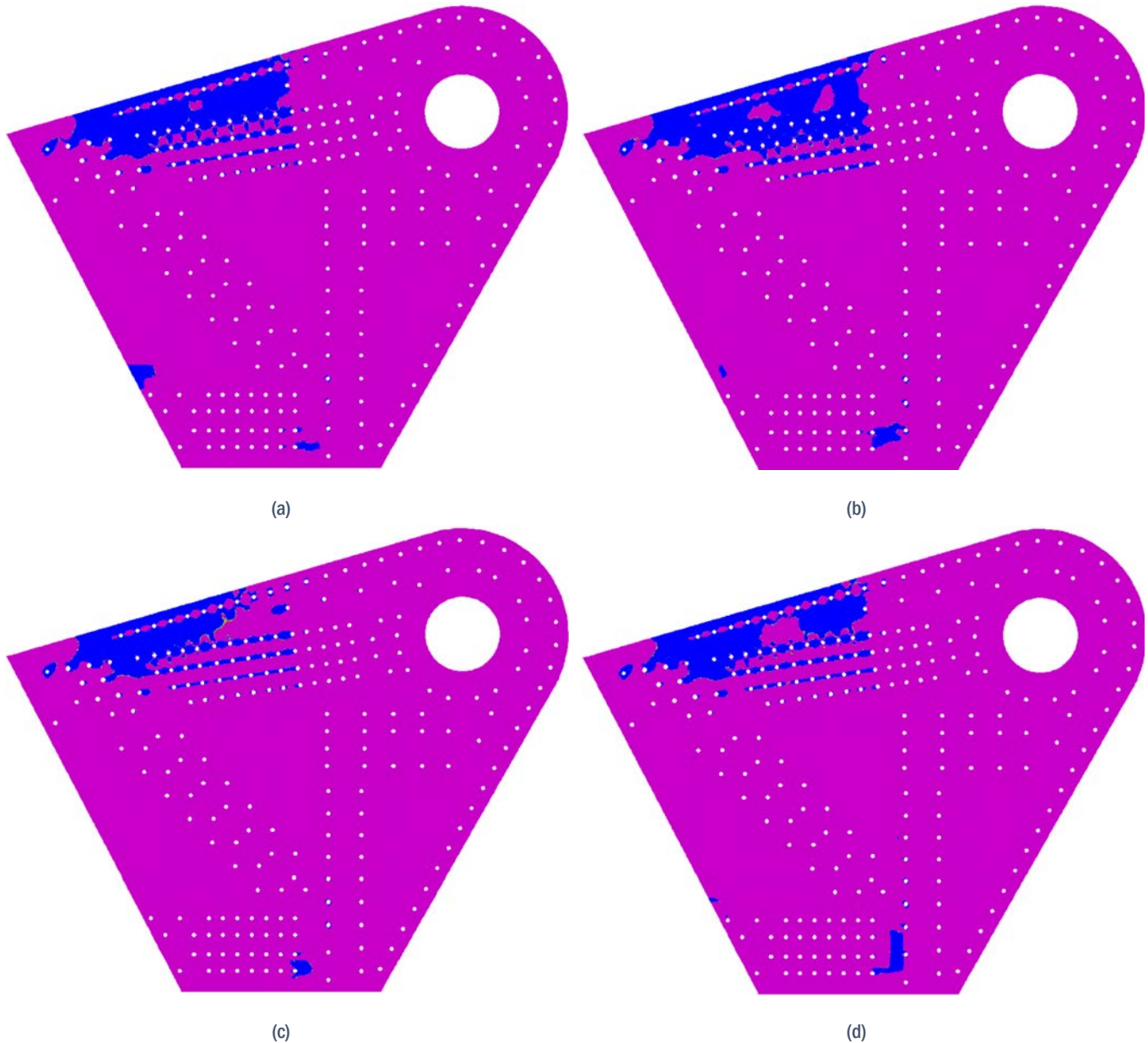


Figure 37 - Gusset plate expected yielding for ULS B1 to B3 according to S6-14 considering deterioration  
 (a) South exterior plate (b) South interior plate  
 (c) North exterior plate (d) North interior plate

Local stress concentrations are expected close to the holes and within areas with important section losses. Even if local redistribution is expected, the gusset plates should be repaired in the areas identified in blue because corrosion can progress in the future and because a brittle failure may initiate and propagate from the areas that yield under principal tensile stress.

Note that, as it was explained in Section 4.3.5.1, both north and south interior plates were modeled with a continuous gusset plate at the location of the cut-out to take into account the influence of the triangular reinforcement plate. A more refined analysis will be necessary for the design of the strengthening.

#### 4.3.6.2 Results with Restrictions during Bridge Operation

As the governing case for gusset plates and fasteners occurs during the operation of the bridge (ULS B1 to ULS B3) and considering the complexity, the cost and impact to traffic of the repair and strengthening of the gusset plates, it is suggested to operate the bridge with some wind restrictions in order to reduce the extent of the strengthening.

An alternative case that deviates from CHBDC has been analyzed and is shown for information purposes in Figure 37. Deviations from the CHBDC as it relates to the wind loads ( $W_0$ ) and the loads caused by the operation of machinery ( $M_0$ ). In this new case, the wind pressure is reduced to correspond to a wind speed of 60 km/h and  $M_0$  is reduced to Level 2. This corresponds exactly to the same case than the one presented in Table 7 for the evaluation of the members.

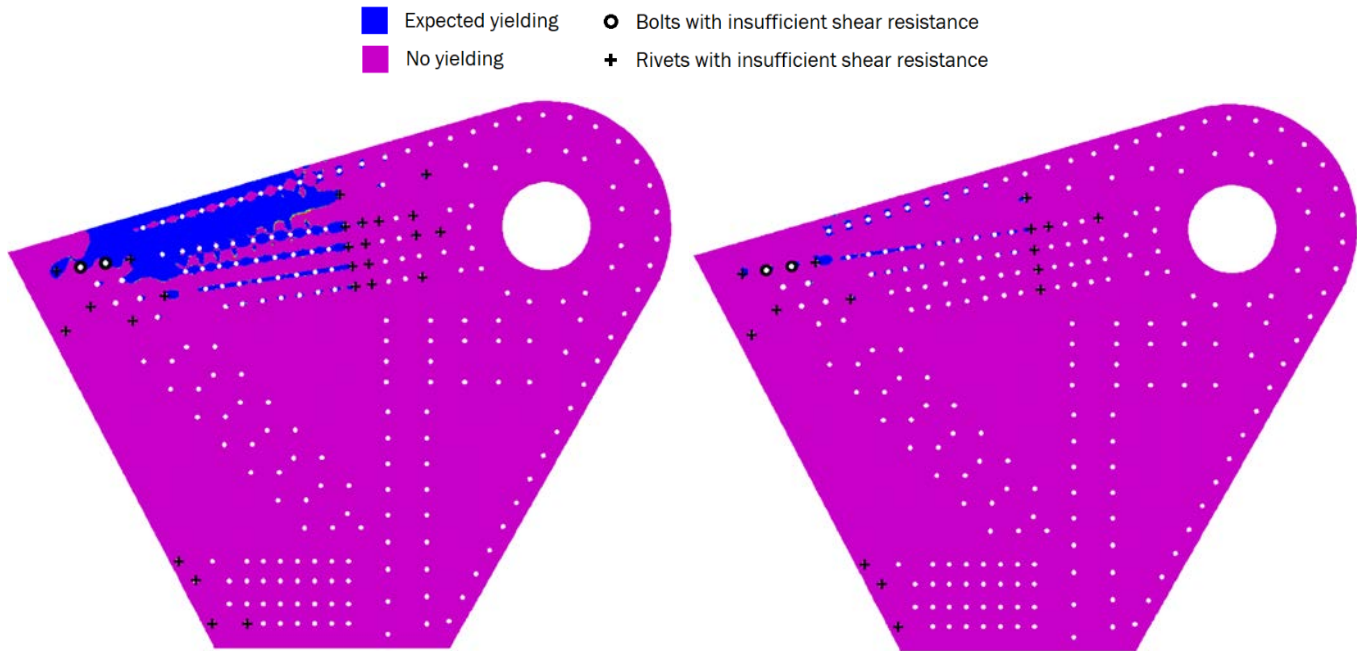


Figure 38 - Gusset plate expected yielding and fasteners with insufficient resistance at undeteriorated state for ULS B1 to B3  
(a) Left: with loads taken according to S6-14 (b) Right: with restrictions during bridge operation

Table 11 shows the results for this alternative case with restrictions during bridge operation (Figure 38 (b)). Results in green means the resistance is sufficient while results in red means the resistance is exceeded.

Table 11 - Results for gusset plates and fasteners at undeteriorated state with restrictions during bridge operation

Results	Fastener stiffness	Special load combinations for bascule bridges		
		ULS B1	ULS B2	ULS B3
MAX. <i>VON MISES</i> STRESS IN GUSSET PLATES $\Phi_s F_Y = 189 \text{ MPa}$	UPPER BOUND	149 MPa	212 MPa <sup>(1)</sup>	190 MPa <sup>(1)</sup>
	<i>VON MISES</i> STRESS / $\Phi_s F_Y$	0.79	1.12	1.01
MAX. RIVET SHEAR FORCE PER SHEAR PLANE $V_R = 45.5 \text{ kN}$	UPPER BOUND	157 kN	215 kN	199 kN
	RIVET SHEAR FORCE / $V_R$	3.45	4.73	4.37
MAX. BOLT SHEAR FORCE PER SHEAR PLANE $V_R = 106 \text{ kN}$	UPPER BOUND	94 kN	126 kN	118 kN
	BOLT SHEAR FORCE / $V_R$	0.89	1.19	1.11

(1) Stress at a localized area, redistribution in surrounding material is expected to occur



## 5 Conclusions and Recommendations

The six connecting members, the gusset plates and the fasteners of the main trunnion assemblies have been evaluated according to the CHBDC.

As previous studies showed that the governing load cases are when the bridge is operated (i.e. opened and closed), in-situ testing with strain gauges was conducted during the bridge opening and closing in order to validate the structural analysis models and to rationalize the dynamic load amplification.

Measured strains in the connecting truss members and in the gusset plates are comparable with those predicted with the structural analysis models. Therefore, the structural models are representative of the true behavior of the bridge for both closed and open positions.

Considering the high variability of the recorded values during the in-situ testing and that the operating impact load ( $I_o$ ) was found to have only a small influence on the forces in the connecting members and on the stresses in the gusset plates, it is recommended to use the operating impact factor of 20% of dead load as specified in the CHBDC for bascule bridges.

The evaluation of the members in accordance to the CHBDC showed that four members (13-16, 14-15, 14-16 and 15-17) are significantly overstressed with D/C ratio greater than 1.6 when the bridge is in the open position. However, the six members evaluated have been found to have an adequate resistance when the bridge is in the closed position.

Gusset plates and fasteners were evaluated with a 2D localized model in which the forces obtained with the 3D global models have been integrated. The *von Mises* yield criterion was used as the failure criterion for the gusset plates at ULS.

When the bridge is in the closed position, results show that both interior gusset plates (north and south) may locally yield in the most deteriorated areas and therefore should be repaired. Some rivets should also be replaced in the four gusset plates according to the most conservative case, i.e. with a non-uniform force distribution within fasteners. When the bridge is operated, i.e. in the open position, results show that the four gusset plates should be repaired when the loads are taken in accordance with CHBDC. This is true for both undeteriorated and deteriorated conditions and regardless of the force distribution considered in the fasteners. Some rivets and bolts should also be replaced.

The analyses show that the greatest loads in the members and gussets are caused by the wind. For structural members of bascule bridges, the CHBDC specifies a wind pressure of 1.5 kPa (Cl. 13.6.4.9), which appears to be a very high wind pressure considering the bridge is normally closed and is not operated in high winds (above 69 km/h). As part of the motor and drive rehabilitation project in 2017, a deviation to the Code was requested (Appendix D) as the existing mechanical components had insufficient capacity to accommodate the full wind pressure. Although mechanical system design is covered by a different section in the CHBDC than structural members, we believe that an approach that is rational, coherent and global should be considered for the retrofit of this existing bridge that has been in service for more than 100 years without any major problem. Therefore, we recommend that PSPC considers applying the deviation from the CHBDC requirements and setting a limit on the maximum permissible wind speed to around 60 km/h. As shown in this report, reducing the wind loads will greatly reduce the amount of strengthening required.

A consideration should also be given to reducing the force caused by the operation of the machinery, especially when it is combined with the wind loads as the brakes have a maximum capacity after which they will allow slippage. This code deviation is very important and will have a significant impact on the strengthening design concept.



Below are the recommendations which are determined based on the evaluation results.

<b>Recommendations</b>	
<b>1</b>	Repair and strengthen the connecting members 13-16, 14-15, 14-16 and 15-17
<b>2</b>	Repair and strengthen the gusset plates
<b>3</b>	Evaluate the possibility of deviating from the CHBDC requirements regarding the loads that need to be considered for the structural capacity evaluation of the bridge in the open position
<b>4</b>	Retrofit the bridge with a global and consistent approach that takes into account both the mechanical and structural capacities and limitations of the bridge

## 6 Closure

We trust that this report contains sufficient information for your present purposes. If you have any questions regarding this report, please do not hesitate to contact us.

Yours truly,

PARSONS INC.

---

PREPARED BY:  
Jimmy Fortier, P.Eng.  
Structural Engineer

---

PREPARED BY:  
Dennis Bascopé, P.Eng.  
Structural Engineer

---

PREPARED BY:  
Kevin Serre, ing.  
Structural Engineer




---

REVIEWED BY:  
Jack Ajrab, P.Eng.  
Structural Engineer

---

REVIEWED BY:  
Peter Harvey, P.Eng.  
Structural Engineer

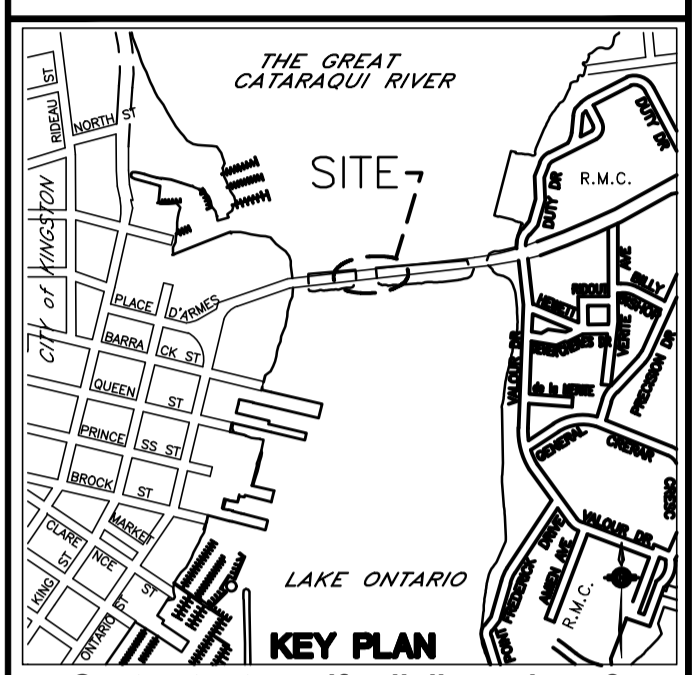
## References

- [1] Lasalle Causeway Trunnion Joint Inspection and Analysis Report, Version 3.0, MMM Group Limited, 2015
- [2] Lasalle Causeway Bascule Bridge 2017 Structural Evaluation Report, Parsons, 2017
- [3] CAN/CSA S6-14 Canadian Highway Bridge Design Code (CHBDC), Canadian Standards Association (CSA), 2014
- [4] AASHTO LRFD Movable Highway Bridge Design Specifications (2nd Edition) with 2008, 2010, 2011, 2012, 2014, 2015 and 2018 Interim Revisions. American Association of State Highway and Transportation Officials (AASHTO).
- [5] Gusset Plate Evaluation Guide: Refined analysis methods, Illinois Department of Transportation, 2014
- [6] Combined Stresses in Gusset Plates, Thornton W. A., 2000
- [7] Guide to Design Criteria for Bolted and Riveted Joints, Second Edition, Kulak G. L., Fisher J. W., Struik J. H. A., American Institute of Steel Construction (AISC), 2001
- [8] CAN/CSA-S16-19: Design of Steel Structures (9th Edition), Canadian Standards Association (CSA), 2019
- [9] Guide to Stability Design Criteria for Metal Structures (5th Edition), T. Galambos, John Wiley & Sons, Inc., 1998
- [10] Calcul des charpentes d'acier, Tome I, Beaulieu and al., Institut canadien de la construction en acier (ICCA), 2003
- [11] H. Huth. Influence of fastener flexibility on the prediction of load transfer and fatigue life for multiple-row joints. Fatigue in Mechanically Fastened Composite and Metallic Joints, ASTM STP927, pages 221-250, 1986

## Appendix A – Updated Mapping of the Trunnion Plate Deterioration



THIS DRAWING IS AN UPDATED VERSION OF THE 2015 DRAWINGS FROM THE REPORT "TRUNNION JOINT INSPECTION AND ANALYSIS" BY MMM GROUP LIMITED. PARSONS RESPONSIBILITY IS LIMITED TO NEW [2018] INFORMATION ADDED ON THE DRAWING.



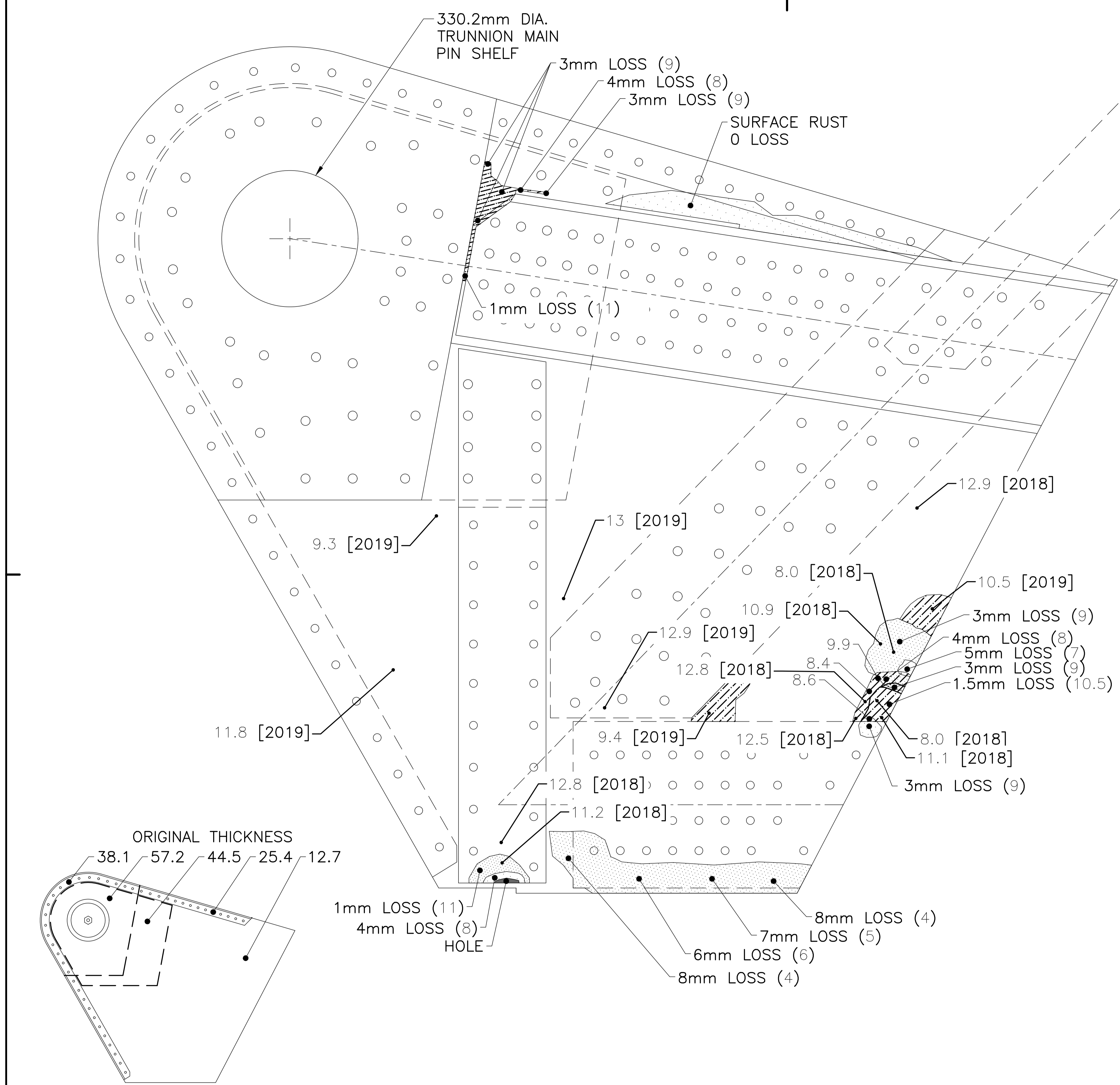
Contractor to verify all dimensions & conditions on site and immediately notify the engineer of all discrepancies.  
L'entrepreneur doit vérifier les dimensions et conditions sur le site et en aviser l'ingénieur immédiatement de toute divergence.

revisions	description	date

project LASALLE CAUSEWAY TRUNNION EVALUATION

drawing NORTH TRUNNION FULL EXTERIOR PLATE DETERIORATION G H

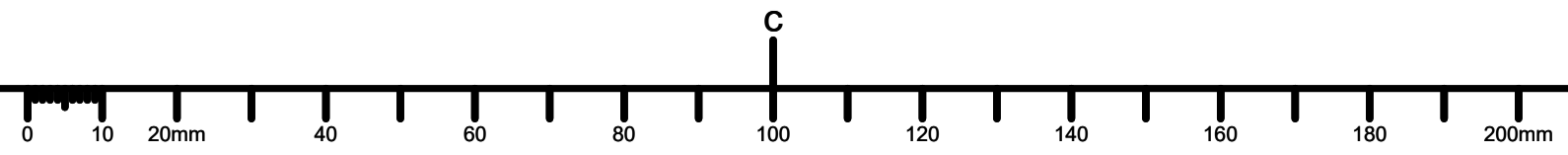
Designed By	Conçu par
Date	(yyyy/mm/dd)
Drawn By	Dessiné par
Date	22 JAN 2020 (yyyy/mm/dd)
Reviewed By	Examiné par
Date	22 JAN 2020 (yyyy/mm/dd)
Approved By	Approuvé par
Date	(yyyy/mm/dd)
Tender	Soumission
Project Manager	Administrateur de projets
Project no.	No. du projet
R.099350.002	
Drawing no.	No. du dessin
0000-4	



MAIN CASTING - CAST STEEL - 11/4" 31.75mm  
 INTERIOR PLATE - PLATE STEEL - 1/2" 12.7mm  
 GUSSET - PLATE STEEL - 1/2" 12.7mm

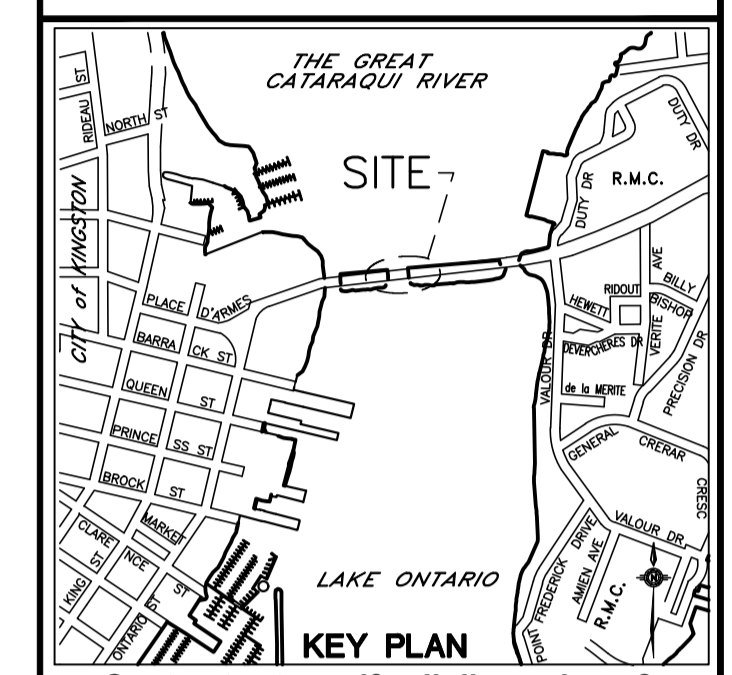
**LEGEND:**

- 4mm LOSS (8) PLATE SECTION LOSS (REMAINING THICKNESS IN MILLIMETRES BASED ON 12mm THICKNESS)
- 9.0 [2018] REMAINING THICKNESS IN MILLIMETRES BASED ON ULTRASONIC MEASUREMENTS [YEAR MEASUREMENT TAKEN]
- 7 REMAINING THICKNESS IN MILLIMETRES BASED ON ULTRASONIC MEASUREMENTS
- 3 DETERIORATED RIVETS PERCENT SECTION REMAINING DIVIDED BY 10 (i.e. 1=10%, 2=20%, 3=30%, ETC.)
- 99 PHOTOGRAPH KEY
- \* PHOTO FROM 2015 MMM GROUP LIMITED REPORT



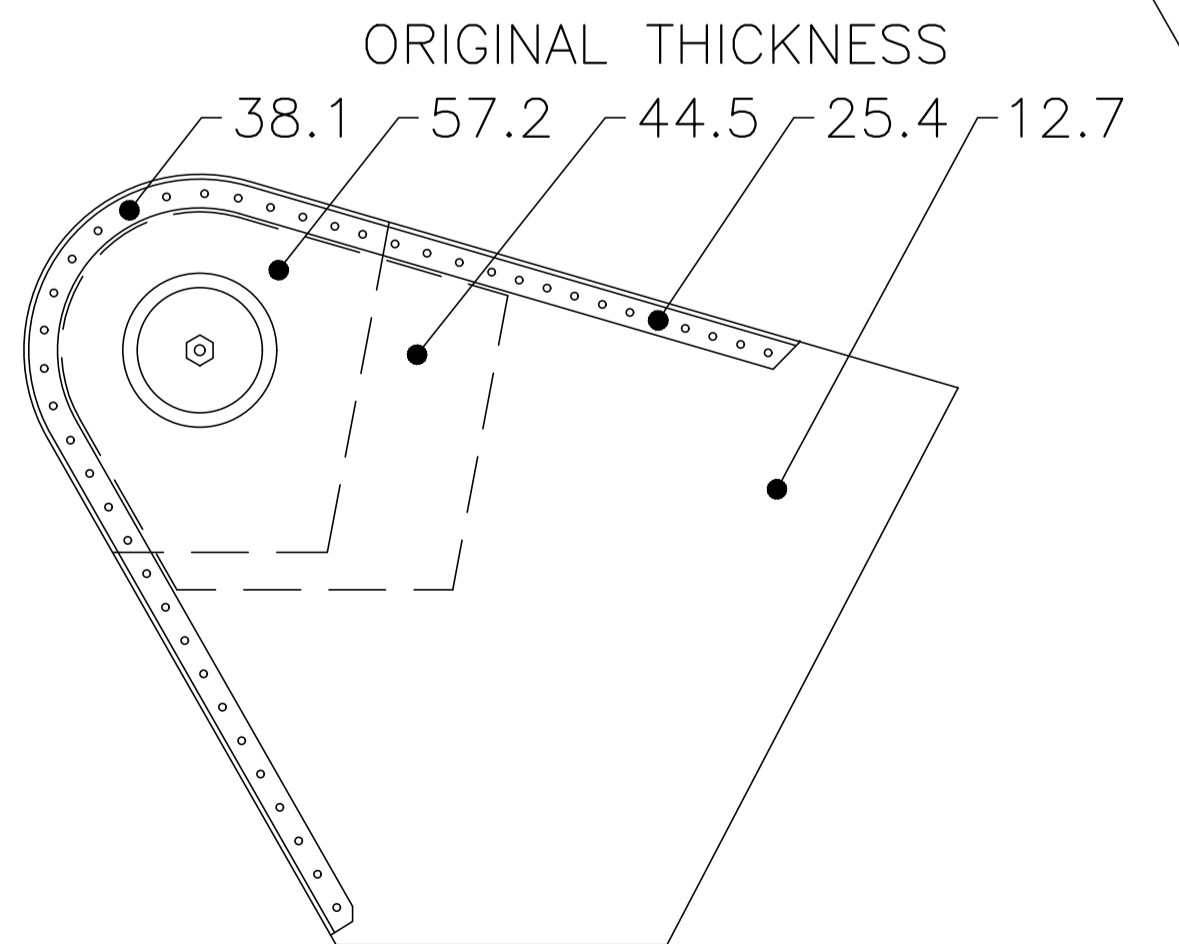
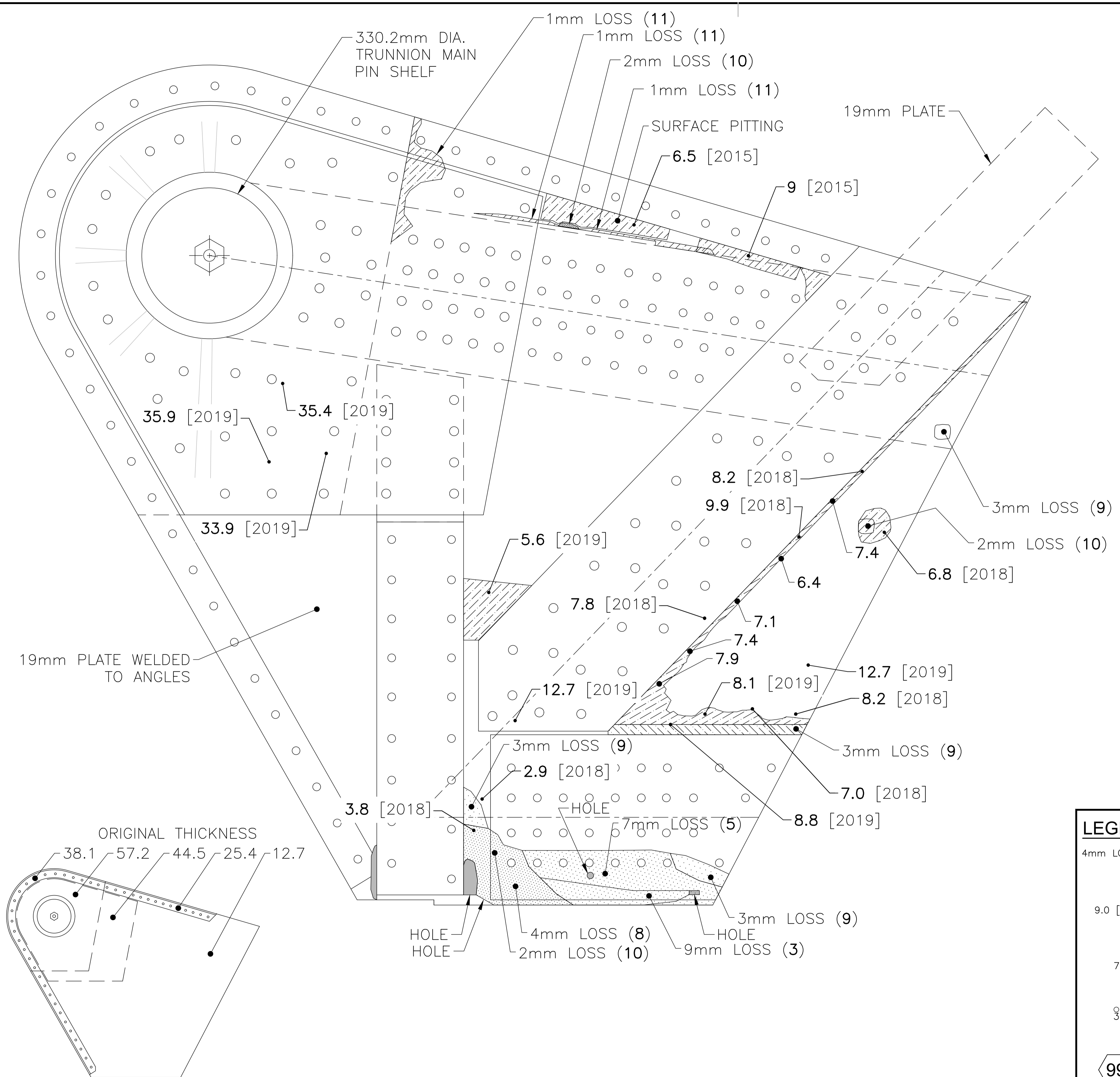


THIS DRAWING IS AN UPDATED VERSION OF THE 2015 DRAWINGS FROM THE REPORT "TRUNNION JOINT INSPECTION AND ANALYSIS" BY MMM GROUP LIMITED. PARSONS RESPONSIBILITY IS LIMITED TO NEW [2018] INFORMATION ADDED ON THE DRAWING.



Contractor to verify all dimensions & conditions on site and immediately notify the engineer of all discrepancies.

L'entrepreneur doit vérifier les dimensions et conditions sur le site et en aviser l'ingénieur immédiatement de toute divergence.



MAIN CASTING - CAST STEEL - 11/4" 31.75mm  
 INTERIOR PLATE - PLATE STEEL - 1/2" 12.7mm  
 GUSSET - PLATE STEEL - 1/2" 12.7mm

**LEGEND:**

4mm LOSS (8) PLATE SECTION LOSS (REMAINING THICKNESS IN MILLIMETRES BASED ON 12mm THICKNESS)

9.0 [2018] REMAINING THICKNESS IN MILLIMETRES BASED ON ULTRASONIC MEASUREMENTS [YEAR MEASUREMENT TAKEN]

7 REMAINING THICKNESS IN MILLIMETRES. BASED ON ULTRASONIC MEASUREMENTS

3 DETERIORATED RIVETS PERCENT SECTION REMAINING DIVIDED BY 10 (i.e. 1=10%, 2=20%, 3=30%, ETC.)

99 PHOTOGRAPH KEY

\* PHOTO FROM 2015 MMM GROUP LIMITED REPORT

revisions	description	date
A	A detail no. no. du detail	A
B	B location drawing no. sur dessin no.	B
C	C drawing no. dessin no.	C

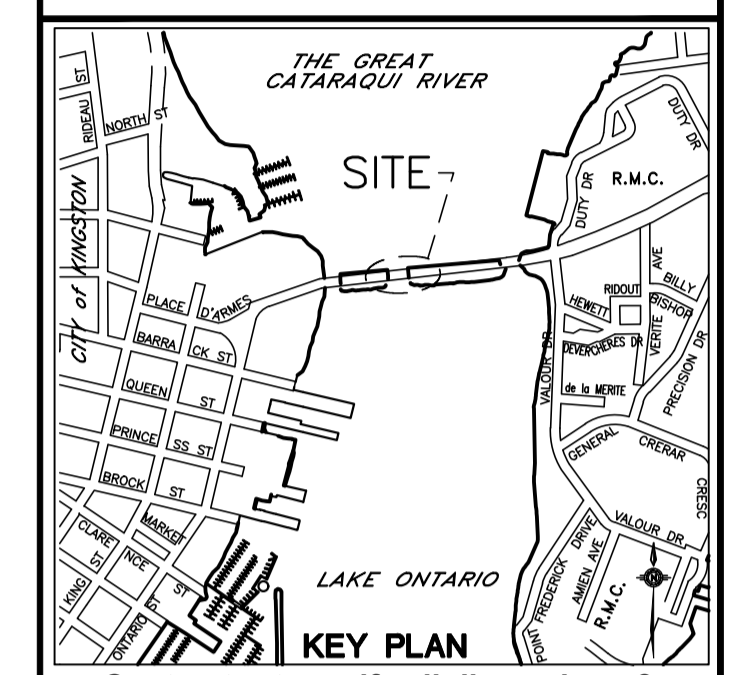
project LASALLE CAUSEWAY TRUNNION EVALUATION

drawing NORTH TRUNNION FULL INTERIOR PLATE DETERIORATION E F

Designed By	Conçu par
Date	(yyyy/mm/dd)
Drawn By	Dessiné par
Date	22 JAN 2020 (yyyy/mm/dd)
Reviewed By	Examiné par
Date	22 JAN 2020 (yyyy/mm/dd)
Approved By	Approuvé par
Date	(yyyy/mm/dd)
Tender	Soumission
Project Manager	Administrateur de projets
Project no.	No. du projet
	R.099350.002
Drawing no.	No. du dessin
	0000-3



THIS DRAWING IS AN UPDATED VERSION OF THE 2015 DRAWINGS FROM THE REPORT "TRUNNION JOINT INSPECTION AND ANALYSIS" BY MMM GROUP LIMITED. PARSONS RESPONSIBILITY IS LIMITED TO NEW [2018] INFORMATION ADDED ON THE DRAWING.



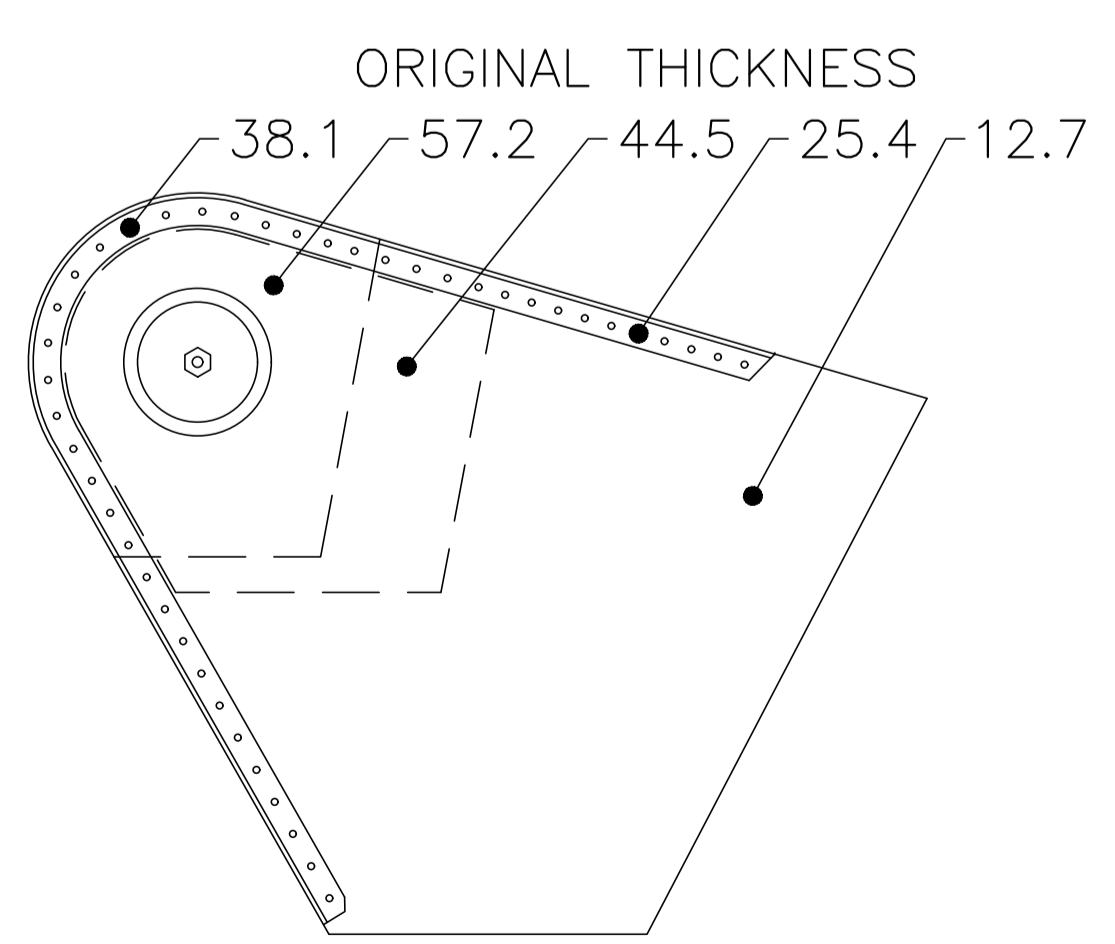
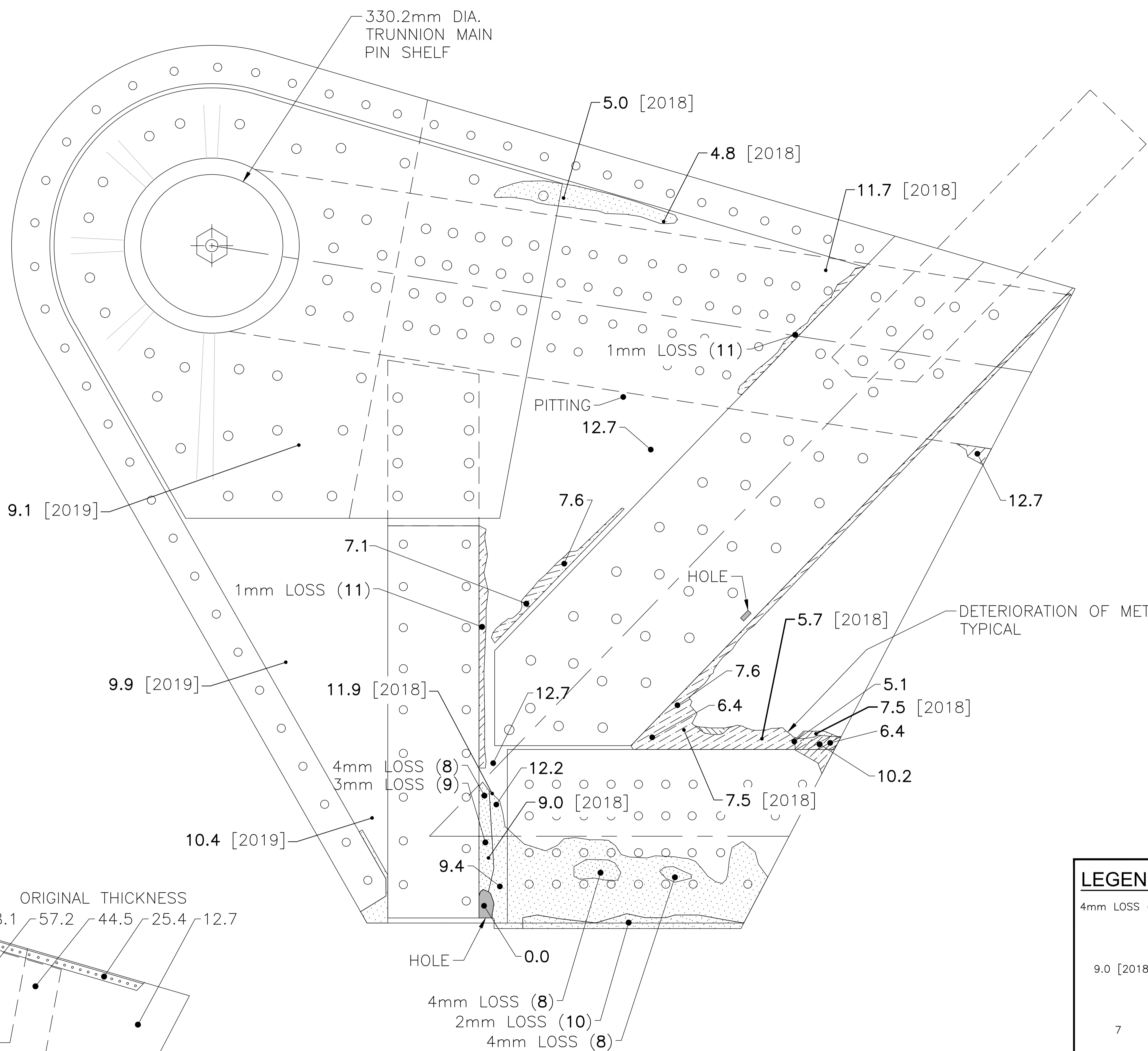
Contractor to verify all dimensions & conditions on site and immediately notify the engineer of all discrepancies.  
L'entrepreneur doit vérifier les dimensions et conditions sur le site et en aviser l'ingénieur immédiatement de toute divergence.

revisions	description	date
A	A detail no. du detail	A
B	B location drawing no. sur dessin no.	B
C	C drawing no. dessin no.	C

project LASALLE CAUSEWAY TRUNNION EVALUATION

drawing SOUTH TRUNNION FULL EXTERIOR PLATE DETERIORATION A B

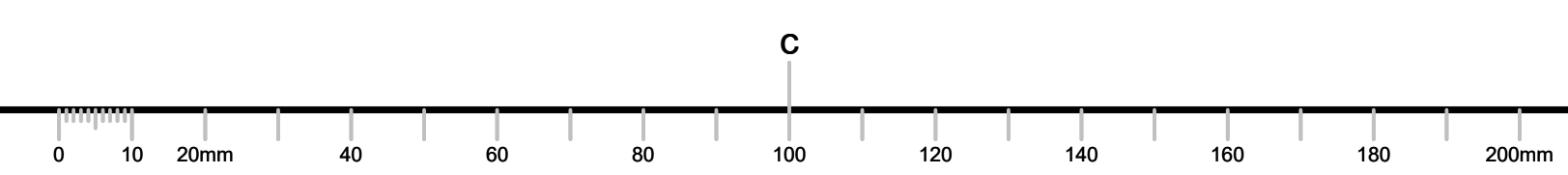
Designed By	Conçu par
Date	(yyyy/mm/dd)
Drawn By	Dessiné par
Date	22 JAN 2020 (yyyy/mm/dd)
Reviewed By	Examiné par
Date	22 JAN 2020 (yyyy/mm/dd)
Approved By	Approuvé par
Date	(yyyy/mm/dd)
Tender	Soumission
Project Manager	Administrateur de projets
Project no.	No. du projet
<b>R.099350.002</b>	
Drawing no.	No. du dessin
<b>0000-1</b>	



MAIN CASTING - CAST STEEL - 1 1/4" 31.75mm  
 INTERIOR PLATE - PLATE STEEL - 1/2" 12.7mm  
 GUSSET - PLATE STEEL - 1/2" 12.7mm

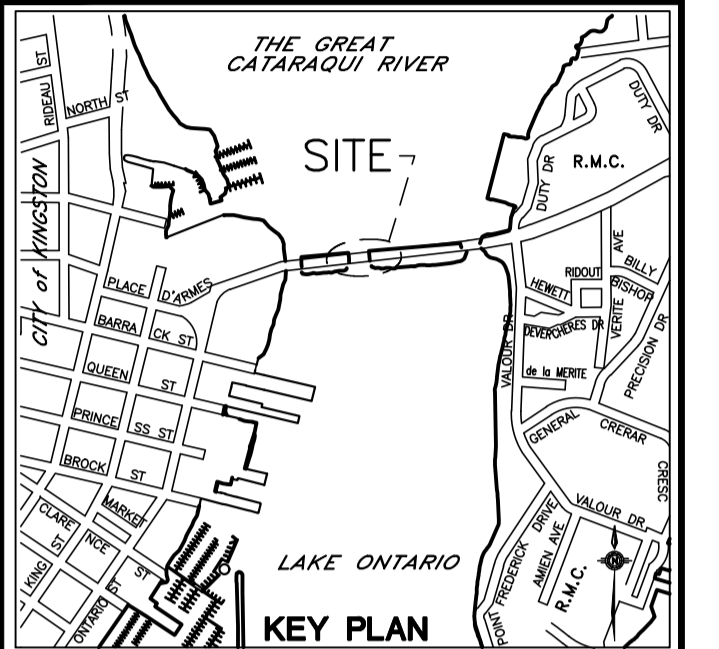
**LEGEND:**

4mm LOSS (8)	PLATE SECTION LOSS (REMAINING THICKNESS IN MILLIMETRES BASED ON 12mm THICKNESS)
9.0 [2018]	REMAINING THICKNESS IN MILLIMETRES BASED ON ULTRASONIC MEASUREMENTS [YEAR MEASUREMENT TAKEN]
7	REMAINING THICKNESS IN MILLIMETRES. BASED ON ULTRASONIC MEASUREMENTS
3	DETERIORATED RIVETS PERCENT SECTION REMAINING DIVIDED BY 10 (i.e. 1=10%, 2=20%, 3=30%, ETC.)
99	PHOTOGRAPH KEY
*	PHOTO FROM 2015 MMM GROUP LIMITED REPORT





THIS DRAWING IS AN UPDATED VERSION OF THE 2015 DRAWINGS FROM THE REPORT "TRUNNION JOINT INSPECTION AND ANALYSIS" BY MMM GROUP LIMITED. PARSONS RESPONSIBILITY IS LIMITED TO NEW [2018] INFORMATION ADDED ON THE DRAWING.



Contractor to verify all dimensions & conditions on site and immediately notify the engineer of all discrepancies.

L'entrepreneur doit vérifier les dimensions et conditions sur le site et en aviser l'ingénieur immédiatement de toute divergence.

revisions	description	date

<b>A</b>	A detail no. / no. du détail	<b>A</b>
<b>B</b>	B location drawing no. / sur dessin no.	<b>B</b>
<b>C</b>	C drawing no. / dessin no.	<b>C</b>

project \_\_\_\_\_ projet \_\_\_\_\_

LASALLE CAUSEWAY  
TRUNNION EVALUATION

drawing \_\_\_\_\_ dessin \_\_\_\_\_

SOUTH TRUNNION  
FULL INTERIOR PLATE  
DETERIORATION  
C D

Designed By \_\_\_\_\_ Conçu par \_\_\_\_\_

Date \_\_\_\_\_ (yyyy/mm/dd)

Drawn By \_\_\_\_\_ Dessiné par \_\_\_\_\_

Date 22 JAN 2020 (yyyy/mm/dd)

Reviewed By \_\_\_\_\_ Examiné par \_\_\_\_\_

Date 22 JAN 2020 (yyyy/mm/dd)

Approved By \_\_\_\_\_ Approuvé par \_\_\_\_\_

Date \_\_\_\_\_ (yyyy/mm/dd)

Tender \_\_\_\_\_ Soumission \_\_\_\_\_

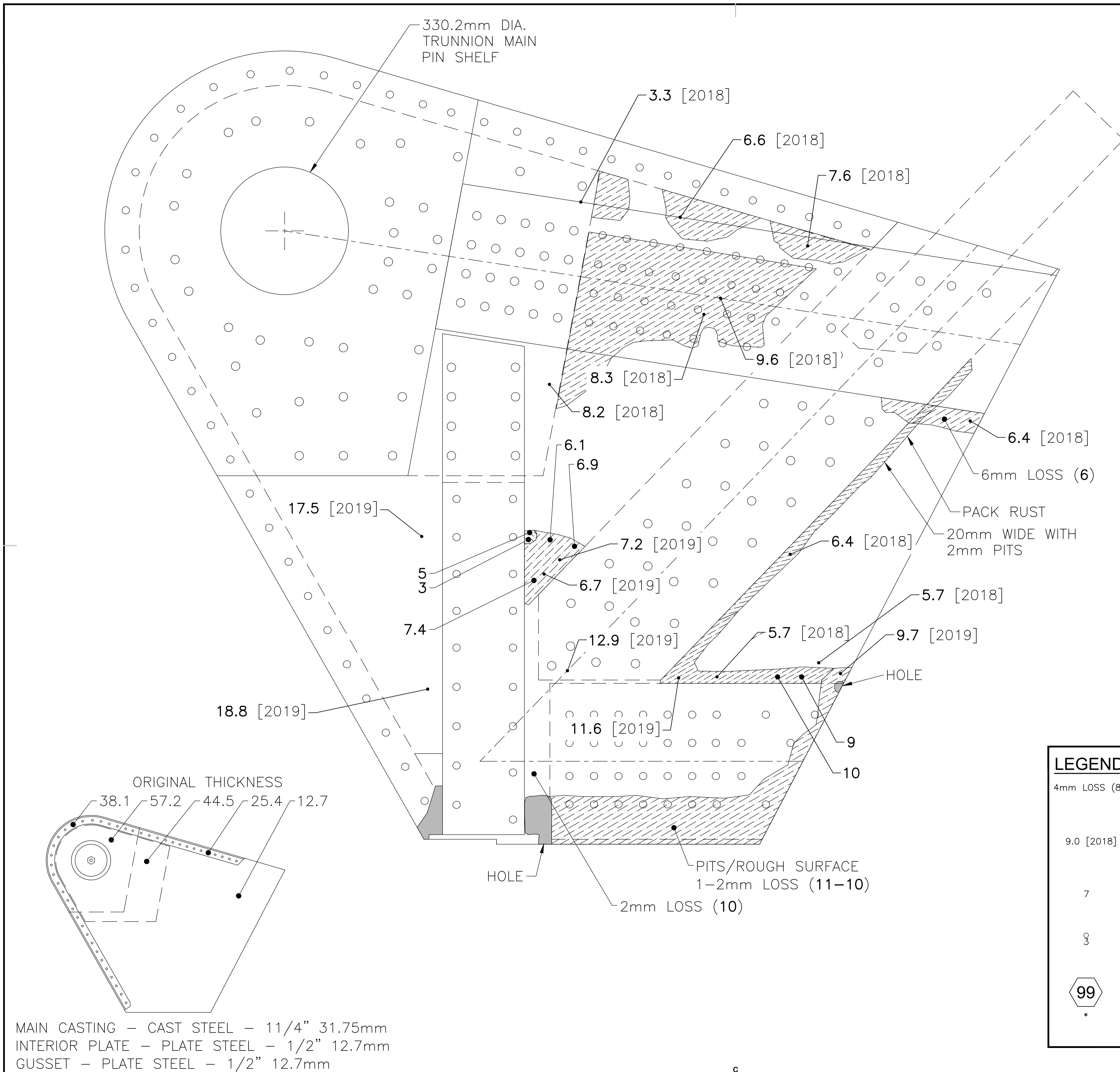
Project Manager \_\_\_\_\_ Administrateur de projets \_\_\_\_\_

Project no. \_\_\_\_\_ No. du projet \_\_\_\_\_

R.099350.002

Drawing no. \_\_\_\_\_ No. du dessin \_\_\_\_\_

0000-2



**LEGEND:**

4mm LOSS (8) PLATE SECTION LOSS (REMAINING THICKNESS IN MILLIMETRES BASED ON 12mm THICKNESS)

9.0 [2018] REMAINING THICKNESS IN MILLIMETRES BASED ON ULTRASONIC MEASUREMENTS [YEAR MEASUREMENT TAKEN]

7 REMAINING THICKNESS IN MILLIMETRES. BASED ON ULTRASONIC MEASUREMENTS

3 DETERIORATED RIVETS PERCENT SECTION REMAINING DIVIDED BY 10 (i.e. 1=10%, 2=20%, 3=30%, ETC.)

**99** PHOTOGRAPH KEY

\* PHOTO FROM 2015 MMM GROUP LIMITED REPORT

## Appendix B – UTT Inspection Report from Brouco NDT



<b>Customer:</b>	<b>Parsons INC.</b>	<b>Job No:</b>	<b>B-NDT- 3164</b>	<b>Date:</b>	<b>October 27, 2019</b>
<b>Project:</b>	<b>LaSalle Causeway – Bascule Bridge Main Trunnion Bearings Rehabilitation Project</b>		<b>Weather Conditions:</b>		<b>N/A</b>
<b>Subject:</b>	<b>Visual and Ultrasonic Thickness Testing of Main Trunnion Plates</b>		<b>Inspection Date:</b>		<b>October 17 and October 18, 2019</b>
<b>References:</b>	<b>CSA W47.1 Standard, CSA W59-13 Standard, CSA W178.1, CSA W178.2, ASTM E797 – Standard Practice for Measuring Thickness by Manual Ultrasonic Pulse-Echo Contact Method</b>				

As requested by Peter Harvey from Parsons INC., inspector Kent Leclair performed Ultrasonic Thickness Testing (UTT) of the Main Trunnion Plates as part of the LaSalle Causeway Bascule Bridge Main Trunnion Bearings Rehabilitation Project. The purpose of the testing was to update the corrosion mapping drawings for the trunnion plates.

**Equipment:**

Panametrics – NDT 37DL Plus Serial #041218711, D799 5MHz .312” diameter probe, Serial #1216107

Milwaukee Battery Powered Grinder (wire wheel and flap disk attachments used for surface preparation)

3400W Gas Powered Inverter Generator with built in spill containment for back-up power

**Results:**

1. Results of UTT Testing at North and South Main Trunnion Locations. Results are as follows:
  - a) **Table 1 through Table 48** contain the ultrasonic thickness test measurements of the North and South Exterior and Interior main Trunnion Plates. Three readings were taken at each location and the tables also show the average of the three readings at each test location. **Figure 1 through Figure 16** shows photos of the test locations and **Figure 17 to Figure 21** shown the mapping of the test locations on the Trunnion Drawings.
  - b) Additional pit gauge readings were taken on the North Trunnion, Interior Plate Location (Near UTT test locations 18 and 19) as shown in **Figure 18**. Two locations of pitting measured showed localized section loss of 0.277" and 0.138" (access was not possible on the backside of the angle member to perform UTT testing).
  - c) Test locations above include readings taken at strain gauge location around and on the main trunnion plates.

<b>Table 1: North Trunnion Exterior Plate Deterioration (At Strain Gauge Location), Test Location #1</b>	
Reading 1	.409
Reading 2	.413
Reading 3	.418
<b>Average:</b>	<b>.413</b>

<b>Table 2: North Trunnion Location 14-15N Exterior Web at Strain Gauge Location, Test Location #2</b>	
Reading 1	.522
Reading 2	.520
Reading 3	.528
<b>Average:</b>	<b>.523</b>

<b>Table 3: North Trunnion Location 14-16N Exterior Web at Strain Gauge Location, Test Location #3</b>	
Reading 1	.391
Reading 2	.392
Reading 3	.393
<b>Average:</b>	<b>.392</b>

<b>Table 4: North Trunnion Plate Interior Plate Deterioration, Test Location #4</b>	
Reading 1	.502
Reading 2	.502
Reading 3	.500
<b>Average:</b>	<b>.501</b>

<b>Table 5: North Trunnion Plate Interior Plate Deterioration at Strain Gauge Location, Test Location #5</b>	
Reading 1	.261
Reading 2	.200
Reading 3	.201
<b>Average:</b>	<b>.221</b>

<b>Table 6: North Trunnion Plate Interior Plate Deterioration at Strain Gauge Location, Test Location #6</b>	
Reading 1	.499
Reading 2	.500
Reading 3	.502
<b>Average:</b>	<b>.500</b>

<b>Table 7: North Trunnion Plate Exterior Plate Deterioration at Strain Gauge Location, Test Location #7</b>	
Reading 1	.509
Reading 2	.511
Reading 3	.510
<b>Average:</b>	<b>.510</b>

<b>Table 8: North Trunnion Plate Exterior Plate Deterioration at Strain Gauge Location, Test Location #8</b>	
Reading 1	.507
Reading 2	.508
Reading 3	.510
<b>Average:</b>	<b>.508</b>

<b>Table 9: North Trunnion Plate Interior Plate Deterioration, Test Location #9a</b>	
Reading 1	.320
Reading 2	.318
Reading 3	.406
<b>Average:</b>	<b>.348</b>

<b>Table 10: North Trunnion Plate Interior Plate Deterioration, Test Location #9b</b>	
Reading 1	.311
Reading 2	.322
Reading 3	.320
<b>Average:</b>	<b>.318</b>

<b>Table 11: North Trunnion Plate Exterior Plate Deterioration, Test Location #10</b>	
Reading 1	.364
Reading 2	.373
Reading 3	.370
<b>Average:</b>	<b>.369</b>

<b>Table 12: North Trunnion Location 14-16N Interior Web at Strain Gauge Location, Test Location #11</b>	
Reading 1	.395
Reading 2	.394
Reading 3	.398
<b>Average:</b>	<b>.396</b>

**Table 13: North Trunnion Location 14-15N Interior Web at Strain Gauge Location, Test Location #12**

Reading 1	.513
Reading 2	.512
Reading 3	.513
<b>Average:</b>	<b>.512</b>

**Table 14: North Trunnion Plate Exterior Plate Deterioration, Test Location #13**

Reading 1	.462
Reading 2	.464
Reading 3	.471
<b>Average:</b>	<b>.466</b>

**Table 15: North Trunnion Plate Exterior Plate Deterioration, Test Location #14**

Reading 1	.338
Reading 2	.392
Reading 3	.364
<b>Average:</b>	<b>.365</b>

**Table 16: North Trunnion Plate Interior Plate Deterioration, Test Location #15**

Reading 1	1.348
Reading 2	1.315
Reading 3	1.344
<b>Average:</b>	<b>1.336</b>

**Table 17: North Trunnion Plate Interior Plate Deterioration, Test Location #16**

Reading 1	1.388
Reading 2	1.369
Reading 3	1.384
<b>Average:</b>	<b>1.380</b>

**Table 18: North Trunnion Plate Interior Plate Deterioration, Test Location #17**

Reading 1	1.422
Reading 2	1.421
Reading 3	1.402
<b>Average:</b>	<b>1.415</b>

**Table 19: North Trunnion Plate Interior Plate Deterioration, Test Location #18**

Reading 1	.242
Reading 2	.237
Reading 3	.217
<b>Average:</b>	<b>.232</b>

**Table 20: North Trunnion Plate Interior Plate Deterioration, Test Location #19**

Reading 1	.363
Reading 2	.353
Reading 3	.357
<b>Average:</b>	<b>.358</b>



<b>Table 21: North Trunnion Plate Batten Plate Deterioration, Test Location #20</b>	
Reading 1	.425
Reading 2	.424
Reading 3	.426
<b>Average:</b>	<b>.425</b>

<b>Table 22: South Trunnion Plate Interior Plate Deterioration, Test Location #21</b>	
Reading 1	.746
Reading 2	.738
Reading 3	.742
<b>Average:</b>	<b>.742</b>

<b>Table 23: South Trunnion Plate Interior Plate Deterioration, Test Location #22a</b>	
Reading 1	.702
Reading 2	.699
Reading 3	.698
<b>Average:</b>	<b>.700</b>

<b>Table 24: South Trunnion Plate Interior Plate Deterioration, Test Location #22b</b>	
Reading 1	.689
Reading 2	.687
Reading 3	.688
<b>Average:</b>	<b>.688</b>

<b>Table 25: South Trunnion Plate Interior Plate Deterioration, Test Location #23</b>	
Reading 1	.338
Reading 2	.369
Reading 3	.363
<b>Average:</b>	<b>.357</b>

<b>Table 26: South Trunnion Plate Exterior Plate Deterioration, Test Location #24</b>	
Reading 1	.404
Reading 2	.411
Reading 3	.409
<b>Average:</b>	<b>.408</b>

<b>Table 27: South Trunnion Plate Exterior Plate Deterioration, Test Location #25</b>	
Reading 1	.436
Reading 2	.439
Reading 3	.449
<b>Average:</b>	<b>.441</b>

<b>Table 28: South Trunnion Plate Exterior Plate Deterioration, Test Location #26</b>	
Reading 1	.389
Reading 2	.384
Reading 3	.390
<b>Average:</b>	<b>.388</b>

<b>Table 29: South Trunnion Plate Exterior Plate Deterioration, Test Location #27</b>	
Reading 1	.327
Reading 2	.302
Reading 3	.292
<b>Average:</b>	<b>.307</b>

<b>Table 30: South Trunnion Plate Exterior Plate Deterioration, Test Location #28</b>	
Reading 1	.429
Reading 2	.441
Reading 3	.444
<b>Average:</b>	<b>.438</b>

<b>Table 31: South Trunnion Plate Exterior Plate Deterioration, Test Location #29</b>	
Reading 1	.477
Reading 2	.476
Reading 3	.475
<b>Average:</b>	<b>.476</b>

<b>Table 32: South Trunnion Plate Interior Plate Deterioration, Test Location #30</b>	
Reading 1	.387
Reading 2	.348
Reading 3	.365
<b>Average:</b>	<b>.367</b>

<b>Table 33: South Trunnion Location 14-15N Interior Web at Strain Gauge Location, Test Location #31</b>	
Reading 1	.521
Reading 2	.528
Reading 3	.522
<b>Average:</b>	<b>.524</b>

<b>Table 34: South Trunnion Location 14-15N Exterior Web at Strain Gauge Location, Test Location #32</b>	
Reading 1	.479
Reading 2	.481
Reading 3	.480
<b>Average:</b>	<b>.480</b>

<b>Table 35: South Trunnion Location 14-16N Exterior Web at Strain Gauge Location, Test Location #33</b>	
Reading 1	.396
Reading 2	.394
Reading 3	.397
<b>Average:</b>	<b>.396</b>

<b>Table 36: South Trunnion Location 14-16N Interior Web at Strain Gauge Location, Test Location #34</b>	
Reading 1	.401
Reading 2	.400
Reading 3	.400
<b>Average:</b>	<b>.400</b>

**Table 37: South Trunnion Plate Exterior Plate Deterioration, Test Location #35**

Reading 1	.491
Reading 2	.492
Reading 3	.491
<b>Average:</b>	<b>.491</b>

**Table 38: South Trunnion Plate Exterior Plate Deterioration at Strain Gauge Location, Test Location #36a**

Reading 1	.496
Reading 2	.497
Reading 3	.496
<b>Average:</b>	<b>.496</b>

**Table 39: South Trunnion Plate Exterior Plate Deterioration, Test Location #36b**

Reading 1	.282
Reading 2	.286
Reading 3	.309
<b>Average:</b>	<b>.292</b>

**Table 40: South Trunnion Plate Interior Plate Deterioration at Strain Gauge Location, Test Location #37a**

Reading 1	.273
Reading 2	.242
Reading 3	.272
<b>Average:</b>	<b>.262</b>

**Table 41: South Trunnion Plate Interior Plate Deterioration, Test Location #37b**

Reading 1	.315
Reading 2	.271
Reading 3	.266
<b>Average:</b>	<b>.284</b>

**Table 42: South Trunnion Plate Interior Plate Deterioration at Strain Gauge Location, Test Location #38**

Reading 1	.508
Reading 2	.509
Reading 3	.511
<b>Average:</b>	<b>.509</b>

**Table 43: South Trunnion Plate Interior Plate Deterioration, Test Location #39**

Reading 1	.394
Reading 2	.363
Reading 3	.382
<b>Average:</b>	<b>.380</b>

**Table 44: South Trunnion Plate Exterior Plate Deterioration, Test Location #40**

Reading 1	.283
Reading 2	.282
Reading 3	.288
<b>Average:</b>	<b>.284</b>

**Table 45: South Trunnion Plate Exterior Plate Deterioration, Test Location #41**

Reading 1	.408
Reading 2	.422
Reading 3	.429
<b>Average:</b>	<b>.420</b>

**Table 46: South Trunnion Plate Interior Plate Deterioration, Test Location #42**

Reading 1	.455
Reading 2	.461
Reading 3	.453
<b>Average:</b>	<b>.456</b>

**Table 47: South Trunnion Exterior Location Deterioration at Batten Plate, Test Location #43**

Reading 1	.158
Reading 2	.169
Reading 3	.196
<b>Average:</b>	<b>.174</b>

**Table 48: South Trunnion Plate Exterior Plate Deterioration, Test Location #44**

Reading 1	.387
Reading 2	.386
Reading 3	.376
<b>Average:</b>	<b>.383</b>



Figure1: Test Locations 5 and 6 at North Trunnion Plate Interior Plate at Strain Gauge Locations (Readings Taken from Inside surface of Plate)

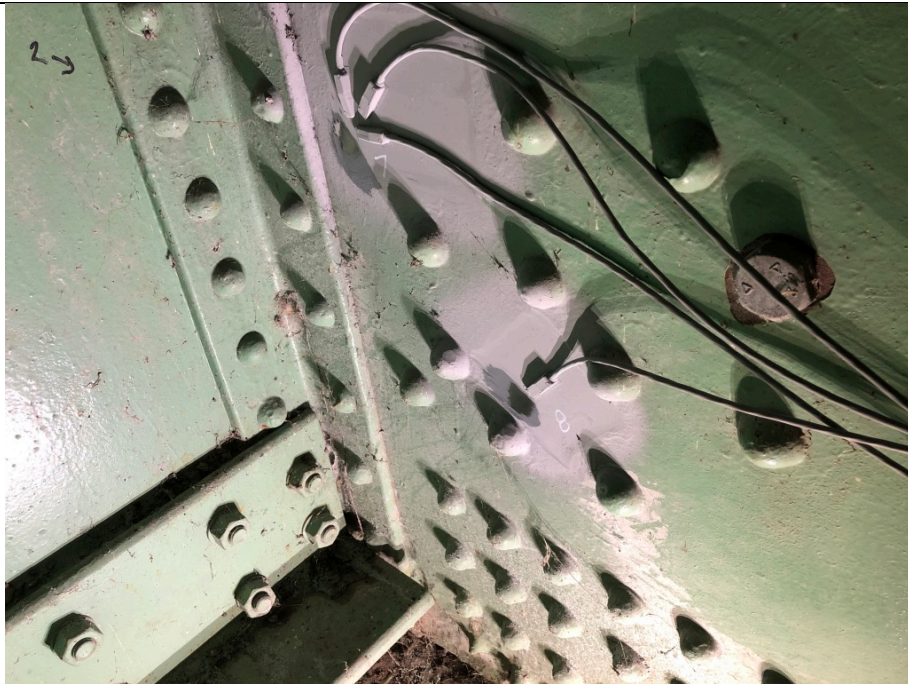


Figure2: Test Locations 7 and 8 at North Trunnion Plate Exterior Plate at Strain Gauge Locations (Readings Taken from Inside surface of Plate)



Figure3: Test Locations 9a and 9b at North Trunnion Plate Interior Plate (Readings Taken from Inside surface of Plate)





Figure4: Test Location 10 at North Trunnion Plate Exterior Plate (Readings Taken from Inside surface of Plate)



Figure4: Test Locations 15, 16, and 17 at North Trunnion Plate Interior Plate



Figure5: Test Location 20 at North Trunnion Location, Batten Plate



Figure6: Test Locations 21 and 22 at South Trunnion Plate Interior Location (Readings Taken on Exterior Plate Surface)





Figure7: Opposite Side of South Trunnion Plate Interior Location (Inside Plate Surface, see Figure 6 for Exterior Plate Surface)



Figure8: Test Locations 25, 26 and 28 at South Trunnion Plate Exterior Location (Readings Taken from Inside Surface)





Figure9: Test Locations 28 and 29 at South Trunnion Plate Exterior Location (Readings Taken from Inside Surface and Bottom Surface of Angle)



Figure10: Test Locations 23 and 30 at South Trunnion Plate Interior Location (Readings Taken from Inside Bottom Surface of Angle)



Figure11: Test Locations 43 and 44 at South Trunnion Exterior Plate at Interior Batten Plate and Angle



Figure12: Test Locations 43 and 44 at South Trunnion Exterior Plate at Interior Batten Plate and Angle





Figure13: Test Location 36 at South Trunnion Exterior Plate Location (Readings Taken on Interior Surface of Plate)



Figure14: Test Locations 37, 38, and 42 at South Trunnion Interior Plate Location (Readings Taken on Interior Surface of Plate)



Figure15: Test Locations 35, and 40 at South Trunnion Exterior Plate Location (Readings Taken on Interior Surface of Plate)



Figure16: Test Location 41 at South Trunnion Exterior Plate Location (Readings Taken on Interior Surface of Plate)



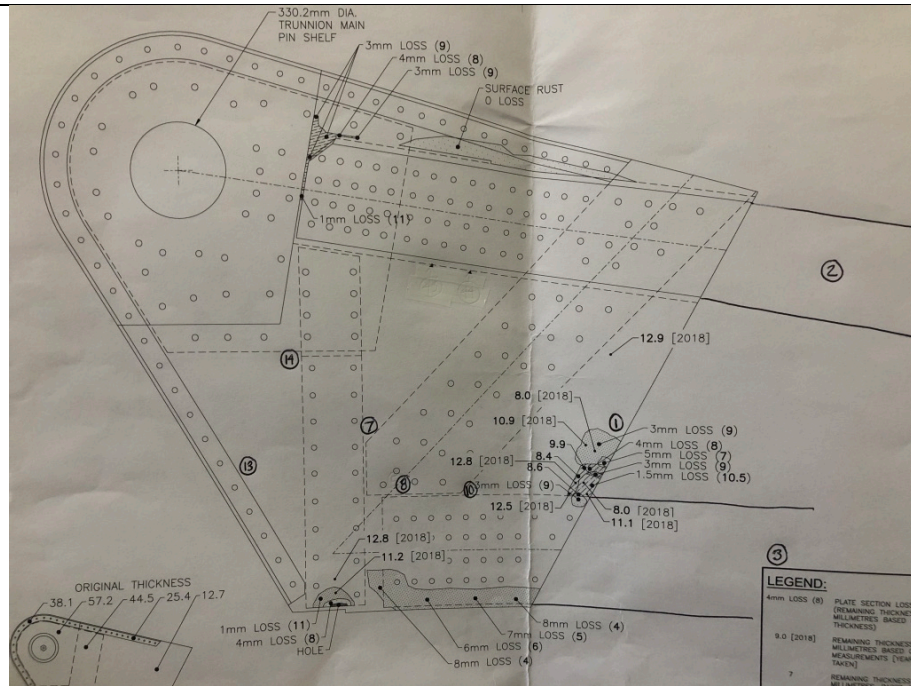


Figure17: North Trunnion Exterior Plate Test Locations

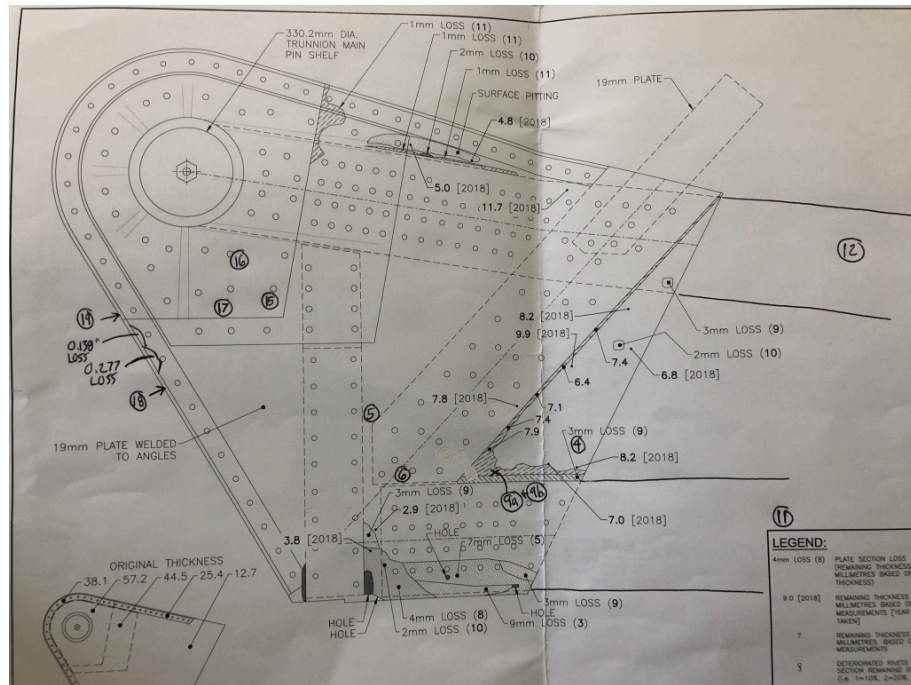


Figure18: North Trunnion Interior Plate Test Locations

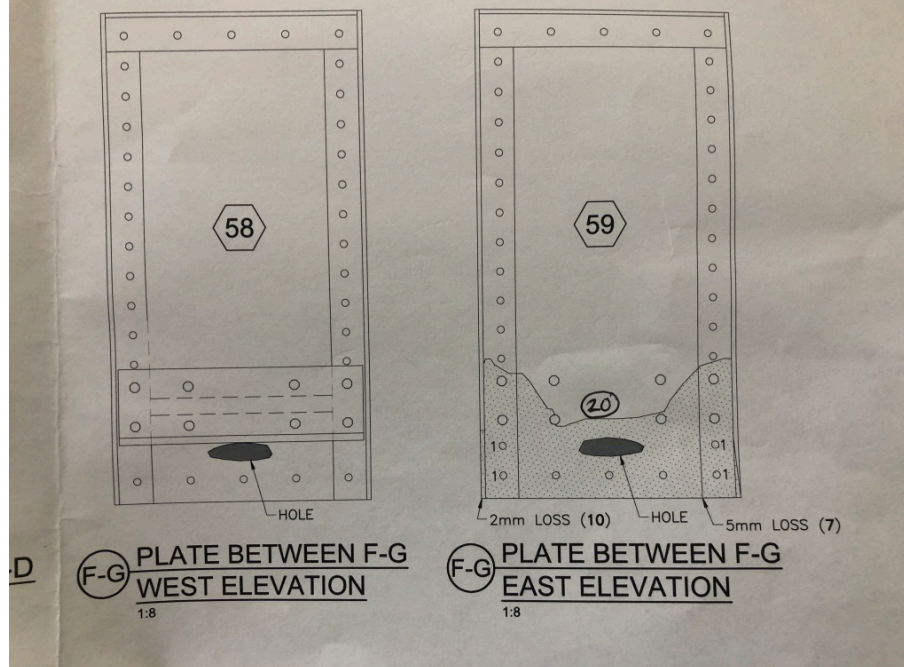


Figure19: North Trunnion Location, Batten Plate Test Location

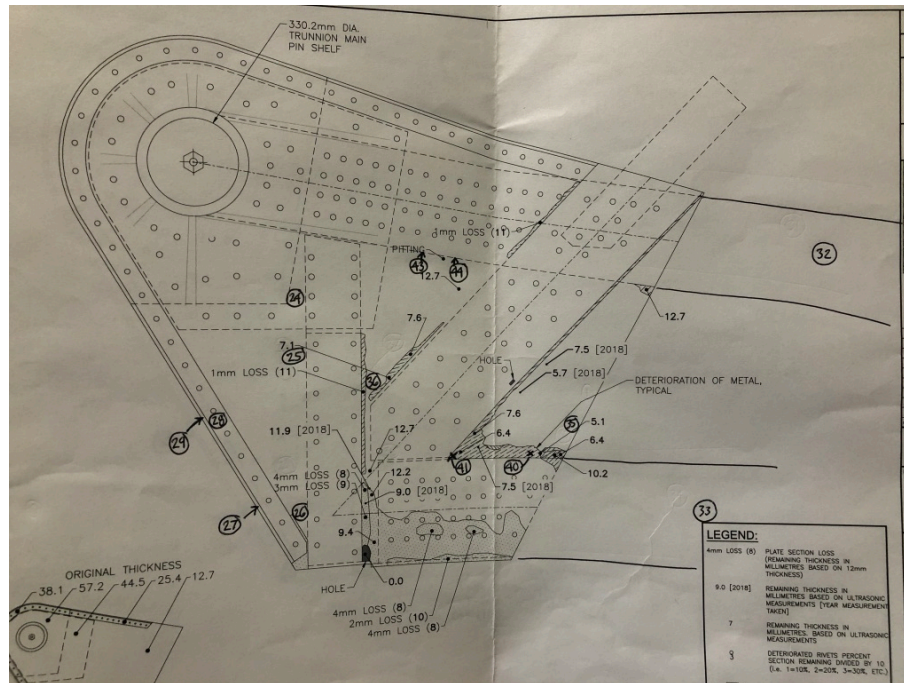


Figure20: South Trunnion Exterior Plate Test Locations



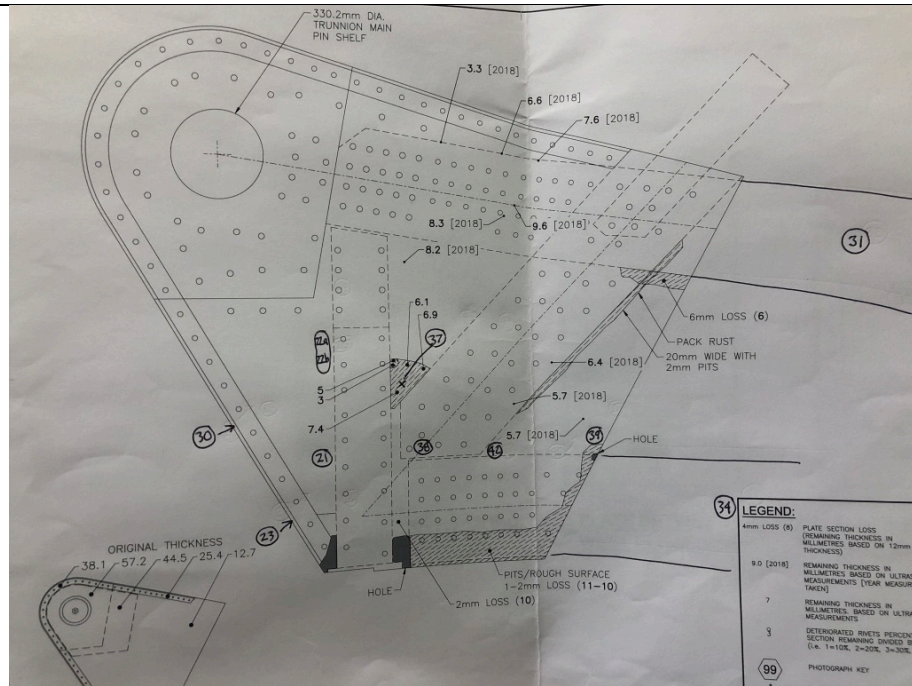


Figure21: South Trunnion Interior Plate Test Locations



**Conclusion:**

The above test results are for the ultrasonic thickness testing for updating the main trunnion plate corrosion mapping. Test locations were also performed at stain gauge locations as reference. Parsons assisted in selecting the above test locations.


**Inspection Date:**

October 17 and  
October 18, 2019


**Report Date:**

October 27, 2018

**Inspection and Report by:** Kent Leclair

CSA W178.2 Level 3 Certified Welding Inspector Reg. #3938  
Level II MT CGSB Reg. #16878 

**Report Reviewed by:** Kent Leclair

CSA W178.2 Level 3 Certified Welding Inspector Reg. #3938  
Level II MT CGSB Reg. #16878 

## Appendix C – Strain Gauge Testing

Considering the size of the raw data, this appendix has been submitted electronically.

## Appendix D – Deviation request for the 2017 Motor and Drive Rehabilitation Project



**STAFFORD BANDLOW ENGINEERING, INC.**

---

July 24, 2017

**Via E-Mail**

[Maurice.Mansfield@parsons.com](mailto:Maurice.Mansfield@parsons.com)

Mr. Maurice Mansfield  
Parsons  
1223 Michael St., Suite 100  
Ottawa, ON K1J 7T2

Maurice,

As part of the LaSalle Causeway Bridge motor and drive rehabilitation design, the existing machinery and prime mover were evaluated with regard to the 2014 edition of the CAN/CSA S6 Canadian Highway Bridge and Design Code (CHBDC), Section 13 requirements. It was determined that the current prime mover, which consists of two 50 HP at 585 RPM motors operating together, were overloaded by a factor of 1.50.

The existing gears, shafts, keys, and bearings were evaluated with regard to the current prime mover using the information provided by the original and 1966 rehab drawings. There was sufficient legible to evaluate the capacity of the gears, shafts and bearings. It was determined that these existing machinery components are appropriately sized for the existing prime mover. However, there is little reserve capacity in the existing gears and therefore increasing the capacity of the prime mover as part of the motor and drive replacement project is not possible unless the scope of the replacement work is increased to include virtually all of the existing gearing.

It should be noted that there is limited legible information on the key sizes and lengths on the available drawings. As such any evaluation of the existing keys is considered preliminary until such time that the existing key dimensions can be verified at the bridge.

Although the existing prime mover is overloaded per Code requirements, the bridge is routinely operated on a single motor and there are no reported issues of the existing motors (individually or operating as a pair) failing to operate the bascule leaf in the recent past or over its' history of operating since circa 1915. As such, it would appear to be reasonable to maintain the current capacity of the motors with the replacement motors which would provide for reliable operation without exceeding the capacity of the existing machinery.

The loads on the prime mover during operation of a bascule leaf are caused by imbalance, friction, inertia, wind and ice as follows per Article 13.7.14.7.2 of the CHBDC:

- (a) Maximum starting torque ( $T_s$ ) shall be determined for span operation against static frictional resistance, unbalanced conditions (if any), a wind load of 0.48 kPa (10 psf) on any vertical projection, and an ice loading of 0.12 kPa (2.5 psf) on the area specified in Clause 13.6.4.5 and shall include inertial resistance due to acceleration.



- (b) Maximum constant velocity torque ( $T_{cv}$ ) shall be determined for span operation against dynamic frictional resistances, unbalanced conditions (if any), and a wind load of 0.12 kPa (2.5 psf) acting normal to the floor on the area specified in Clause 13.6.4.5.

Maximum starting torque is the limiting case for sizing the prime mover. Imbalance, friction, inertia are not practical to modify. As such, limitations on wind pressure (and therefore maximum wind speeds) must be modified if the prime mover does not have adequate capacity to fully comply with CHBDC requirements. The existing (and proposed new) prime mover has sufficient capacity to operate the span with a wind pressure of 0.24 kPa (5 psf).

Wind loads for movable bridge operation are given in the Code as a wind pressure. The commentary on Annex CA3.1 – Climate and environmental data in CAN/CSA S6-14 provides a formula describing the relationship between the reference pressure,  $q$  (in Pa), and the corresponding mean hourly wind speed,  $v$  (in km/h):

$$q = 0.05 v^2$$

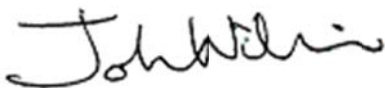
Using this formula, the wind speed corresponding to the Code required design wind pressure (480 Pa) is 98 km/hr and the wind speed corresponding to the proposed maximum permissible wind pressure (240 Pa) is 69 km/hr.

In order to implement the wind speed restrictions for the bascule leaf operation it would be necessary to revise operating procedures to check wind speeds. This may be done using dedicated wind speed monitoring equipment installed at the bridge (which does not presently exist), or by checking wind speeds at a nearby weather station via the internet.

Please advise if it is acceptable to deviate from CAN/CSA S6-14 Canadian Highway Bridge and Design Code requirements and design the new motors and drives with the same capacity as the existing prime movers at the bridge which will require implementation of operating restrictions to periods when the wind speeds are less than 69 km/hr and adopting new operating procedures for verifying acceptable wind speeds.

If you have any questions or would like to discuss any of the above in further detail, please do not hesitate to contact me at (215) 340-5830.

Sincerely,



John Williams, P.Eng.

# Lasalle Causeway Bascule Bridge Main Trunnion Rehabilitation Study - Structural Evaluation Report

---

**Jimmy Fortier, P.Eng.**

1800 McGill College Avenue,  
Suite 510  
Montréal, QC H3A 3J6  
514.375.4949

**Dennis Bascopé, P.Eng.**

1800 McGill College Avenue,  
Suite 510  
Montréal, QC H3A 3J6  
514.375.4949

**Kevin Serre, ing.**

1800 McGill College Avenue,  
Suite 510  
Montréal, QC H3A 3J6  
514.375.4949

**Jack Ajrab, P.Eng.**

1223 Michael Street North,  
Suite 100  
Ottawa, ON K1N 7X4  
613.738-4160

**Peter Harvey, P.Eng.**

1223 Michael Street North,  
Suite 100  
Ottawa, ON K1N 7X4  
613.738-4160



5875 Trinity Parkway, Suite 300  
Centreville, Virginia 20120  
Direct: +1 703.988.8500  
parsons.com

© Copyright 2020 Parsons Corporation.  
All Rights Reserved.